4-17-2013

Investigations of Substrate Channeling in the Proline Oxidative Pathway

Nikhilesh Sanyal
University of Nebraska-Lincoln, nikhilesh1@gmail.com

INVESTIGATIONS OF SUBSTRATE CHANNELING IN THE PROLINE OXIDATIVE PATHWAY

by

Nikhilesh Sanyal

A DISSERTATION

Presented to the Faculty of

The Graduate College at the University of Nebraska

In Partial Fulfillment of Requirements

For the Degree of Doctor of Philosophy

Major: Biochemistry

Under the Supervision of Professor Donald F. Becker

Lincoln, Nebraska

April, 2013

INVESTIGATIONS OF SUBSTRATE CHANNELING IN THE PROLINE OXIDATIVE PATHWAY

Nikhilesh Sanyal, Ph.D.

University of Nebraska, 2013

Advisor: Donald F. Becker

In cell metabolism, substrate channeling is a phenomenon where the product of one reaction is transported to a second enzyme active site without equilibrating into bulk solvent. Chapter 1 reviews the rationale and evidence for substrate channeling with the specific example of proline metabolism. Oxidation of proline to glutamate is catalyzed in consecutive reactions by proline dehydrogenase (PRODH) and pyrroline-5-carboxylate dehydrogenase (P5CDH). The intermediate Δ^1-pyrroline-5-carboxylate reportedly tends to be labile and inhibitory towards several metabolic pathways.

One of the main objectives of this dissertation was to investigate substrate channeling between independent proline oxidative enzymes from *Thermus thermophilus*- TtPRODH and TtP5CDH. Chapter 2 establishes that TtPRODH and TtP5CDH are capable of interacting with a dissociation constant (K_D) of 3.03 μM as demonstrated using Surface Plasmon Resonance (SPR). As observed in the present study, this interaction is possible only with a specific orientation of TtPRODH relative to TtP5CDH. A docking model of the two enzymes predicts an orientation of the active sites which is supportive of substrate channeling. Corroborating observations are made with kinetic studies. We observe that interference of TtPRODH-TtP5CDH complex by catalytically inactive mutants TtPRODH R288M/R289M and TtP5CDH C322A lead to significant decrease in

glutamate formation. The results pave the way for testing substrate channeling in eukaryotic enzymes. In chapter 3, two novel eukaryotic enzymes from *Saccharomyces cerevisiae*, Put1p (PRODH) and Put2p (P5CDH), have been characterized. Particular attention was focused on the oxidative half-reaction of Put1p for gaining insight into possible redox functions of human PRODH.

Previous studies show that bifunctional enzyme from Gram-negative *Bradyrhizobium japonicum* (BjPutA) containing PRODH and P5CDH domains, exhibits substrate channeling via an elegant internal tunnel. BjPutA and its channeling variants were used to test the role of substrate channel in hydrolysis of P5C, an essential step in proline oxidation. These aspects of substrate channeling are discussed in chapter 4.

Overall, this study provides an improved understanding of: (1) Substrate channeling in proline oxidation; and (2) a model for investigating substrate channeling between other individual enzymes that catalyze consecutive reactions.

ACKNOWLEDGEMENTS

Firstly, I would like to express sincere gratitude to my advisor, Dr. Donald F. Becker, for his invaluable guidance throughout my graduate career. His constant encouragement and thoughtful critique of experimental ideas have shaped me into a better scientist. I will always be inspired by his dedication to fostering young students towards a career in scientific research.

I would also like to thank the members of my Ph.D. committee, Dr. Joseph Barycki, Dr. Jaekwon Lee, Dr. Mark Wilson and Dr. Greg Somerville for their helpful suggestions and willingness to evaluate my research. I thank Dr. Somerville for his broad advice during my first year of graduate school.

Special thanks go to our research collaborator, Dr. John Tanner, and his lab members from University of Missouri-Columbia for continued discussion and helpful suggestions. I sincerely appreciate and acknowledge current and former members of Becker Lab for creating a healthy work atmosphere and especially Ben Arentson for his exchange of experimental ideas.

I am thankful to the Biochemistry office personnel and departmental colleagues for creating a helpful and pleasant environment. I acknowledge Prof. Rekha Gupta whose lectures during my undergraduate years steered my interest towards Biochemistry.

Finally, I would like to acknowledge the unbound love and support of my parents and my friends, which have made these years in graduate school meaningful and complete.

TABLE OF CONTENTS

ABBREVIATIONS

AAK	amino acid kinase
ATP	adenosine-5'-triphosphate
BIAM	N-(Biotinoyl)-N'-(iodoacetyl)ethylenediamine
CoQ_1	ubiquinone-1
DCPIP	2,6-dichlorophenolindophenol
DMSO	dimethyl sulfoxide
DrP5CDH	*Deinococcus radiodurans* Δ^1-pyrroline-5-carboxylate dehydrogenase
EDTA	ethylenediaminetetraacetic acid
FAD	flavin adenine dinucleotide
γ-GP	γ-glutamyl phosphate
GK	γ-glutamyl kinase
GPR	γ-glutamyl phosphate reductase
GSA	γ-glutamic semialdehyde
HEPES	4-(2-Hydroxyethyl)piperazine-1- ethanesulfonic acid
IPTG	isopropyl β-D-1-thiogalactopyranoside
MES	2-(N-morpholino)ethanesulfonic acid
NAD^+	nicotinamide adenine dinucleotide
NADPH	nicotinamide adenine dinucleotide phosphate
o-AB	o-aminobenzaldehyde
P5C	Δ^1-pyrroline-5-carboxylate
P5CDH	Δ^1-pyrroline-5-carboxylate dehydrogenase
P5CR	pyrroline-5-carboxylate reductase
P5CS	pyrroline-5-carboxylate synthase
PIPES	piperzaine-N,N'-bis(2-ethanesulfonic acid)
POX	proline oxidase
PRODH	proline dehydrogenase
Put1p	*Saccharomyces cerevisiae* PRODH
Put2p	*Saccharomyces cerevisiae* P5CDH
PutA	proline utilization A

put	proline utilization
SA	Streptavidin
SDS-PAGE	sodium dodecyl sulfate polyacrylamide gel electrophoresis
TAPS	N-[Tris(hydroxymethyl)methyl]-3-aminopropanesulfonic acid
THFA	tetrahydro-2-furoic acid
TtP5CDH	*Thermus thermophilus* Δ^1-pyrroline-5-carboxylate dehydrogenase
TtPRODH	*Thermus thermophilus* proline dehydrogenase

CHAPTER 1

Introduction: Substrate channeling in proline metabolism

Note: This chapter has been published as a review article: “Substrate channeling in proline metabolism.” Arentson BW, Sanyal N, Becker DF. Front Biosci. 2012 Jan 1;17:375-88. Permission for usage in thesis obtained from Frontiers of Bioscience.

INTRODUCTION

It is well known that proline metabolism has important roles in carbon and nitrogen flux and protein synthesis. Proline metabolism has also emerged as a relevant pathway in other processes such as cell signaling, cellular redox balance, and apoptosis [1-3]. Proline homeostasis is important in human disease, where inborn errors in proline metabolism are thought to lead to neurological dysfunctions such as schizophrenia and febrile seizures, as well as errors in systemic ammonia detoxification and developmental disorders such as skin hyperelasticity [4-7]. Recently it was shown that mutations that disrupt proline biosynthesis are linked with progeroid features and osteopenia that are part of the autosomal recessive cutis laxa syndrome [8]. In bacteria and plants, proline metabolism is responsive to various environmental stresses such as drought, osmotic pressure, or ultraviolent irradiation leading to proline accumulation as a survival mechanism [9-11]. Overall proline has become a very important metabolite that is thought to be involved in many cellular processes.

Fundamental to understanding the roles of proline metabolism in various processes is knowledge of the relevant enzymes and mechanisms used to maintain proper proline homeostasis. In this review, the unique aspect of substrate channeling in proline metabolism will be explored. Insights into the channeling mechanisms of enzymes responsible for the catabolism and biosynthesis of proline are helping to reveal the many roles of proline within the cell. Here we review the structural and kinetic data that support substrate channeling of P5C/GSA and gamma–glutamyl phosphate in the proline catabolic and biosynthetic pathways, respectively. The data indicate that both intermediates are channeled which increases the efficiency of proline metabolic flux.

PROLINE METABOLIC ENZYMES

Proline catabolism

The catabolic and anabolic reactions of proline metabolism are shown in Figure 1. The catabolic pathway generates glutamate from the four electron oxidation of proline, which occurs in two catalytic steps [12]. In the first step, proline dehydrogenase (PRODH; EC 1.5.99.8) uses a flavin adenine dinucleotide (FAD) cofactor as an electron acceptor to remove two electrons from proline, rendering the intermediate Δ^1-pyrroline-5-carboxylate (P5C). P5C then undergoes a non-enzymatic hydrolysis, which opens the ring structure and generates γ-glutamate semialdehyde (GSA). Pyrroline-5-carboxylate dehydrogenase (P5CDH; EC 1.5.1.12) next pulls off two additional electrons from GSA using nicotinamide adenine dinucleotide (NAD^+) to complete the conversion of proline to glutamate [12].

The PRODH and P5CDH enzymes involved in the oxidation of proline are highly conserved in both eukaryotes and prokaryotes, but differ in whether they are fused into a bifunctional enzyme called proline utilization A (PutA). As reviewed by Tanner, PRODH enzymes can be divided into three branches [13]. One branch consists of monofunctional enzymes, where the PRODH and P5CDH domains are found as separate enzymes. The other two branches have the PRODH and P5CDH domains on a single PutA polypeptide [13]. Originally it was thought that all prokaryotes contain bifunctional PutAs, and that all eukaryotes contain monofunctional enzymes. However, it is now known that Gram-positive bacteria contain monofunctional enzymes, thus limiting PutAs to Gram-negative bacteria [14].

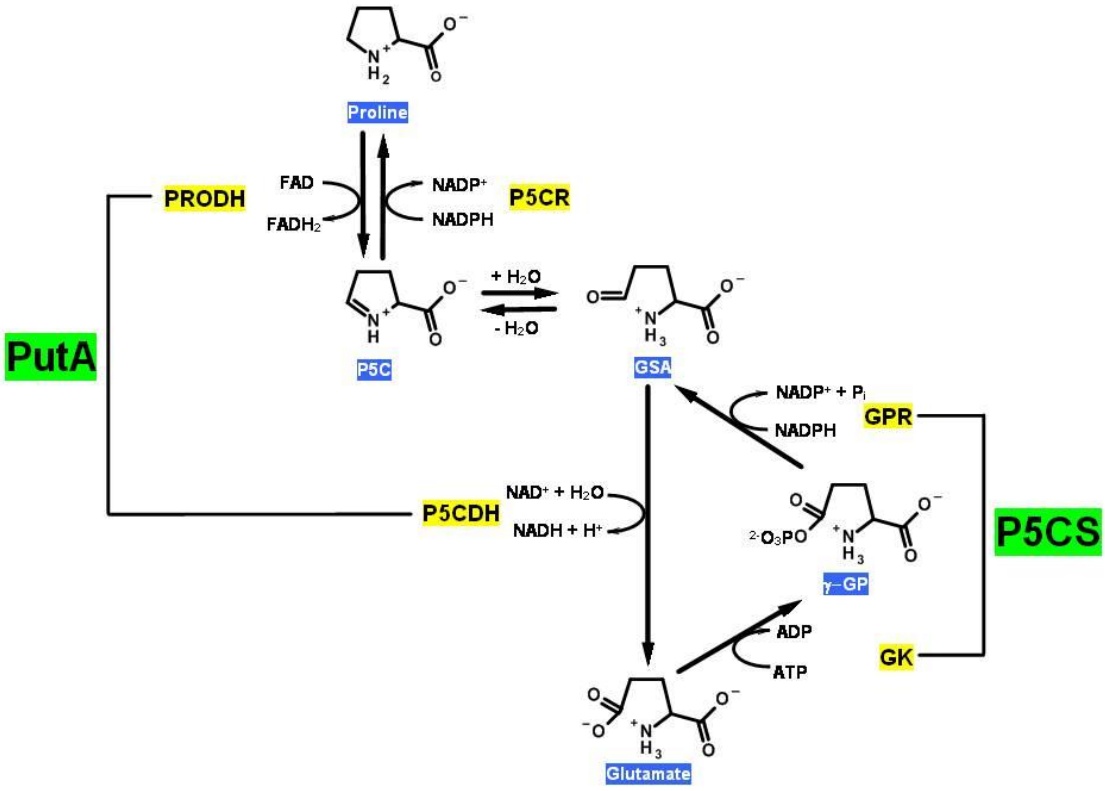

Figure 1- Reactions of the proline metabolic pathway. In the catabolic pathway, proline is converted to glutamate via a four electron oxidation process. Proline dehydrogenase (PRODH) performs the first oxidative step, resulting in the intermediate pyrroline-5-carboxylate (P5C). P5C is subsequently hydrolyzed to glutamic semialdehyde (GSA), which is then further oxidized by P5C dehydrogenase (P5CDH) to generate glutamate. In Gram-negative bacteria, PRODH and P5CDH are fused together on a bifunctional enzyme called proline utilization A (PutA). Proline anabolism begins with phosphorylation of glutamate by γ-glutamyl kinase (GK) to generate γ-glutamyl phosphate (gamma-GP). gamma-GP is reduced by γ-glutamyl phosphate reductase (GPR) to GSA , which cyclizes to form P5C. P5C is then reduced to proline via pyrroline-5-carboxylate reductase (P5CR). In higher eukaryotes such as plants and animals, GPR and GK are fused together in the bifunctional enzyme pyrroline-5-carboxylate synthase (P5CS).

Figure 2 summarizes the domain organization of PRODH and P5CDH enzymes. Monofunctional PRODHs typically are 200-540 amino acid residues in length, while monofunctional P5CDHs are composed of 400-600 residues. *Thermus thermophilus* PRODH and P5CDH are currently the only structures of monofunctional enzymes that have been solved (PDB IDs: 2G37, 2EKG, 2BHP, 2BJA) [14-16]. PutAs consist of 1000-1350 residues with the P5CDH domain linked to the C-terminal end of the PRODH domain [13]. The two branches of PutA enzymes are distinguished by whether or not PutA also contains an N-terminal ribbon-helix-helix (RHH) DNA binding domain. PutAs that contain a DNA binding domain are trifunctional and are generally longer polypeptides than PutAs that lack a DNA binding domain [17-19].

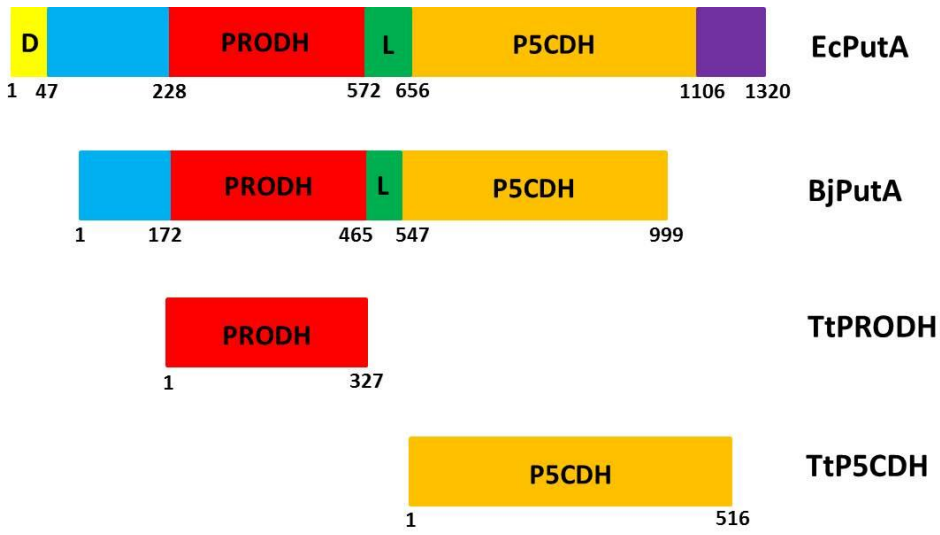

Figure 2- Domain mapping of PRODH and P5CDH from *E. coli* (EcPutA), *B. japonicum* (BjPutA), and *T. thermophilus.* In PutAs, the PRODH and P5CDH domains are connected by a linker region (**L**). Trifunctional PutAs such as EcPutA also have a DNA binding domain (**D**). TtPRODH and TtP5CDH are separate enzymes (monofunctional) in the Gram-positive bacteria, *T. thermophilus*.

Trifunctional PutAs act as transcriptional repressors—when cellular proline is scarce, PutA binds DNA and represses expression of the *putA* and *putP* (Na^+/proline transporter) genes [20, 21]. Regulation of PutA is achieved through a functional switching mechanism, where the redox state of flavin determines whether PutA is bound to the DNA and acts as a transcriptional repressor or is peripherally bound to the membrane where it efficiently catabolizes proline [22].

Recently, the first crystal structure of a complete PutA protein (*Bradyrhizobium japonicum*) was solved by Tanner's group (PDB ID: 3HAZ). Previously, the only structures available for PutA were of the isolated PRODH and DNA binding domains. The PRODH domain structure was solved for PutA from *Escherichia coli* (PDB IDs: 1K87, 1TJ2, ITIW, 1TJ0, 3ITG) [23-26], and the DNA binding domain of PutA was solved by solution NMR (*Pseudomonas putida*) and X-ray diffraction (*E. coli*) (PDB IDs: 2JXG, 2GPE, 2RBF) [27-29]. These structures show that the PRODH domain is a conserved $\beta_8\alpha_8$-barrel, while the P5CDH domain contains a well conserved Rossmann fold domain. The evolutionary divergence from bifunctional PutA to monofunctional PRODH and P5CDH is of interest due to substrate channeling between the active sites in bifunctional PutA. Substrate channeling between monofunctional enzymes would necessitate functional PRODH-P5CDH interactions, which have not yet been explored and are the focus of Chapter 2 in this thesis.

Proline biosynthesis

Proline biosynthesis from glutamate involves three enzymatic steps (Figure 1). The initial two steps are catalyzed by γ-glutamyl kinase (GK; EC 2.7.2.11) and γ-glutamyl phosphate reductase (GPR; EC 1.2.1.41). GK uses adenosine-5'-triphosphate

(ATP) to generate γ-glutamyl phosphate, which is subsequently reduced by GPR using nicotinamide adenine dinucleotide phosphate (NADPH) to produce GSA [12]. GSA next cyclizes to P5C, which is a crossroads intermediate that, in principle, can be converted not only to proline, but also to ornithine or back to glutamate via P5CDH [12]. The reduction of P5C to proline is catalyzed by P5C reductase (P5CR; EC 1.5.1.2), while the production of ornithine from P5C requires ornithine aminotransferase (OAT; EC 2.6.1.13), an enzyme that is important for balancing cellular nitrogen levels [12].

In bacteria and lower eukaryotes such as yeast, GK and GPR are discrete monofunctional enzymes. In animals and plants, the GK and GPR domains are fused together into the bifunctional enzyme P5C synthase (P5CS) (Figure 3). The GK and GPR domains are well conserved in lower eukaryotes and bacteria. The GK domain is normally between 250-450 residues in length with an N-terminal amino acid kinase (AAK) domain. In bacteria, GK contains a C-terminal pseudo uridine synthase and archaeosine-specific transglycosylase (PUA) domain, which has no known function [30]. It has been suggested, however, that the PUA domain may enable bacterial GK to have a gene regulatory role [31]. The structures of GK enzymes from *E. coli* and *Campylobacter jejuni* have been solved (PDB IDs: 2J5T, 2AKO) [32]. *E. coli* GK is composed of an N-terminal catalytic domain made up of eight nearly parallel β-sheets sandwiched by two layers of three and four α-helices. It is connected by a linker region to the PUA domain, which contains a distinctive β sandwich [32].

GPR typically contains 400-500 residues and consists of an N-terminal Rossmann fold domain for NADPH binding, a catalytic domain, and an oligomerization domain at the C-terminus [33]. The X-ray crystal structure of GPR from *Thermotoga maritima*

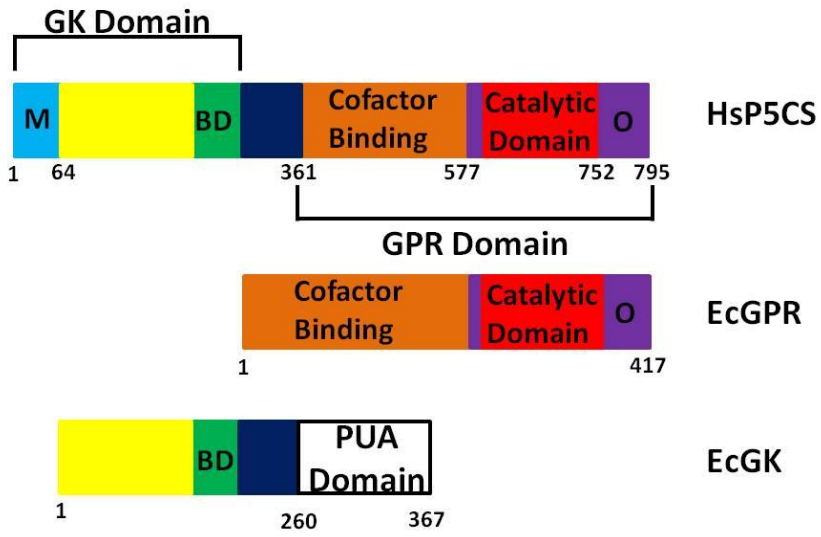

Figure 3- Domain mapping of monofunctional γ-glutamyl phosphate reductase (EcGPR) and γ-glutamyl kinase (EcGK) enzymes from *E. coli* and bifunctional pyrroline-5-carboxylate synthase (P5CS) from *Homo sapiens*. M, putative mitochondrial signaling peptide, **BD**, binding domain for glutamate and ATP, **O,** oligomerization domain, and **PUA**, pseudo uridine synthase and archaeosine-specific transglycosylase domain with no known function in EcGK.

reveals that the catalytic domain has an α/β architecture with a five-stranded parallel β-sheet (PDB ID: 1O20) [33]. To date, no complete structure of bifunctional P5CS has been reported. However, the structure of the isolated GPR domain (PDB ID: 2H5G; unpublished) from human P5CS is available. The last enzyme of the proline biosynthetic pathway, P5CR, ranges from 400-500 residues in length and has a conserved N-terminal Rossmann fold for NADPH binding. Several crystal structures of P5CR have been determined including the human form (PDB ID: 2GRA) [34]. Human P5CR has an active site cleft made of an 8-stranded β-sheet sandwiched by α-helices on either side and oligomerizes to form a decameric structure of dimers [34].

INTERMEDIATES OF PROLINE METABOLISM

The P5C/GSA and γ–glutamyl phosphate intermediates of proline metabolism are appreciably labile and reactive. Figure 4 shows examples of undesirable fates that can occur with these intermediates. The instability of the intermediates implies substrate channeling may be important for maintaining efficient proline metabolic flux. The intermediate shared by the catabolic and biosynthetic pathways, P5C/GSA, has been shown to inhibit other enzymes, react with metabolites, and act as a signaling molecule. GSA has been reported to inhibit glucosamine-6-phosphate synthase from *E. coli*, cytidine 5'-triphosphate synthase, and the amidotransferase domain of carbamoyl phosphate synthetase [35-37]. Additionally, P5C forms adducts with other metabolites such as pyruvic acid, oxaloacetic acid, and acetoacetic acid [38]. P5C can also react with pyridoxal phosphate in patients with type II hyperprolinemia.

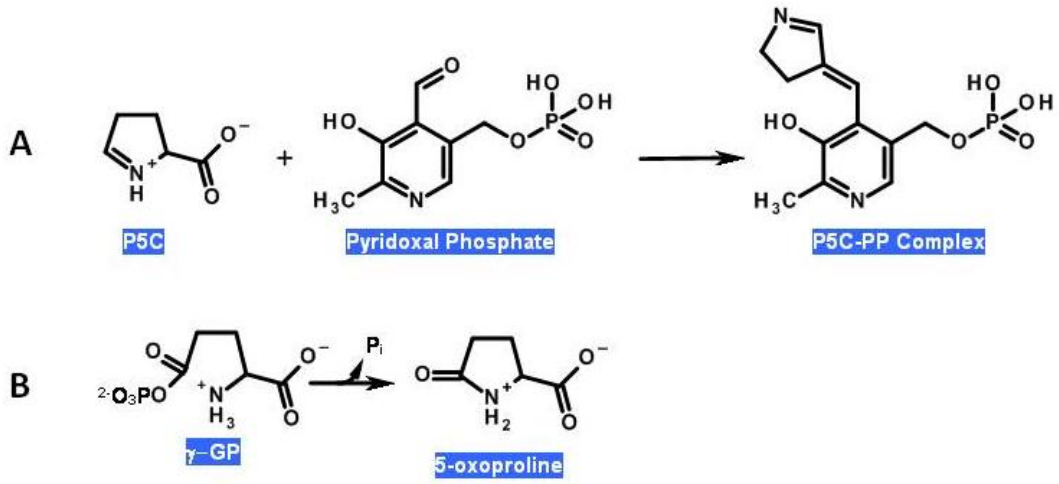

Figure 4- Side reactions of intermediates pyrroline-5-carboxylate (P5C) and γ-glutamyl phosphate (γ-GP). (A) P5C can deactivate pyridoxal phosphate by forming an adduct, resulting in vitamin B6 deficiency in individuals with hyperprolinemia type II. (B) γ-GP can cyclize and dephosphorylate to form 5-oxoproline, which is suggested to be a neurotoxin in rats.

Type II hyperprolinemia is characterized by elevated plasma levels of P5C/GSA due to deficient P5CDH activity [39]. The high levels of P5C/GSA generates inactive adducts with pyridoxal phosphate, leading to lower amounts of functional vitamin B6 in patients (Figure 4) [38]. P5C also acts as a signaling molecule in eukaryotes and is thought to induce apoptosis by increasing intracellular reactive oxygen species [40, 41]. Altogether, it seems that controlling levels of free P5C/GSA would be beneficial.

The reactive intermediate in proline biosynthesis is γ–glutamyl-phosphate. The carbonyl phosphate group is susceptible to nucleophilic attack, resulting in the spontaneous cyclization of γ–glutamyl-phosphate into 5-oxoproline as shown in Figure 4 [42, 43]. It has been suggested that 5-oxoproline is a neurotoxin. Interstitial injection of 5-oxoproline into rats produces behavioral and neuropathological effects that resemble Huntington's disease [44, 45]. The instability of γ–glutamyl phosphate seems to necessitate its channeling between GK and GPR during proline biosynthesis.

OVERVIEW OF SUBSTRATE CHANNELING

Rationale for substrate channeling

Substrate channeling is a phenomenon where the product of one reaction is transported to a second active site without equilibrating into bulk solvent [46]. Three mechanisms of substrate channeling have been defined, two of which are reviewed by Miles *et al.* [47]. The most common form of substrate channeling occurs when a cavity exists within a protein that sequesters the intermediate from solvent, allowing for a means of travel between active sites [47]. To date, several enzymes are known to utilize these intramolecular tunnels, with the classic example being tryptophan synthase [48]. The

second form of channeling does not use intramolecular cavities; rather, electrostatic residues on the surface of the enzyme guide the intermediate from the first active site to the second active site [47]. Dihydrofolate reductase-thymidylate synthase complex stands as the common example for this form of channeling [49]. A third form of channeling exists in protein complexes such as pyruvate dehydrogenase, which uses cofactor lipoic acid to transfer substrate to multiple active sites using a swinging arm [50].

Substrate channeling has been proposed to be advantageous in the cellular environment for several reasons, as outlined by Ovadi and others [46, 51]. First and foremost it increases the efficiency of coupled reactions both by preventing the loss of intermediates to diffusion and by decreasing transit time between active sites. This allows the steady-state flux through the coupled steps to be attained more rapidly [46]. Secondly, it prevents labile intermediates from decaying and reacting with other metabolites or enzymes within the cell [46]. Third, channeling segregates intermediates that may require a specific environment (e.g., pH) to retain structure or reactivity. Channels can provide an environment that facilitates an equilibrium step that normally would be unfavorable in the bulk solution. Finally, channeling limits intermediates from being siphoned out into competing reactions or pathways [46].

All of the benefits listed above are not necessarily relevant for every channeling system. In the proline catabolic pathway, channeling of P5C/GSA may be most critical for making the hydrolysis of P5C to GSA more favorable at physiological pH values. The P5C/GSA equilibrium is highly pH dependent [35]. GSA is favored only below pH 6.5 due to protonation of the pyrrolinium ring, which facilitates the hydrolysis of P5C to

GSA. Thus, one benefit of channeling between PRODH and P5CDH would be to increase the pK_a of the pyrrolinium species above pH 6.6, making the hydrolysis of P5C to GSA more favorable at physiological pH conditions. If we only consider the P5C/GSA hydrolysis step, substrate channeling is likely more critical for the proline catabolic pathway than for proline biosynthesis, since P5C formation is favored at physiological pH. In the proline biosynthetic pathway, protecting the highly labile γ–glutamyl phosphate would be a clear benefit of substrate channeling between GK and GPR.

KINETIC APPROACHES TO TEST FOR SUBSTRATE CHANNELING

Different strategies have been devised to examine whether channeling occurs between enzymes. Before reviewing the evidence for substrate channeling in proline metabolism, a short description of various experimental methods is described here.

Transient time estimation

A common strategy to test for channeling is to evaluate whether there is a lag time in reaching steady-state formation of the final product in a coupled assay. Figure 5 shows substrate (S) being converted to the final product (P) via the coupled action of two enzymes (E1 and E2). The lag time or transient time, Tau, is the time preceding the build-up to steady-state formation of the final product using the substrate of the first enzyme [52]. If no channeling occurs, Tau should be equal to the ratio of K_m/V_{max} of the second enzyme. If the observed lag time is shorter than the K_m/V_{max} ratio, then it infers that the intermediate is transferred between the enzymes, E1 and E2. The extent of the observed lag time may vary among different channeling systems with a shorter transient time being interpreted as more efficient transfer or channeling [53]. Along with steady-state assays,

pre-steady state measurements can also be made to evaluate the lag time prior to product formation.

Trapping the intermediate

The effect of a reagent that specifically traps the intermediate species (I, Figure 5) on the kinetics of product formation can also be used to evaluate channeling. For example, *o*-aminobenzaldehyde (*o*-AB) which reacts with P5C to form a yellow complex can be used as a trapping agent for the PRODH and P5CDH coupled reaction. *o*-AB would be anticipated to decrease the overall rate of glutamate formation if no channeling occurs, while in a channeling system *o*-AB would have a negligible effect on the reaction kinetics. Using a third enzyme that competes with E2 for the intermediate can also be an effective strategy to test for substrate channeling.

Inactive mutants

Another useful tool is to generate active site mutants of the two enzymes being studied (Figure 5B). In the case of suspected channeling partners, an active site mutant (e.g., E2) would be expected to compete with its native counterpart for interaction with the cognate enzyme (E1). If channeling occurs, adding the inactive E2 mutant in amounts excess to that of native E2 would decrease product formation. If no channeling occurs, adding the inactive E2 mutant to the coupled enzyme assay would have no effect on the rate of product formation. This strategy was effectively used to rule out channeling between aspartate aminotransferase (AAT) and malate dehydrogenase (MDH) [54].

If the channeling involves two enzyme active sites that are covalently linked, active site mutants can be used to generate a non-channeling control. Figure 5C illustrates that combining active site mutants of E1 and E2 creates a mixture of monofunctional

enzyme variants that can only generate product via a diffusion mechanism. The transient times of the native enzyme and the mixed enzyme variants can then be compared to distinguish between channeling and non-channeling mechanisms. This strategy was used recently to demonstrate channeling in bifunctional PutA [23].

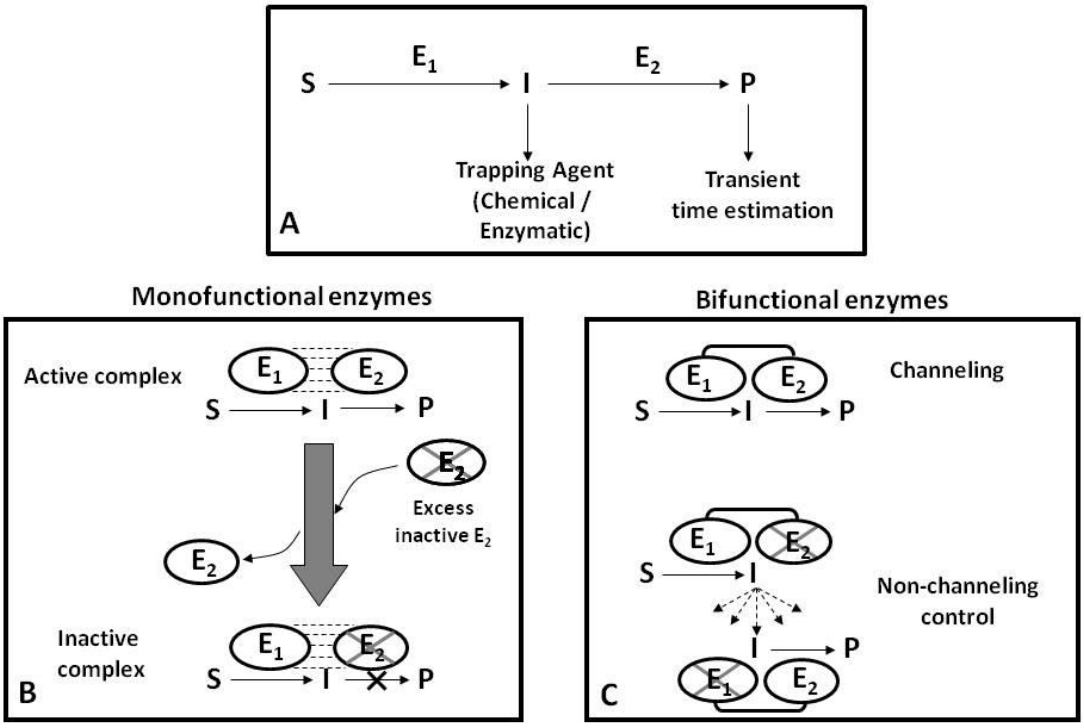

Figure 5- Strategies for examining substrate channeling. (A) Transient time analysis of a coupled reaction involving two enzymes, E1 and E2, which convert substrate A into product C. A trapping agent can also be used to test whether intermediate B is released into bulk solvent during the reaction. (B) Inactivation of one of the enzyme pairs by site-directed mutagenesis. If channeling occurs, adding inactive E2 would disrupt the active E1-E2 complex resulting in lower steady-state activity. (C) Testing channeling in bifunctional enzymes. Inactivation of the individual domains results in monofunctional variants that can only catalyze the coupled reaction via a diffusion mechanism. The mixture of monofunctional variants is thus a non-channeling control.

Designing fusion proteins

Two active sites that are in close proximity can sometimes exhibit kinetic behavior that resembles direct channeling [55]. One strategy for distinguishing between active channeling and proximity effects is to change the relative orientation of two active sites, which is important for interacting enzymes [56]. A polypeptide linker can be engineered to covalently link the two enzymes with various degrees of flexibility and in different orientations [55]. If the enzymes are truly channeling, changes in the orientation of the active sites will have a dramatic effect on the kinetics of production formation.

CHANNELING OF P5C/GSA

The oxidation of proline to glutamate is catalyzed in consecutive reactions by PRODH and P5CDH (Figure 1). Avoiding release of P5C/GSA into bulk solvent during proline oxidation may be beneficial due to the chemical properties of P5C/GSA as discussed in the previous section. Evidence for channeling P5C/GSA has recently been shown for bifunctional PutA from *B. japonicum* (BjPutA). Srivastava *et al* reported a 2.1 Å resolution crystal structure of BjPutA (999-residue polypeptide) that reveals an interior channel connecting the PRODH and P5CDH active sites (PDB ID: 3HAZ) [23]. Figure 6 shows a structural model of BjPutA, which purifies as a homodimer. Both PRODH and P5CDH domains contribute to the formation of the channel, with the two active sites separated by a distance of 41 Å. The connecting channel appears to start at the *si* face of the isoalloxazine ring of FAD and end at the catalytic cysteine (Cys792) of the P5CDH domain (Figure 6). Within the channel, the central cavity is lined by fifteen basic residues

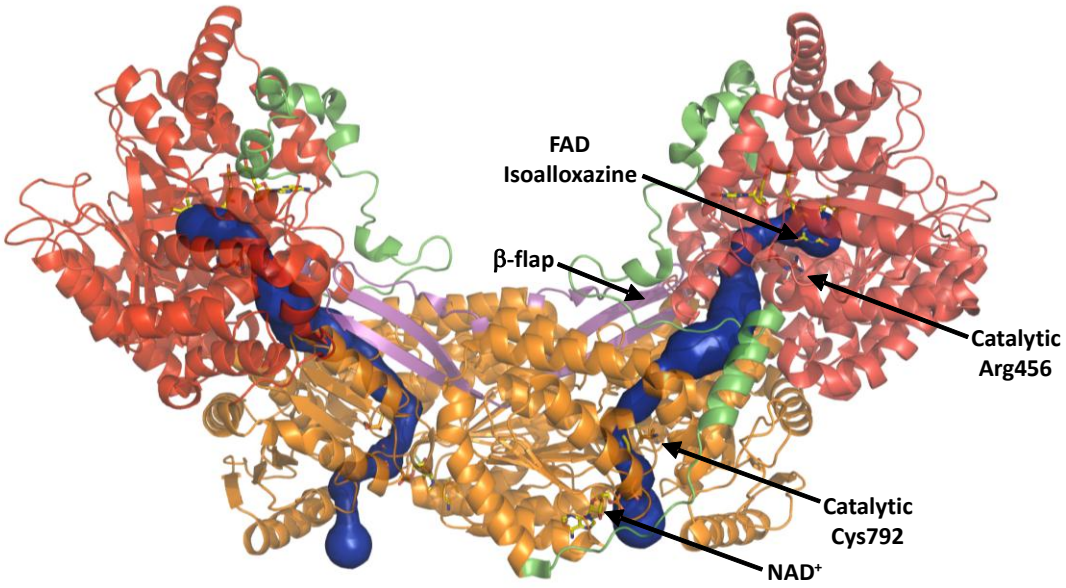

Figure 6- Structure of dimeric BjPutA shown in ribbon representation. The PRODH domain (red) and the P5CDH domain (orange) of each protomer are connected by a linker region (green). Active site residues (Arg456, Cys792), FAD and NAD^+ are displayed as sticks. β-flap of each protomer is colored as magenta. The substrate channel of each BjPutA protomer is shown as blue surface. This model was made using PyMol [57] and PDB ID: 3HAZ.

(Lys and Arg) and seventeen acidic residues (Glu and Asp), imparting a hydrophilic nature to the channel. Each of the PutA protomers has an individual channel connecting PRODH and P5CDH active sites.

Interestingly, the dimeric structure of BjPutA seems to be critical for sealing the channel and minimizing access to bulk solvent. A beta-flap protrudes from the P5CDH domain (β strands, residues 628-646, 977-989) from one protomer and forms intermolecular interactions with the P5CDH domain of the second protomer (Figure 6). This β-flap is structurally conserved in *Thermus thermophilus* P5CDH (PDB ID 1UZB, residues 163-174,506-516) as well as a class I aldehyde dehydrogenase isolated from

sheep liver (PDB ID: 1BXS, residues 147-159, 486-498) [58] [16]. Thus, in BjPutA, the β-flap not only helps stabilize dimer formation but is also important for sealing the central cavity.

Along with these structural features of channeling, kinetic evidence for channeling was also reported for BjPutA by Srivastava *et al*. Different experiments have provided strong evidence for channeling. First, the amount of P5C released into bulk solvent was estimated using *o*-aminobenzaldehyde (*o*-AB) as a trapping agent. P5C and *o*-AB react to form a yellow complex that can be monitored at 443 nm [59]. In the absence of NAD^+, the P5CDH domain is inactive and leads to significant release of P5C into the bulk solvent, as detected by the yellow complex formation. In the presence of NAD^+, however, the P5CDH domain is active, resulting in significantly lower *o*-AB-P5C complex formation, as the majority of P5C is converted into glutamate [23]. The apparent fraction of P5C that is channeled in BjPutA from PRODH to P5CDH was estimated to be 0.7 by these measurements.

Substrate channeling in BjPutA was also examined by estimating the transient time to reach steady-state turnover of the second enzyme, P5CDH, using proline as a substrate [23, 60, 61]. With native BjPutA, steady-state formation of NADH (product of the P5CDH reaction) occurred without any apparent lag time [23]. The absence of a lag time in the approach to steady-state indicates substrate channeling. A non-channeling control was also analyzed using active site mutants of BjPutA that lack PRODH (R456M) and P5CDH (C792A) activity [23]. The R456M mutation inactivates PRODH but does not impair P5CDH activity, whereas the C792A mutation inactivates P5CDH but does not impair PRODH activity. The mixture of these monofunctional variants was

used as a non-channeling control as described above. In this non-channeling control, P5C formed by the C792A variant must diffuse out into bulk solvent and bind to the R456M variant before NADH is formed. In the assays with the non-channeling variants, a lag time of about seven minutes for NADH formation was observed [23]. The observed lag time was similar to the theoretical Tau value calculated from the independent PRODH activity and P5CDH kinetic parameters. An example of these steady-state assays is shown in Figure 7. Figure 7 illustrates the clear difference in the kinetic behavior of native BjPutA and the non-channeling control. With native BjPutA, NADH formation is observed without a lag time, while with the mixed variants a lag time of around 6.5 minutes is observed. The results from these assays are consistent with a substrate channeling mechanism in BjPutA. Kinetic profiles of native BjPutA and the mixed variants were also compared by rapid-reaction kinetics under anaerobic, single-turnover conditions. Rapid mixing of native BjPutA and proline generated NADH with no apparent lag time. For the non-channeling variants, a 10 s lag time for NADH formation was observed after mixing the enzymes with proline. These results show native BjPutA efficiently channels P5C/GSA.

Evidence for channeling in PutA has also been reported from *Salmonella typhimurium* PutA (StPutA). Similar to EcPutA, StPutA contains the N-terminal DNA binding domain and is thus trifunctional. Maloy *et al* demonstrated that the P5CDH domain shows a 14-fold greater steady-state production of NADH using P5C generated endogenously from proline by PRODH, as compared to exogenously added P5C [63]. In addition, they showed exogenous P5C was unable to compete against endogenous P5C.

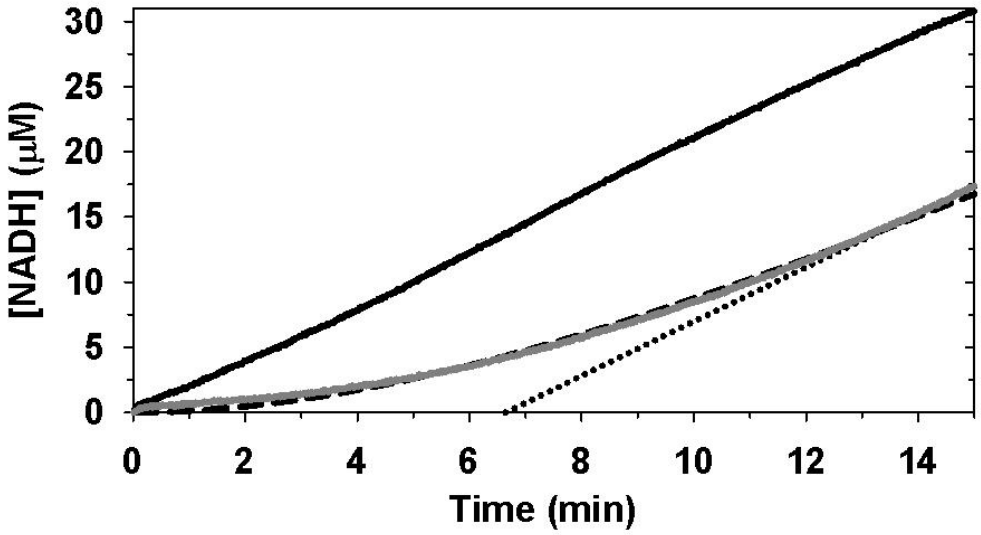

Figure 7- Example of transient time analysis of BjPutA. Steady-state formation of NADH using proline as a substrate by native BjPutA (solid black curve) and an equimolar mixture of monofunctional variants R456M and C792A (solid grey curve). The mixture of the monofunctional variants serves as a non-channeling control. The dotted line represents the extrapolation used for estimating the lag-time. Native BjPutA shows no apparent lag in NADH formation, while a lag time of about 6.5 min is observed for the non-channeling control. The dashed line overlaying the grey curve of the non-channeling control reaction was simulated using the kinetic parameters of PRODH and P5CDH as described previously and the following equation: $[NADH] = v_1 t + (v_1/v_2)K_m(e^{-v2t/Km} - 1)$ [62]. Assays were performed at pH 7.5.

Despite two-fold excess of exogenous P5C, 86 % of glutamate was produced from endogenous P5C. Due to a lack of structural information on trifunctional PutAs, it is not clear whether a channel similar to that characterized in BjPutA exists. Future structural and kinetic experiments will need to be performed to fully address the channeling mechanism in trifunctional PutAs.

CHANNELING OF GAMMA-GLUTAMYL PHOSPHATE

As mentioned previously, channeling of the intermediate γ-glutamyl phosphate would be beneficial because of its instability. Channeling of γ-glutamyl phosphate is also

implicated by the fusion of GK and GPR in bifunctional P5CS. Kinetically speaking, data has existed for over forty years suggesting that a complex forms between bacterial GK and GPR in order to conceal γ-glutamyl-phosphate from solvent [64, 65]. A typical assay to measure GK activity is to add hydroxylamine along with the substrates, glutamate and ATP. Hydroxylamine reacts with the product γ-glutamyl phosphate to make γ-glutamyl hydroxamate, which can be measured at 535 nm [64]. Multiple groups have documented that GK activity is dependent on the presence of GPR. GK is inactive or exhibits very low activity in the absence of GPR, suggesting GPR is required for GK activity [42, 43, 64, 66, 67]. It was found that a 10:1 GPR:GK ratio was necessary to obtain maximal GK activity, indicating that a GK/GPR complex forms with excess GPR [66]. To test for a complex, Smith *et al.* tried incubating different ratios of bacterial GK and GPR, then looked for co-elution of the enzymes by chromatography [66]. Both proteins eluted separately meaning either a complex does not form or complex formation is transient and is dependent on substrate binding. Other work suggesting a GK-GPR complex includes assays which contained GK and GPR, but lacked NADPH, the cofactor necessary for GPR activity [43]. In this case the GPR enzyme was inactive, but it still activated GK. GK has also been shown to be activated by incubation with GPR mutants, further demonstrating that GK activation by GPR does not require GPR activity [68]. Other experiments that have explored GK/GPR interactions include Chen *et al*, who created a mutant GK/GPR fusion protein that was able to over-produce proline, making the host *E. coli* strain more resistant to osmotic stress [69]. While this work does not support channeling directly, it does show that enhancing the proximity of two active sites can significantly increase the efficiency of a metabolic pathway [69].

Structural data supporting channeling is not directly available for GK and GPR enzymes [70]. Figure 8 shows the individual structures of *E. coli* GK (EcGK) and *T. maritima* GPR (TtGPR). Marco-Marin *et al* modeled a possible interaction between monofunctional GK and GPR, showing GPR in both an open and closed conformation, depending on the binding status of the substrate [32]. The model shows a tetrameric form

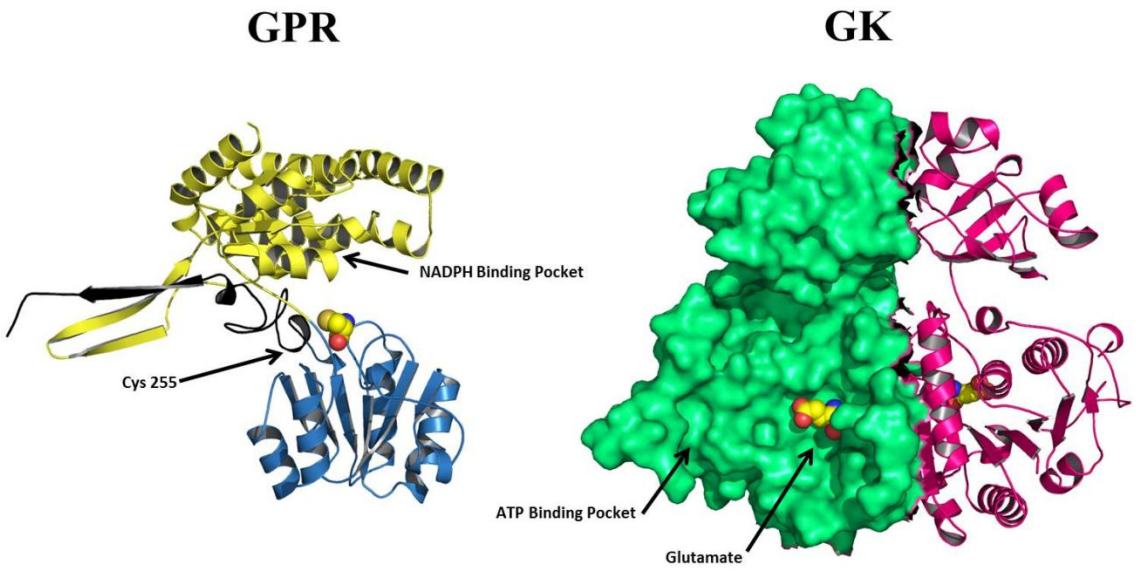

Figure 8- Structures of GPR from *T. maritima* (TmGPR) and GK from *E. coli* (EcGK). EcGK is shown as a dimer with one monomer shown in surface representation and the other monomer as a ribbon cartoon illustration. Glutamate is shown as spheres in the substrate binding pocket, which is solvent accessible. Only one monomer of GPR (open conformation) is shown, which contains three domains: NADPH binding domain (yellow), catalytic domain (blue) with the catalytic cysteine shown in spheres, and the oligomerization domain (black). The solvent-exposed glutamate binding pocket of GK suggests that the γ-glutamyl phosphate intermediate would be accessible to GPR in a potential GK-GPR complex. A GK-GPR complex in which the catalytic domain of GPR is aligned with the glutamate binding pocket of GK has been proposed and modeled by Marco-Marin *et al* [32]. Models shown here were made using PyMol [57] and PDB IDs: 2J5T (EcGK) and 1O20 (TmGPR).

of GK from *E. coli* complexed with a dimer of GPR from T. maritime [32]. In solving the crystal structure EcGK, Marco-Marin et al. noted that GK was well suited for channeling [32]. They suggested that channeling is possible if the GK and GPR active sites are positioned so that the active site cysteine of GPR is able to react with γ-glutamyl phosphate while still bound at the GK active site. A complex as described would allow for a favorable environment and timely transfer of γ-glutamyl-phosphate to the second active site thereby preventing cyclization to 5-oxoproline [32]. Additionally it has been suggested that leucine zipper motifs found in the GK and GPR domains of plants, as well as the GK and GPR enzymes of some bacteria are evidence for a functional complex [71]. The leucine zipper of plant P5CS may help with oligomerization or it may be an artifact of evolution. Several domain swapping experiments have shown that leucine zippers mediate protein-protein dimerization in eukaryotic and prokaryotic enzymes. Thus, the leucine zippers in bacterial GK and GPR enzymes and plant P5CS may support a possible channeling complex [72].

SUMMARY

Proline metabolism has become a very important area of study due to its involvement in many different cellular processes from maintaining redox balance to countering environmental stress. As described in this review, substrate channeling is a relevant mechanism in proline metabolism for translocating important intermediates between active sites. Rational for substrate channeling in proline metabolism is two-fold. First, the equilibrium for the hydrolysis of P5C to GSA is unfavorable at physiological pH indicating channeling may be necessary to increase the overall conversion efficiency of proline into glutamate. Second, P5C/GSA and γ-glutamyl-phosphate are reactive and

labile intermediates. Channeling of these intermediates would protect against the formation of unwanted products, such as 5-oxoproline from γ-glutamyl-phosphate.

Future kinetic and structural studies are important for understanding the mechanisms of substrate channeling in proline metabolism. In proline catabolism, BjPutA provides structural and kinetic data supporting channeling, but more work needs to be done on trifunctional and monofunctional enzymes. Substrate channeling in PutAs suggests that bacteria have evolved a strategy to limit the availability of P5C to other competing pathways. P5C is at the crossroads of important metabolic pathways, which include proline oxidation, urea cycle, TCA cycle via glutamate, and the proline biosynthetic pathway [73]. Substrate channeling by PutA may help maintain flux through the proline oxidative pathway, which would be especially important under poor nutrient conditions in cells starved for nitrogen and glutamate and other downstream products such as α–ketoglutarate. Whether P5C/GSA is channeled in Gram-positive bacteria and eukaryotes is not yet known. Studies of PRODH-P5CDH coupled kinetics and potential PRODH-P5CDH interactions are needed to address channeling between monofunctional PRODH and P5CDH enzymes. In proline biosynthesis, evidence for interactions between monofunctional GPR and GK has been reported, but structural evidence for channeling in bifunctional P5CS is currently not available. Although channeling interactions between GK and GPR seem likely and are supported by several studies, additional work is required to define the channeling pathway and mechanisms in proline biosynthesis. To date, a full-length structure of P5CS has not been reported. Solving a crystal structure of P5CS would be a significant step toward understanding channeling of γ-glutamyl phosphate. Not only would a complete structure of P5CS act as a template for modeling

the interaction between monofunctional GK and GPR, but it could also be used to identify cavities within the protein that may act as channels for transporting γ-glutamyl phosphate between active sites.

REFERENCES

1. Phang, J.M., W. Liu, and O. Zabirnyk, *Proline metabolism and microenvironmental stress.* Annu Rev Nutr, 2010. **30**: p. 441-63.
2. Donald, S.P., et al., *Proline oxidase, encoded by p53-induced gene-6, catalyzes the generation of proline-dependent reactive oxygen species.* Cancer Res, 2001. **61**(5): p. 1810-5.
3. Krishnan, N., M.B. Dickman, and D.F. Becker, *Proline modulates the intracellular redox environment and protects mammalian cells against oxidative stress.* Free Radic Biol Med, 2008. **44**(4): p. 671-81.
4. Chakravarti, A., *A compelling genetic hypothesis for a complex disease: PRODH2/DGCR6 variation leads to schizophrenia susceptibility.* Proc Natl Acad Sci U S A, 2002. **99**(8): p. 4755-6.
5. Baumgartner, M.R., et al., *Hyperammonemia with reduced ornithine, citrulline, arginine and proline: a new inborn error caused by a mutation in the gene encoding delta(1)-pyrroline-5-carboxylate synthase.* Hum Mol Genet, 2000. **9**(19): p. 2853-8.
6. Mitsubuchi, H., et al., *Inborn errors of proline metabolism.* J Nutr, 2008. **138**(10): p. 2016S-2020S.
7. Kamoun, P., B. Aral, and J.M. Saudubray, *[A new inherited metabolic disease: delta1-pyrroline 5-carboxylate synthetase deficiency]*. Bull Acad Natl Med, 1998. **182**(1): p. 131-7; discussion 138-9.
8. Reversade, B., et al., *Mutations in PYCR1 cause cutis laxa with progeroid features.* Nat Genet, 2009. **41**(9): p. 1016-21.
9. Wood, J.M., et al., *Osmosensing and osmoregulatory compatible solute accumulation by bacteria.* Comp Biochem Physiol A Mol Integr Physiol, 2001. **130**(3): p. 437-60.
10. Yoshiba, Y., et al., *Correlation between the induction of a gene for delta 1-pyrroline-5-carboxylate synthetase and the accumulation of proline in Arabidopsis thaliana under osmotic stress.* Plant J, 1995. **7**(5): p. 751-60.
11. Szabados, L. and A. Savoure, *Proline: a multifunctional amino acid.* Trends Plant Sci, 2010. **15**(2): p. 89-97.
12. Adams, E. and L. Frank, *Metabolism of proline and the hydroxyprolines.* Annu Rev Biochem, 1980. **49**: p. 1005-61.
13. Tanner, J.J., *Structural biology of proline catabolism.* Amino Acids, 2008. **35**(4): p. 719-30.
14. White, T.A., et al., *Structure and kinetics of monofunctional proline dehydrogenase from Thermus thermophilus.* J Biol Chem, 2007. **282**(19): p. 14316-27.
15. White, T.A., et al., *Structural basis for the inactivation of Thermus thermophilus proline dehydrogenase by N-propargylglycine.* Biochemistry, 2008. **47**(20): p. 5573-80.
16. Inagaki, E., et al., *Crystal structure of Thermus thermophilus Delta1-pyrroline-5-carboxylate dehydrogenase.* J Mol Biol, 2006. **362**(3): p. 490-501.

17. Becker, D.F. and E.A. Thomas, *Redox properties of the PutA protein from Escherichia coli and the influence of the flavin redox state on PutA-DNA interactions.* Biochemistry, 2001. **40**(15): p. 4714-21.
18. Vilchez, S., M. Manzanera, and J.L. Ramos, *Control of expression of divergent Pseudomonas putida put promoters for proline catabolism.* Appl Environ Microbiol, 2000. **66**(12): p. 5221-5.
19. Menzel, R. and J. Roth, *Regulation of the genes for proline utilization in Salmonella typhimurium: autogenous repression by the putA gene product.* J Mol Biol, 1981. **148**(1): p. 21-44.
20. Ostrovsky de Spicer, P., K. O'Brien, and S. Maloy, *Regulation of proline utilization in Salmonella typhimurium: a membrane-associated dehydrogenase binds DNA in vitro.* J Bacteriol, 1991. **173**(1): p. 211-9.
21. Brown, E.D. and J.M. Wood, *Redesigned purification yields a fully functional PutA protein dimer from Escherichia coli.* J Biol Chem, 1992. **267**(18): p. 13086-92.
22. Zhang, W., et al., *Redox-induced changes in flavin structure and roles of flavin N(5) and the ribityl 2'-OH group in regulating PutA--membrane binding.* Biochemistry, 2007. **46**(2): p. 483-91.
23. Srivastava, D., et al., *Crystal structure of the bifunctional proline utilization A flavoenzyme from Bradyrhizobium japonicum.* Proc Natl Acad Sci U S A, 2010. **107**(7): p. 2878-83.
24. Lee, Y.H., et al., *Structure of the proline dehydrogenase domain of the multifunctional PutA flavoprotein.* Nat Struct Biol, 2003. **10**(2): p. 109-14.
25. Zhang, M., et al., *Structures of the Escherichia coli PutA proline dehydrogenase domain in complex with competitive inhibitors.* Biochemistry, 2004. **43**(39): p. 12539-48.
26. Srivastava, D., et al., *The structure of the proline utilization a proline dehydrogenase domain inactivated by N-propargylglycine provides insight into conformational changes induced by substrate binding and flavin reduction.* Biochemistry, 2010. **49**(3): p. 560-9.
27. Halouska, S., et al., *Solution structure of the Pseudomonas putida protein PpPutA45 and its DNA complex.* Proteins, 2009. **75**(1): p. 12-27.
28. Larson, J.D., et al., *Crystal structures of the DNA-binding domain of Escherichia coli proline utilization A flavoprotein and analysis of the role of Lys9 in DNA recognition.* Protein Sci, 2006. **15**(11): p. 2630-41.
29. Zhou, Y., et al., *Structural basis of the transcriptional regulation of the proline utilization regulon by multifunctional PutA.* J Mol Biol, 2008. **381**(1): p. 174-88.
30. Perez-Arellano, I., V. Rubio, and J. Cervera, *Mapping active site residues in glutamate-5-kinase. The substrate glutamate and the feed-back inhibitor proline bind at overlapping sites.* FEBS Lett, 2006. **580**(26): p. 6247-53.
31. Perez-Arellano, I., J. Gallego, and J. Cervera, *The PUA domain - a structural and functional overview.* FEBS J, 2007. **274**(19): p. 4972-84.
32. Marco-Marin, C., et al., *A novel two-domain architecture within the amino acid kinase enzyme family revealed by the crystal structure of Escherichia coli glutamate 5-kinase.* J Mol Biol, 2007. **367**(5): p. 1431-46.

33. Page, R., et al., *Crystal structure of gamma-glutamyl phosphate reductase (TM0293) from Thermotoga maritima at 2.0 A resolution.* Proteins, 2004. **54**(1): p. 157-61.
34. Meng, Z., et al., *Crystal structure of human pyrroline-5-carboxylate reductase.* J Mol Biol, 2006. **359**(5): p. 1364-77.
35. Bearne, S.L. and R. Wolfenden, *Glutamate gamma-semialdehyde as a natural transition state analogue inhibitor of Escherichia coli glucosamine-6-phosphate synthase.* Biochemistry, 1995. **34**(36): p. 11515-20.
36. Bearne, S.L., O. Hekmat, and J.E. Macdonnell, *Inhibition of Escherichia coli CTP synthase by glutamate gamma-semialdehyde and the role of the allosteric effector GTP in glutamine hydrolysis.* Biochem J, 2001. **356**(Pt 1): p. 223-32.
37. Thoden, J.B., et al., *The small subunit of carbamoyl phosphate synthetase: snapshots along the reaction pathway.* Biochemistry, 1999. **38**(49): p. 16158-66.
38. Farrant, R.D., et al., *Pyridoxal phosphate de-activation by pyrroline-5-carboxylic acid. Increased risk of vitamin B6 deficiency and seizures in hyperprolinemia type II.* J Biol Chem, 2001. **276**(18): p. 15107-16.
39. Geraghty, M.T., et al., *Mutations in the Delta1-pyrroline 5-carboxylate dehydrogenase gene cause type II hyperprolinemia.* Hum Mol Genet, 1998. **7**(9): p. 1411-5.
40. Nomura, M. and H. Takagi, *Role of the yeast acetyltransferase Mpr1 in oxidative stress: regulation of oxygen reactive species caused by a toxic proline catabolism intermediate.* Proc Natl Acad Sci U S A, 2004. **101**(34): p. 12616-21.
41. Maxwell, S.A. and G.E. Davis, *Differential gene expression in p53-mediated apoptosis-resistant vs. apoptosis-sensitive tumor cell lines.* Proc Natl Acad Sci U S A, 2000. **97**(24): p. 13009-14.
42. Hayzer, D.J. and V. Moses, *The enzymes of proline biosynthesis in Escherichia coli. Their molecular weights and the problem of enzyme aggregation.* Biochem J, 1978. **173**(1): p. 219-28.
43. Seddon, A.P., K.Y. Zhao, and A. Meister, *Activation of glutamate by gamma-glutamate kinase: formation of gamma-cis-cycloglutamyl phosphate, an analog of gamma-glutamyl phosphate.* J Biol Chem, 1989. **264**(19): p. 11326-35.
44. Rieke, G.K., A.D. Scarfe, and J.F. Hunter, *L-pyroglutamate: an alternate neurotoxin for a rodent model of Huntington's disease.* Brain Res Bull, 1984. **13**(3): p. 443-56.
45. McGeer, E.G. and E. Singh, *Neurotoxic effects of endogenous materials: quinolinic acid, L-pyroglutamic acid, and thyroid releasing hormone (TRH).* Exp Neurol, 1984. **86**(2): p. 410-3.
46. Ovadi, J., *Physiological significance of metabolic channelling.* J Theor Biol, 1991. **152**(1): p. 1-22.
47. Miles, E.W., S. Rhee, and D.R. Davies, *The molecular basis of substrate channeling.* J Biol Chem, 1999. **274**(18): p. 12193-6.
48. Hyde, C.C., et al., *Three-dimensional structure of the tryptophan synthase alpha 2 beta 2 multienzyme complex from Salmonella typhimurium.* J Biol Chem, 1988. **263**(33): p. 17857-71.

49. Knighton, D.R., et al., *Structure of and kinetic channelling in bifunctional dihydrofolate reductase-thymidylate synthase.* Nat Struct Biol, 1994. **1**(3): p. 186-94.
50. Perham, R.N., *Swinging arms and swinging domains in multifunctional enzymes: catalytic machines for multistep reactions.* Annu Rev Biochem, 2000. **69**: p. 961-1004.
51. Huang, X., H.M. Holden, and F.M. Raushel, *Channeling of substrates and intermediates in enzyme-catalyzed reactions.* Annu Rev Biochem, 2001. **70**: p. 149-80.
52. Anderson, K.S., *Fundamental mechanisms of substrate channeling.* Methods Enzymol, 1999. **308**: p. 111-45.
53. Bera, A.K., J.L. Smith, and H. Zalkin, *Dual role for the glutamine phosphoribosylpyrophosphate amidotransferase ammonia channel. Interdomain signaling and intermediate channeling.* J Biol Chem, 2000. **275**(11): p. 7975-9.
54. Geck, M.K. and J.F. Kirsch, *A novel, definitive test for substrate channeling illustrated with the aspartate aminotransferase/malate dehydrogenase system.* Biochemistry, 1999. **38**(25): p. 8032-7.
55. Iturrate, L., et al., *Substrate channelling in an engineered bifunctional aldolase/kinase enzyme confers catalytic advantage for C-C bond formation.* Chem Commun (Camb), 2009(13): p. 1721-3.
56. Tsuji, S.Y., D.E. Cane, and C. Khosla, *Selective protein-protein interactions direct channeling of intermediates between polyketide synthase modules.* Biochemistry, 2001. **40**(8): p. 2326-31.
57. DeLano, W.L., *The PyMOL Molecular Graphics System.* DeLano Scientific, San Carlos, CA, USA., 2002.
58. Moore, S.A., et al., *Sheep liver cytosolic aldehyde dehydrogenase: the structure reveals the basis for the retinal specificity of class 1 aldehyde dehydrogenases.* Structure, 1998. **6**(12): p. 1541-51.
59. Mezl, V.A. and W.E. Knox, *Properties and analysis of a stable derivative of pyrroline-5-carboxylic acid for use in metabolic studies.* Anal Biochem, 1976. **74**(2): p. 430-40.
60. Purcarea, C., et al., *Aquifex aeolicus aspartate transcarbamoylase, an enzyme specialized for the efficient utilization of unstable carbamoyl phosphate at elevated temperature.* J Biol Chem, 2003. **278**(52): p. 52924-34.
61. Wimalasena, D.S. and K. Wimalasena, *Kinetic evidence for channeling of dopamine between monoamine transporter and membranous dopamine-beta-monooxygenase in chromaffin granule ghosts.* J Biol Chem, 2004. **279**(15): p. 15298-304.
62. Meek, T.D., E.P. Garvey, and D.V. Santi, *Purification and characterization of the bifunctional thymidylate synthetase-dihydrofolate reductase from methotrexate-resistant Leishmania tropica.* Biochemistry, 1985. **24**(3): p. 678-86.
63. Surber, M.W. and S. Maloy, *The PutA protein of Salmonella typhimurium catalyzes the two steps of proline degradation via a leaky channel.* Arch Biochem Biophys, 1998. **354**(2): p. 281-7.
64. Baich, A., *Proline synthesis in Escherichia coli. A proline-inhibitable glutamic acid kinase.* Biochim Biophys Acta, 1969. **192**(3): p. 462-7.

65. Gamper, H. and V. Moses, *Enzyme organization in the proline biosynthetic pathway of Escherichia coli.* Biochim Biophys Acta, 1974. **354**(1): p. 75-87.
66. Smith, C.J., A.H. Deutch, and K.E. Rushlow, *Purification and characteristics of a gamma-glutamyl kinase involved in Escherichia coli proline biosynthesis.* J Bacteriol, 1984. **157**(2): p. 545-51.
67. Perez-Arellano, I., V. Rubio, and J. Cervera, *Dissection of Escherichia coli glutamate 5-kinase: functional impact of the deletion of the PUA domain.* FEBS Lett, 2005. **579**(30): p. 6903-8.
68. Hayzer, D.J. and T. Leisinger, *The gene-enzyme relationships of proline biosynthesis in Escherichia coli.* J Gen Microbiol, 1980. **118**(2): p. 287-93.
69. Chen, M., et al., *Directed evolution of an artificial bifunctional enzyme, gamma-glutamyl kinase/gamma-glutamyl phosphate reductase, for improved osmotic tolerance of Escherichia coli transformants.* FEMS Microbiol Lett, 2006. **263**(1): p. 41-7.
70. Perez-Arellano, I., et al., *Pyrroline-5-carboxylate synthase and proline biosynthesis: from osmotolerance to rare metabolic disease.* Protein Sci, 2010. **19**(3): p. 372-82.
71. Hu, C.A., A.J. Delauney, and D.P. Verma, *A bifunctional enzyme (delta 1-pyrroline-5-carboxylate synthetase) catalyzes the first two steps in proline biosynthesis in plants.* Proc Natl Acad Sci U S A, 1992. **89**(19): p. 9354-8.
72. Abel, T. and T. Maniatis, *Gene regulation. Action of leucine zippers.* Nature, 1989. **341**(6237): p. 24-5.
73. Downing, S.J., et al., *Proline oxidase in cultured mammalian cells.* J Cell Physiol, 1977. **91**(3): p. 369-76.

CHAPTER 2

Investigation of substrate channeling between monofunctional PRODH and P5CDH enzymes of *Thermus thermophilus*

Note: The results discussed in this chapter are being prepared for manuscript "Evidence for substrate channeling in monofunctional proline metabolic enzymes of *Thermus thermophilus*." Sanyal N, Tanner JJ, Becker DF. *Manuscript in preparation*.

INTRODUCTION

The oxidative conversion of proline to glutamate involves two enzymes, a flavin dependent proline dehydrogenase (PRODH) and a NAD^+-dependent Δ^1-pyrroline-5-carboxylate (P5C) dehydrogenase (P5CDH). PRODH and P5CDH help organisms respond to changes in the nutritional environment by initiating the breakdown of proline as a source for nitrogen, carbon, and energy [1-6] (Scheme 1). In Gram negative bacteria such *Escherichia coli* and *Bradyrhizobium japonicum*, PRODH and P5CDH catalytic domains are fused into one polypeptide known as proline utilization A or PutA [7].

P5C and γ-glutamate semialdehyde (GSA) are the intermediates of the proline and ornithine metabolic pathways [8]. The interconversion of P5C and GSA occurs via a non-enzymatic pH-dependent hydrolysis. P5C/GSA are appreciably labile and have been shown to react with metabolites, inhibit enzymes, and act as signaling molecules. GSA has been reported to inhibit glucosamine-6-phosphate synthase from *E. coli*, cytidine 5'-triphosphate synthase, and the amidotransferase domain of carbamoyl phosphate synthetase [9-11].

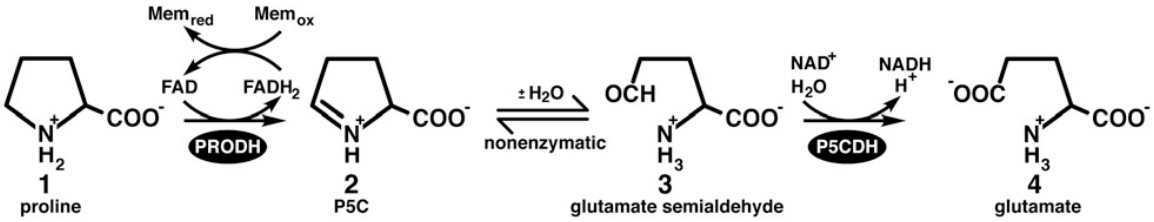

Scheme 1- An overview of the two-step oxidation of proline by proline dehydrogenase (PRODH) and Δ^1-pyrroline-5-carboxylate dehydrogenase (P5CDH). The physiological electron acceptor for PRODH during catalytic turnover is assumed to be a membrane bound electron carrier such as ubiquinone. Figure is adapted from [15].

Additionally, P5C forms adducts with other metabolites such as pyruvic acid, oxaloacetic acid, and acetoacetic acid [12]. P5C can also react with pyridoxal phosphate in patients with type II hyperprolinemia. The high levels of P5C/GSA generates inactive adducts with pyridoxal phosphate, leading to lower amounts of functional vitamin B6 in patients [12]. P5C also acts as a signaling molecule in eukaryotes and is thought to induce apoptosis by increasing intracellular reactive oxygen species [13, 14].

Altogether, it seems that controlling the levels of free P5C/GSA would be beneficial for the cell. The instability of the intermediates and competition from proline biosynthetic and ornithine metabolic pathways implies substrate channeling may be important for maintaining efficient proline catabolic flux. Substrate channeling is a phenomenon where the product of one reaction is transported to a second active site without equilibrating into bulk solvent [16].

Our previous study using enzyme kinetic measurements and X-ray crystallography in collaboration with Dr. John Tanner's laboratory (University of Missouri-Columbia) has shown that the PRODH and P5CDH domains of bifunctional PutA (BjPutA) from Gram-negative *Bradyrhizobium japonicum* are connected by a large, elongated channel [15]. Kinetic data have shown that substrate channeling in BjPutA facilitates product formation by decreasing the transient time for glutamate production. Using small-angle X-ray scattering (SAXS), similar occurrence of substrate channeling has also been proposed in PutA from *Escherichia coli* [17]. Thus, a general feature of PutA's may be the sequestering of the P5C/GSA intermediate and efficient transfer of P5C/GSA from PRODH to the P5CDH active site without equilibrating with the contents of the cytoplasm.

The 4e- oxidation of proline to glutamate by PRODH and P5CDH enzymes is highly conserved in all domains of life [7]. However, unlike Gram-negative bacteria, organisms such as Gram-positive bacteria and eukaryotes express separate monofunctional PRODH and P5CDH enzymes (Figure 1). Table 1 shows that intracellular proline concentrations are within an order of magnitude in various representative organisms.

It is thus anticipated that the oxidation of proline by PRODH would lead to significant amounts of P5C/GSA formation and, as mentioned above lead to deleterious effects such as inhibition of nucleoside synthesis, PLP-dependent enzymes and other metabolic processes impacted by P5C/GSA. To prevent substantial build-up of P5C/GSA in these organisms, the expression and activity levels of PRODH and P5CDH would need to be highly coordinated. As part of the mechanism by which organisms regulate proline metabolic flux, it is feasible that PRODH and P5CDH form a bienzyme complex. To date, however, no studies have been performed to test substrate channeling and potential interactions between monofunctional PRODH and P5CDH enzymes. It is not known whether monofunctional PRODH and P5CDH enzymes physically interact to form an internal cavity and to facilitate P5C/GSA channeling similar to bifunctional PutAs.

The main objective of this study is to investigate substrate channeling between monofunctional PRODH and P5CDH from *Thermus thermophilus*. PRODH from *Thermus thermophilus* (TtPRODH) was previously characterized and shown to be a 35 kDa flavoprotein containing a triosephosphate isomerase (TIM) barrel ($\beta_8\alpha_8$) catalytic domain [18, 19]. TtPRODH shares the catalytic $\beta_8\alpha_8$ fold domain previously reported for bifunctional PutA (White, Krishnan et al. 2007). P5CDH from *Thermus thermophilus*

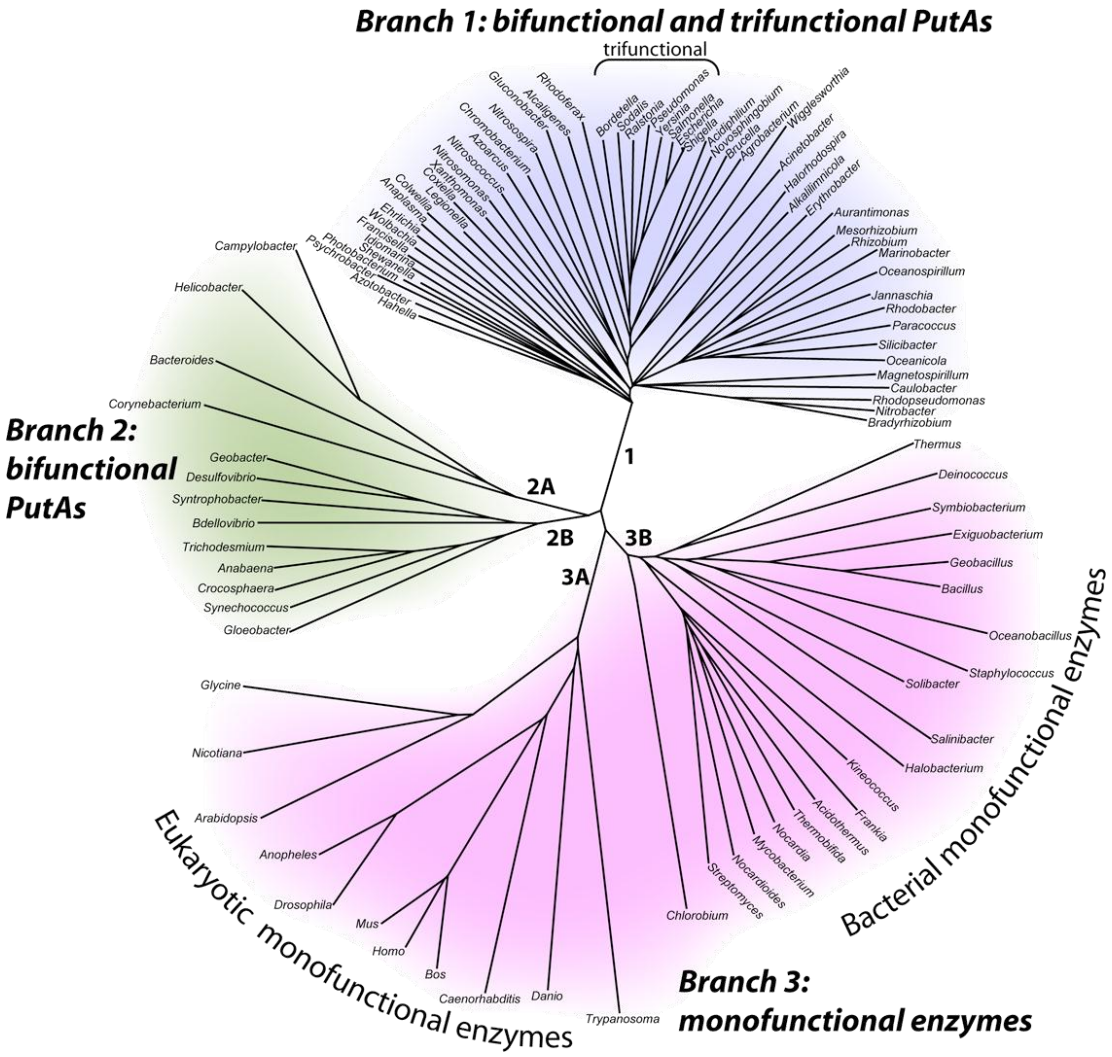

Figure 1- Phylogenetic tree representation of proline oxidative enzymes. Branch 1 and Branch 2 organisms, most of which are Gram-negative bacteria, encode for the bifunctional enzyme, PutA. Branch 3B displays organisms from Archaea and bacteria that express monofunctional PRODH and P5CDH. Examples of such organisms include *Thermus thermophilus, Deinococcus radiodurans, and Staphylococcus aureus.* Branch 3A includes all eukaryotic organisms. Figure from [7] with permission from source.

Table 1- Intracellular proline concentrations in various organisms under non-stressed conditions.

Organism	Intracellular Proline	Source
Escherichia coli	27.8 mM	(Chen, Cao et al. 2006) [51]
	0.39 mM	(Bennett, Kimball et al. 2009) [52]
Salmonella typhimurium	0.11 mM	(Csonka 1988) [53]
Bacillus subtilis	16.4 mM	(Whatmore, Chudek et al. 1990; Roesser and Muller 2001) [54, 55]
Thermus thermophilus	8.78 mM	(Kosuge and Hoshino 1998) [56]
Saccharomyces cerevisiae	3.15 mM	(Chen, Wanduragala et al. 2006) [57]
	2.9 mM	(Morita, Nakamori et al. 2003) [58]
Human plasma	0.1 – 0.26 mM	(Jaksic, Wagner et al. 1990) [59]

(TtP5CDH) has also been previously characterized and is a 57kDa protein that exists as hexamer in crystal form [18, 19]. Because TtPRODH and TtP5CDH are the best characterized pair of monofunctional enzymes in proline metabolism, they were chosen for studying substrate channeling *in vitro*.

The main strategy for testing substrate channeling is adapted from the work of Geck and Kirsch [20] and is illustrated in Figure 2. Using proline as a substrate, the amount of NADH generated, which is equivalent to the amount of glutamate product, is measured in assays using an equimolar mixture of TtPRODH andTtP5CDH. This coupled assay is called a channeling assay. The experiment is carried out in the presence of increasing amounts of catalytically inactive mutants of TtP5CDH or TtPRODH. In these assays, evidence for channeling between TtPRODH and TtP5CDH is considered when NADH formation decreases with increased amounts of the inactive mutant. For example, if PRODH and P5CDH form a channeling complex, the addition of an excess amount of a

P5CDH inactive mutant would compete with native P5CDH for binding to TtPRODH. This would result in formation of a complex where the second enzyme is inactive and, thus, the rate of the coupled proline to glutamate conversion would decrease (Figure 2). Conversely, inactive mutants of TtPRODH could also interfere with a TtPRODH/TtP5CDH channeling complex and yield similar results. If substrate channeling does not occur, the presence of the inactive mutant should not affect the rate of NADH formation.

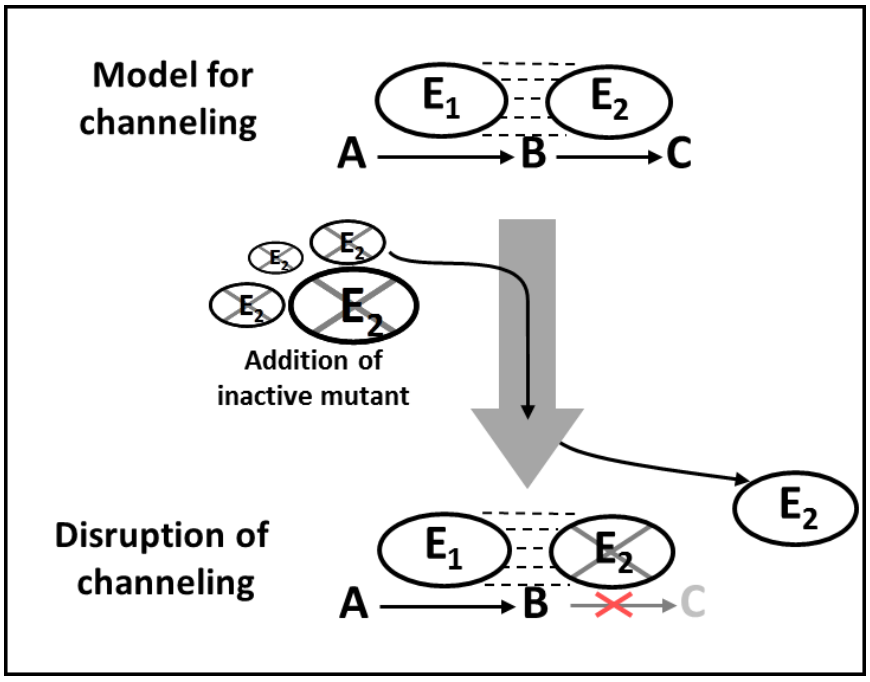

Figure 2- Strategy for testing substrate channeling between monofunctional PRODH and P5CDH. E_1 and E_2 represent PRODH and P5CDH respectively. A, B and C represent proline, P5C/GSA and glutamate, respectively.

The strategy outlined in Figure 2 has been used previously to demonstrate substrate channeling between muscle aldolase and fructose 1,6-bisphosphatase [21] and between aspartokinase and aspartate semialdehyde dehydrogenase [22]. More frequently, however, the above strategy has been used to rule out substrate channeling such as between aspartate aminotransferase and malate dehydrogenase [20] and for methyl erythritol phosphate biosynthetic enzymes IspDF and IspE [23].

Channeling of an intermediate requires some form of interaction between the pair of enzymes, regardless of how transient or stable the interactions might be. Without sufficient interactions between enzyme pairs, the intermediate is likely to quickly diffuse into the bulk solvent. Hence, to support the kinetic studies on substrate channeling, protein-protein interactions between TtPRODH and TtP5CDH were also investigated using surface plasmon resonance (SPR). SPR is a sensitive and powerful tool for detecting and measuring biomolecular interactions [24]. Properly designed SPR experiments not only provide estimates of protein-protein binding affinities but also the kinetic parameters of the binding event.

Substrate channeling has been demonstrated for PutA and other multifunctional enzymes [25-27] and, individual enzymes proximally docked onto a scaffold [28, 29]. The scientific novelty of this study is the evidence for substrate channeling between two separate enzymes.

EXPERIMENTAL PROCEDURES

Materials

All chemicals and buffers were obtained from Sigma-Aldrich or Fisher Scientific unless otherwise noted. DL-P5C was chemically synthesized from DL-hydroxylysine as described previously by Williams and Frank and stored in 1M HCl at 4^{o}C. [30]. D,L-P5C contains equimolar concentration of D-P5C and L-P5C. N-(Biotinoyl)-N'-(iodoacetyl)ethylenediamine (BIAM) and dimethyl sulfoxide (DMSO) were obtained from Molecular Probes. The streptavidin (SA) sensor chip and PD-10 desalting columns were purchased from GE Healthcare. The molecular interaction between TtPRODH and TtP5CDH was studied using a BIAcore 3000 (BIACORE AB, Uppsala, Sweden) instrument maintained in the Molecular Interaction Core Facility at the University of Nebraska Medical Center. Assays for enzymatic activities of PRODH and P5CDH were carried out on a Cary-50 UV-Vis spectrophotometer (Varian) or Powerwave XS Microplate reader (BioTek). Substrate channeling assays were carried out on a SF-61DX2 stopped-flow spectrophotometer (TgK Scientific, UK). The TtP5CDH-pKA8H construct and purified DrP5CDH inactive mutant (C325A) were generous gifts from Dr. John Tanner at the University of Missouri-Columbia.

Constructs and site-directed mutagenesis

The TtPRODH and TtP5CDH genes were expressed from a pKA8H expression vector as previously described [18, 19]. The PUT2 gene encoding P5CDH from *Saccharomyces cerevisiae* (Put2p) was cloned into a pET14b expression vector (pET14b-PUT2) as described in Chapter 3 of this thesis. Site-directed mutagenesis for active site and surface mutations was performed using the GeneTailor mutagenesis kit (Invitrogen).

The mutants generated in this study and the corresponding primers used for introducing active site mutations are listed in Table 2. The codon change for mutagenesis is highlighted in bold letters. All mutations were confirmed by DNA sequencing.

Table 2 – List of primers used for site-directed mutagenesis

Mutation	Primer	Sequence
TtP5CDH C322A	Forward primer	5' acggcttccaggggcagaag**gcc**tccgcggcga 3'
	Reverse primer	5' cttctgcccctggaagccgtaggcggagac 3'
TtPRODH R288M/R289M	Forward primer	5' actggtacccctacctcacc**atgatg**atcgcggagag 3'
	Reverse Primer	5' ggtgaggtaggggtaccagtcccggccgtag 3'
TtPRODH S8C	Forward primer	5' cctggacctggcttaccgt**tgc**ttcgtgctcgg 3'
	Reverse primer	5' aacggtaagccaggtccaggttcat 3'
TtPRODH A88C	Forward primer	5' ttgagctcgtctgggcccttt**tgc**gggaagccct 3'
	Reverse Primer	5' a agggcccagacgagctcaaggagcccccct 3'
Put2 C351A	Forward primer	5' tcgagttccaaggccaaaag**gcc**tctgccgctt 3'
	Reverse Primer	5' agaggcactttcgagttccaaggccaaaag 3'

Purification of TtPRODH and TtP5CDH enzymes

All proteins were expressed and purified from *E. coli* strain BL21(DE3) pLysS with a N-terminal 6xHis tag using the pKA8H construct as described here. pKA8H constructs for expressing wild-type TtPRODH, TtPRODH R288M/R289M, TtPRODH S8C, TtPRODH A88C, wild-type TtP5CDH, and TtP5CDH C322A, and pET14b-PUT2 were transformed separately into *E. coli* BL21(DE3) pLysS. For enzyme expression and purification, newly transformed cells were plated onto Luria-Bertani (LB) agar

containing chloramphenicol (34 µg/ml) and ampicillin (50 µg/ml). Resulting colonies were inoculated in 5 ml of LB broth containing the necessary antibiotics and grown to an optical density at 600 nm (OD_{600}) of 1.0. 1 ml of the LB culture was then used to inoculate 1 L of LB Broth media containing chloramphenicol (34 µg/ml) and ampicillin (50 µg/ml). The 1 L cultures were incubated at 37^{o}C with shaking (250 rpm) until OD_{600} of 0.8 at which point protein expression was induced with 0.5 mM IPTG overnight at 20^{o}C.

The overnight cultures were centrifuged at 6000 rpm for 20 min at 4^{o}C. The resulting pellets were resuspended in a final 50 ml volume of binding buffer (20 mM Tris, 5 mM imidazole, 0.5 M NaCl, 10% glycerol, pH 7.9) supplemented with protease inhibitors (3 mM ε-amino-N-caproic acid, 0.3 mM phenyl methyl sulfonyl chloride, 1.2 µM leupeptin, 48 µM N-p-tosyl-L-phenyl alanine chloromethyl ketone, 78 µM N- p -tosyl-L-lysine chloromethylketone). 1 mM FAD and 0.25% Triton-X 100 was additionally supplemented for purification of wild-type TtPRODH and TtPRODH mutant R288M/R289M. Cell suspensions were disrupted by sonication at 4^{o}C for a total of 5 min (5 sec pulse on, 15 sec pulse off, 40% power). The cell extract was centrifuged at 16000 rpm (4^{o}C) for 60 min. The supernatant (50 ml) was passed through a 0.8 µm filter (VWR) and applied to a Ni-NTA superflow (Qiagen) resin (25 ml bed volume in a 2.8 cm x 30 cm column) equilibrated with 1X binding buffer. Wash buffer (125 ml, 20 mM Tris, 60 mM imidazole, 0.5 M NaCl, 10% glycerol, pH 7.9) was then applied to the column followed by elution buffer (20 mM Tris, 500 mM imidazole, 0.5 M NaCl, 10% glycerol, pH 7.9) with a flow rate of 3 ml/min to elute His-tagged recombinant proteins. Fractions from the elution step were then analyzed by SDS-PAGE and pooled. Pooled protein was

then dialyzed into 50 mM Tris buffer (pH 8.0) containing 25 mM NaCl, 10% glycerol, 0.5 mM Tris (3-hydroxypropyl) phosphine (THP) and concentrated using an Amicon 30-kDa cutoff filter (Millipore). The final concentration of purified protein was determined using the BCA method and is expressed as concentration of monomer unless stated otherwise [23]. The 6xHis tag was not removed after purification.

Measurement of PRODH and P5CDH activities

PRODH Activity

TtPRODH activity was measured at 25^{o}C using Coenzyme Q_1 (CoQ_1) as the terminal electron acceptor. For measurement of kinetic parameters for proline and CoQ_1, TtPRODH (0.5 μM) was mixed in 50 mM phosphate buffer at pH 8.0 with varying proline (0-100 mM) and fixed CoQ_1 concentrations (150 μM) or varying CoQ_1 (0-300 μM) and fixed proline concentrations (150 mM). Reaction progress was monitored by following reduction of CoQ_1 at 275 nm (ε= 13700 cm^{-1} M^{-1}) using a 0.15 cm path length on a Hi-Tech Scientific SF-61DX2 stopped-flow instrument at 25^{o}C [31]. The kinetic parameters K_m and k_{cat} were estimated by regression analysis of the initial reaction velocity versus proline concentration using the Michaelis-Menten equation and Lineweaver-Burk plot analysis [32]. Proline:dichlorophenolindophenol (DCPIP) oxidoreductase assay was used for measurement of specific activity of TtPRODH in a 1-ml reaction volume using Cary 100 and Cary 50 UV-visible spectrophotometers [33]. The DCPIP assay mixture contained 0.2 μM of TtPRODH enzyme, 0.27 mM phenazine methosulfate, 75 μM DCPIP and 300 mM proline in 20 mM Tris at pH 8.0. The rate of DCPIP reduction was measured at 595 nm (ε = 16100 cm^{-1} M^{-1}) [33]. One unit of PRODH is defined as the amount of enzyme that reduces 1 μmole of DCPIP per min.

Test for the effect of TtP5CDH C322A and BSA on TtPRODH activity was done using the proline:DCPIP oxidoreductase assay with 1 mM proline as substrate and 1 to 25 µM concentrations of TtP5CDH C322A and BSA.

P5CDH Activity

P5CDH activity was measured by monitoring the formation of NADH at 340 nm (ε = 6400 cm^{-1} M^{-1}) at 25 °C. The assay buffer contained 50 mM potassium phosphate (pH 7.5) and 25 mM NaCl. P5CDH enzyme concentration was 0.5 µM (30 µg/ml) and NAD^+ concentration was 0.2 mM. Varying concentrations of L-P5C ranging from 1 to 300 µM were used. Initial rates were fitted to a Michaelis-Menten equation (equation 2.1).

$$v = \frac{V_{max}[S]}{K_m + [S]} \qquad (2.1)$$

Inhibition studies of P5CDH activity were carried out using the assays conditions described above with increasing concentrations of proline (0-15 mM). Initial velocities as function of P5C concentration at different proline concentrations were fitted to a competitive inhibition model (equation 2.2) using SigmaPlot 12 Enzyme Kinetics Module (Systat Inc.), where v is P5CDH velocity (µM/sec), $[E]_T$ is P5CDH concentration (µM), k_{cat} (sec^{-1}) and K_m (µM) are the Michaelis-Menten constants for P5CDH, $[S]$ is L-P5C concentration (µM), $[I]$ is the proline concentration (µM) and K_I is the competitive inhibition constant for L-proline.

$$\frac{v}{E_T} = \frac{K_{cat}[S]}{K_m\left(1 + \frac{[I]}{K_I}\right) + [S]} \qquad (2.2)$$

The effect of TtPRODH R288M/R289M on TtP5CDH was carried out similarly to the assays described above using 100 μM L-P5C as a substrate and varying TtPRODH R288M/R289M from 1 to 25 μM in the assays.

Test for substrate channeling

Optimization of the TtPRODH:TtP5CDH ratio for channeling assays

Varying concentrations of TtPRODH (0.1 μM to 10 μM) were mixed with 0.5 μM of TtP5CDH in 50 mM potassium phosphate (pH 7.5) and 25 mM NaCl. A separate substrate solution was prepared by mixing proline (1 mM), CoQ_1 (0.1 mM), and NAD^+ (0.2 mM) in 50 mM potassium phosphate (pH 7.5) and 25 mM NaCl. Equal volumes of the substrate and enzyme solutions were then mixed via single-mixing on a SF-61DX2 stopped-flow spectrophotometer. The reaction was monitored at 340 nm with a 1 cm path length observation cell. A molar extinction coefficient of 6400 cm^{-1} M^{-1} [34] was used to calculate concentration of NADH formed during the coupled assay.

The strategy described by Geck and Kirsch [20] was used for testing substrate channeling between TtPRODH and TtP5CDH. The experiment uses proline as the substrate for PRODH and monitors formation of NADH, a product of P5CDH activity. This coupled reaction (channeling assay) is performed at increasing concentrations of inactive mutants of TtP5CDH and TtPRODH. The inactive mutants of P5CDH were TtP5CDH C322A, DrP5CDH C325A, and Put2p C351A. The inactive mutant of TtPRODH used for these assays was TtPRODH R288M/R289M. The lack of enzymatic activity in the TtPRODH and TtP5CDH mutants was confirmed by activity assays described above. Bovine serum albumin (BSA), a protein unrelated to proline metabolism, was used as negative control in the channeling assays. The final

concentration of TtPRODH and TtP5CDH used in these assays was 0.5 μM of monomer each. The final concentrations of catalytically inactive mutants were 0, 1, 2, 3, 5, 12.5, and 25 μM (monomer). This resulted in 0 – 50 fold inactive mutant to wild-type enzyme ratio.

For the channeling assays, a mixture of TtPRODH (0.5 μM) and TtP5CDH (0.5 μM) was prepared in 50 mM potassium phosphate (pH 7.5) and 25 mM NaCl. A separate substrate solution was prepared by mixing proline (1 mM), CoQ_1 (0.1 mM), and NAD^+ (0.2 mM) in 50 mM potassium phosphate (pH 7.5) and 25 mM NaCl. Equal volumes of the substrate and enzyme solutions were then mixed via single-mixing on a SF-61DX2 stopped-flow spectrophotometer. The reaction was monitored at 340 nm with 1 cm path length observation cell. Molar extinction coefficient of 6400 cm^{-1} M^{-1} [34] was used to calculate the concentration of NADH formed during the channeling assay. Reduction of CoQ_1 alone causes a minor spectral decrease at 340 nm due to the absorbance overlap of CoQ_1 at 340 nm. To correct for this interference, the absorbance decrease at 340 nm due to CoQ_1 reduction was subtracted from the channeling assays by recording changes at 340 nm in the absence of NAD^+. Linear regression analysis was used for determining the rate of NADH formation in each assay. The change in NADH formation rates are also presented as the percent channeling activity relative to assays without inactive mutant.

The non-channeling PRODH-P5CDH reaction was simulated as previously described [35] using a diffusion-limited two-enzyme model (Equation 2.3, 2.4).

$$[NADH] = v_1 t + \left(\frac{v_1}{v_2}\right) K_{m2} \left(e^{-\frac{v_2 t}{K_{m2}}} - 1\right) \qquad (2.3)$$

$$\tau = \frac{K_{m2}}{v_2} \qquad (2.4)$$

In the above equation, v_1 is the experimentally determined rate of PRODH activity under the specified assay conditions with 1 mM proline, t is time in sec, K_{m2} (42.5 μM L-P5C) and v_2 (0.26 μM/sec) are the steady-state Michaelis-Menten constants K_m and V, respectively, for TtP5CDH, and τ is the transient time (sec) required to attain steady-state formation of product (i.e., NADH).

Biotin labeling of TtPRODH

TtPRODH mutants S8C and A88C were purified as described above and labeled with biotin at the newly incorporated cysteine residue using the thiol-reactive N-(Biotinoyl)-N'-(iodoacetyl)ethylenediamine (BIAM) reagent. A 5 mM stock of BIAM was prepared by dissolving in DMSO. Under anaerobic conditions, purified TtPRODH mutants S8C and A88C and BIAM were mixed at final concentrations of 51 μM (TtPRODH) and 715 μM (BIAM). After allowing the labeling reaction to proceed overnight at 4^{o}C, 25 mM β-mercaptoethanol was added to quench the unreacted BIAM. Crude biotin-labeled TtPRODH was separated from the quenched BIAM using a PD-10 desalting column. The concentration of total protein was measured using the Pierce 660 nm Protein Assay Reagent (Pierce). Biotin labeling of TtPRODH was confirmed by Western blot analysis using streptavidin-conjugated Horse Radish Peroxidase (Pierce). ECLprime reagents (GE Healthcare) were used for detection and visualization of biotin-labeled TtPRODH.

Protein-protein interaction analysis by SPR

Immobilization of TtPRODH on streptavidin sensor chip

The streptavidin (SA) sensor chip was first washed with HBS-EP buffer (10 mM HEPES, pH 7.4, 0.15 M NaCl, 3.4 mM EDTA, and 0.05% surfactant P20) for 6 min (20 µl/min flow rate). Prior to immobilization, the SA sensor chip was activated with three consecutive 40 µl injections of activating buffer (1 M NaCl and 50 mM NaOH). Biotinylated TtPRODH mutants S8C and A88C were then diluted in HBS-EP to a final concentration of 250 µM and injected with a flow rate of 5 µl/min onto flow cells 2 (TtPRODH S8C) and 4 (TtPRODH A88C). Sensor chip flow cells 1 and 3 were not exposed to TtPRODH mutants and were used as reference cells.

Preliminary experiments were carried out to test the interaction of immobilized TtPRODH S8C and A88C ligands with analytes such as TtP5CDH, DrP5CDH and BSA. The analytes were equilibrated in HBS-EP buffer and diluted to a concentration of 1 µM immediately prior to injection. Each protein analyte was then injected onto flow cells 1-4 for 2 min followed by a 5 min dissociation phase at a flow rate of 30 µl/min.

Binding analysis of TtP5CDH

The SA sensor chip with immobilized TtPRODH A88C on flow cell 4 was first washed with regeneration buffer (2 M NaCl) at a flow rate of 30 µl/min for 3 min followed by equilibration with HBS-EP buffer (30 µl/min). Wild-type TtP5CDH was equilibrated with HBS-EP buffer and diluted to different concentrations ranging from 0.5 to 7.5 µM (monomer). From lowest to highest concentration, wild-type TtP5CDH was injected for 2 min (30 µl/min) followed by a 5 min dissociation phase at a flow rate of 30

µl/min with HBS-EP buffer. The SA sensor chip was regenerated using 90 µl of 2 M NaCl (30 µl/min) and equilibrated with HBS-EP buffer (30 µl/min, 5 min) after each injection of TtP5CDH. The resulting sensorgrams were globally fitted to 1:1 Langmuir PRODH-P5CDH binding model using BIA-evaluation software 3.1. The experiments were carried out at 25^{o}C. All buffers were filtered and degassed prior to injection on SA sensor chip. Signals from the reference flow cells were subtracted from the sensorgrams.

RESULTS

Competitive inhibition of TtP5CDH by proline

The crystal structure of TtP5CDH [19] shows several ligands containing a carboxylate moiety (COO^-) bind at the TtP5CDH active site. L-proline (PDB ID:2J40) and glutamate (PDB ID:2BHQ) were among these ligands. The carboxyl moiety of proline is 2.7 Å from the hydroxyl group of active site Ser321 and 3.0 Å from the backbone amide nitrogen atoms of Gly477 and Ala478 (Figure 3A). Such bond distances can favor hydrogen bonding or electrostatic interaction and thereby stabilize ligand binding [36]. The orientation of the carboxyl group of the other ligands is identical to proline and glutamate. This suggests that the binding of proline to the active site is stable and not an artifact of TtP5CDH crystallization. Hence, we decided to test the possibility of proline as an inhibitor of TtP5CDH.

The effect of proline on P5CDH initial velocity was determined and is shown as a direct plot in Figure 3B and a double reciprocal plot of 1/v versus 1/[S] with varying proline concentrations in Figure 3C. The steady-state kinetic parameters for TtP5CDH were estimated as K_m of 42.7 µM DL-P5C and k_{cat} of 0.52 s^{-1} (Table 3). As is

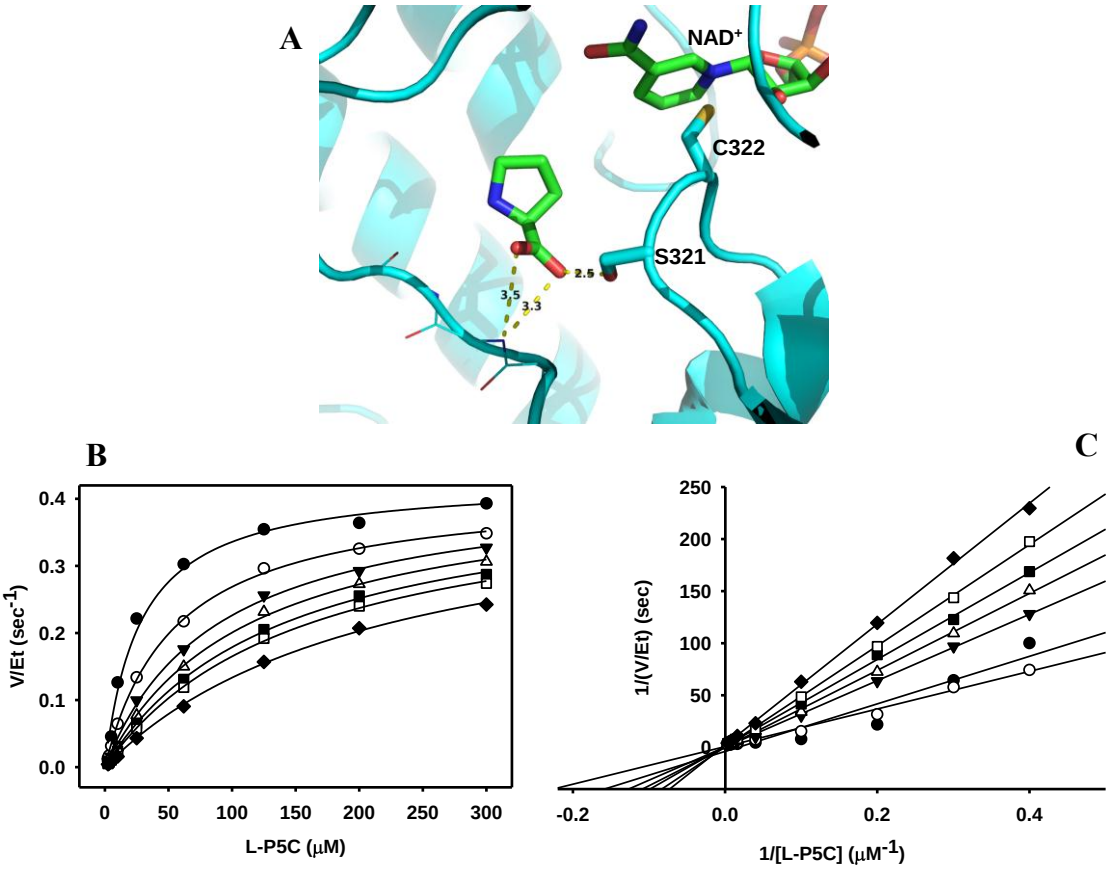

Figure 3- Competitive inhibition of TtP5CDH by L-Proline. A) Molecular representation of L-proline bound to TtP5CDH active site (PDB ID:2J40). Ligands L-proline and NAD^+ are represented as sticks. Distance between carboxyl moiety of proline and active site residues are shown using yellow dotted line with distance represented in Å. TtP5CDH is represented as cartoon (cyan). Figure was generated using PyMol molecular graphics system [37]. B) Michaelis-Menten plot and C) Double reciprocal plot of initial velocity TtP5CDH versus L-P5C substrate concentration with proline as competitive inhibitor with concentrations 0 mM (●); 2 mM (○); 4 mM (▼); 6 mM (△) ; 8 mM (■); 10 mM (□); and 15 mM (◆). Regression analysis was performed by global fitting of data to Michaelis-Menten equation using Sigmaplot 12 (Systat Software Inc.). Kinetic parameters from the fitting are k_{cat} = 0.43 ± 0.02 sec^{-1}, K_m = 27.7 ± 4.3 μM, and $K_{I(pro)}$ = 3.9 ± 0.7 mM proline.

characteristic of competitive inhibition, the apparent V of P5CDH does not change with inhibitor (proline) concentration. The data fits well with a competitive inhibition model (equation 2.2) with an inhibition constant (K_I) of 3.9 mM proline. In order to eliminate interference from proline acting as a competitive inhibitor of P5CDH, we chose to test TtPRODH-TtP5CDH substrate channeling using proline concentrations < 3.9 mM. The subsequent channeling assays were thus performed with 1 mM proline, which is not only < $K_{I(pro)}$, but is also below $K_{m(pro)}$ for TtPRODH. The kinetics parameters determined for TtPRODH are K_m of 8.19 ± 0.34 mM proline and 162.2 ± 7.6 µM CoQ_1 with overall k_{cat} of 17.04 ± 0.42 sec^{-1}.

TtPRODH-TtP5CDH coupled reaction and non-channeling two-enzyme modeling

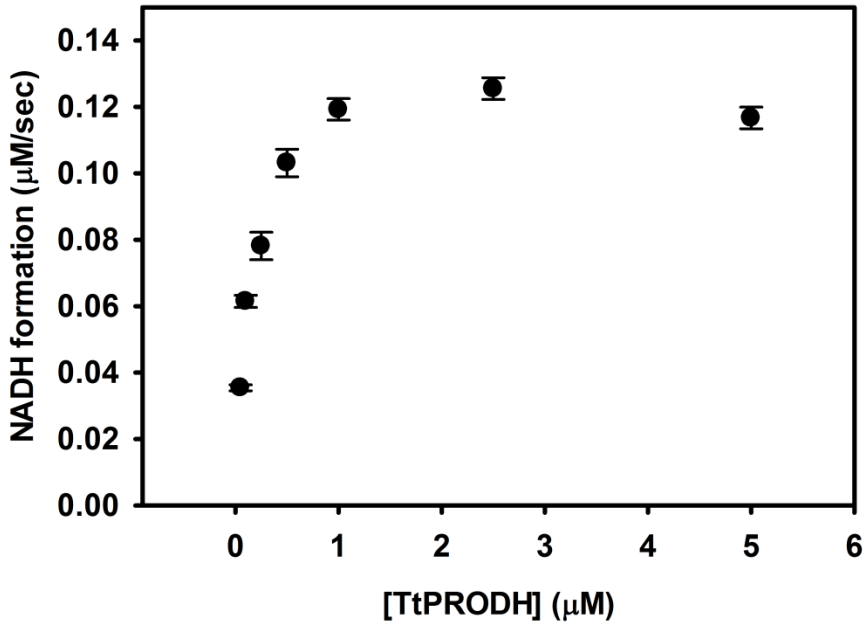

Figure 4 – Effect of TtPRODH enzyme concentration on channeling reaction. NAD^+ reduction rate was calculated from slope of progress curves at 340 nm. The reaction mixture contained 0.5 µM TtP5CDH, 1 mM proline, 0.2 mM NAD^+, and 0.1 mM CoQ_1. TtPRODH was varied from 0.1 µM to 10 µM. Assays for each TtPRODH concentration was carried out in triplicate.

Before performing TtPRODH-TtP5CDH channeling assays, the ratio of TtPRODH:TtP5CDH was first optimized. This was done to ensure that the coupled TtPRODH-TtP5CDH reaction was not limited by the concentration of either enzyme. Figure 4 shows the dependence of NADH formation on the concentration of TtPRODH. Keeping TtP5CDH fixed at 0.5 μM, NADH formation plateaus above 1 μM TtPRODH. Thus, an equimolar mixture of 0.5 μM TtPRODH and 0.5 μM TtP5CDH was considered to be appropriate for testing substrate channeling.

The rate of NADH formation using an equimolar mixture of TtPRODH-TtP5CDH (0.5 μM:0.5 μM) was compared to that of a diffusion-limited two-enzyme reaction model (equation 2.3). Figure 5 shows that an equimolar mixture of TtPRODH-TtP5CDH exhibits a velocity of 0.0803 μM NADH/sec. Simulating a non-channeling reaction for the formation of NADH by TtPRODH and TtP5CDH using equation 2.3 generates a rate of 0.0804 μM/sec. The simulated steady-state rate of NADH formation is identical to the experimental rate, however, the transient time for TtPRODH-TtP5CDH to attain steady-state formation of NADH is much longer for the simulated non-channeling reaction than for the experimentally observed reaction. The predicted transient time for a non-channeling TtPRODH-TtP5CDH mixture is 164.2 sec, whereas the experimentally observed transient time is 38.5 sec. The 4-fold decrease in transient time in the experimental curve relative to the simulated curve is suggestive of substrate channeling between TtPRODH and TtP5CDH. The shorter time to reach steady-state formation of NADH may be due to increased local concentration of P5C/GSA at the P5CDH active site [38].

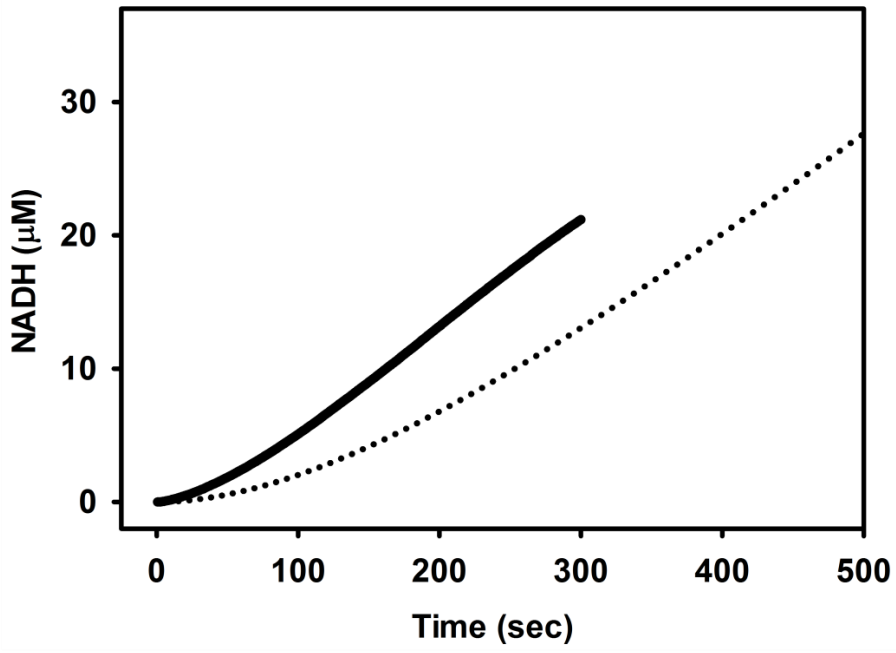

Figure 5- Observed NADH formation from TtPRODH-TtP5CDH channeling assay and simulated non-channeling TtPRODH-TtP5CDH reaction. Solid line represents NADH formed in a channeling assay by an equimolar mixture of TtPRODH and TtP5CDH using 1 mM proline as substrate. Dotted line represents simulated NADH formation by a non-channeling two-enzyme model (equation 2.3) using experimentally determined values of v_1 (0.08 μM/sec), K_{m2} (42.7 μM), and v_2 (0.26 μM/sec).

An explanation for decreased lag time to NADH formation could be allosteric activation by one of the two enzymes [39]. In a proline:DCPIP oxidoreductase assay with 1 mM proline, 0.5 μM TtPRODH alone reduces 24.9 μM DCPIP/min whereas addition of 50-fold excess of inactive TtP5CDH C322A or Put2p C351A changes the rate to 19.26 and 23.11 μM DCPIP reduced/min, respectively. TtP5CDH was also tested for allosteric effects by TtPRODH. With 100 μM L-P5C present as P5CDH substrate, 50-fold excess of TtPRODH R288M/R289M caused a slight decrease in TtP5CDH activity from 14.6 μM NADH formed/min to 11 μM NADH/min. Both TtPRODH and TtP5CDH exhibit a negligible inhibitory effect on each other but no evidence of allosteric activation was observed.

Effect of inactive mutants on TtPRODH-TtP5CDH channeling assays

To further test the channeling hypothesis, inactive mutants of TtP5CDH and TtPRODH were used as competitors of the putative TtPRODH-TtP5CDH channeling complex. Inactive TtPRODH (TtPRODH mutant R288M/R289M) was created by replacing two catalytic arginine residues (Arg288 and Arg289) which are responsible for ionic interactions with the carboxylate moiety of proline thereby stabilizing proline binding [40]. The inactive variant of TtP5CDH (TtP5CDH C322A) was generated by mutating Cys322 which is the active site nucleophile that attacks the aldehyde carbon of GSA and forms an essential thiohemiacetal tetrahedral intermediate. Active site mutations did not significantly alter the oligomeric structures of TtPRODH and TtP5CDH as observed by size-exclusion chromatography and small-angle X-ray scattering (personal communications Dr. John Tanner's group, University of Missouri-Columbia).

Figure 6 shows that the addition of the TtP5CDH inactive mutant (TtP5CDH C322A) to a mixture of TtPRODH-TtP5CDH caused a severe decrease in the rate of NADH formation (Figure 6A). In the absence of TtP5CDH C322A, the velocity of NADH formation by the TtPRODH-TtP5CDH mixture was 0.1 μM NADH/sec whereas in the presence of 50-fold excess of TtP5CDH C322A (25 μM) the rate decreased 5-fold to 0.02 μM NADH/sec. This is about an 80% decrease in the rate of product formation (Figure 6B). The rate of decrease in NADH formation has a linear correlation with the amount of TtP5CDH C322A added to the reaction. From an extrapolation on the x-axis, it is predicted that 63-fold excess of TtP5CDH C322A would lead to complete inhibition of the channeling reaction. The amount of inactive mutant added to the reaction was limited

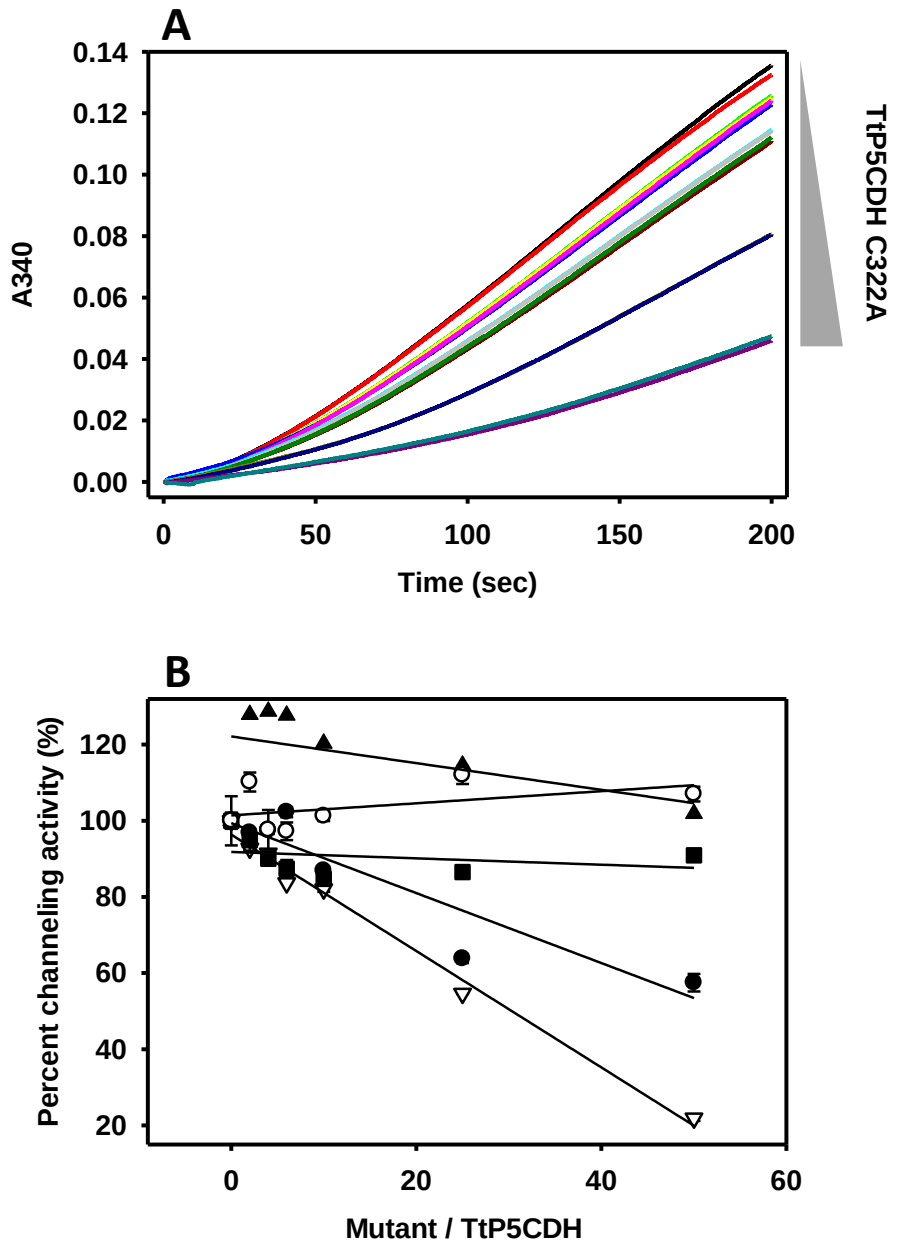

Figure 6- Test for substrate channeling. A) Time course of NADH formation at 340 nm with varying concentrations of TtP5CDH C322A. The concentration of inactive mutant was varied from 0 to 25 µM. Grey bar corresponds to increasing TtP5CDH C322A concentration. NADH formation decreases with increasing TtP5CDH C322A concentration. The reaction mixture contained 0.5 µM TtP5CDH, 0.5 µM TtPRODH, 1 mM proline, 0.2 mM NAD^+, 0.1 mM CoQ_1 and increasing concentrations of TtP5CDH C322A. Percent channeling rate is calculated from slope of progress curve. B) Percent channeling rates are plotted for the different inactive P5CDH and TtPRODH mutants. Shown in the plot are- TtP5CDH C322A (▽), TtPRODH R288M/R289M (●), DrP5CDH C325A (■), Put2p C351A (○), and BSA (▲). A linear fit for the effect of each mutant on the NADH formation rate is shown.

to 50-fold excess due to experimental constraints such as volume of protein added, concentration of glycerol and buffering agents required for protein solubility. Addition of buffer components alone did not have any effect on the rate of NADH formation. The effect of adding the TtPRODH inactive mutant (TtPRODH R288M/R289M) to the channeling reaction was similar to TtP5CDH inactive mutant albeit to a lesser extent. At a 50-fold excess of TtPRODH R288M/R289M (25 μM) relative to wild-type TtPRODH, a 2-fold decrease in the rate of NADH formation was observed from 0.1 μM/sec to 0.054 μM/sec.

To test the effects of inactive P5CDH from another organism, inactive mutants of P5CDH from *D. radiodurans (*DrP5CDH C325A) and *S. cerevisiae* (Put2p C351A) were added to the TtPRODH:TtP5CDH reaction mixture. In contrast to inactive TtP5CDH, DrP5CDH and Put2p inactive mutants had no significant effect on NADH formation rates as shown in Figure 6B. In addition, BSA showed no effect on the TtPRODH:TtP5CDH reaction mixture. Interestingly, a slight increase in NADH formation was observed with BSA. The slight increase in activity may be attributed to a general stabilizing effect of BSA on enzymatic activity [41-44]. Although the mechanism is not fully understood, it has been proposed that BSA increases protein stability and decreases interaction of enzymes with the reaction vessel and air-solvent interface by acting as a surfactant [42]. In summary, the results shown in Figure 6 show that only TtP5CDH C322A and TtPRODH R288M/R289M cause a decrease in NADH formation rate.

Because the highest concentration of inactive mutant in the test for channeling assays is 25 μM and, approximately 20 μM P5C is generated during a 200 sec assay, one possible explanation for the decrease in NADH formation caused by TtP5CDH C322A is

the binding of P5C/GSA by the inactive mutant. Binding of P5C/GSA by an inactive P5CDH mutant could possibly decrease the amount of P5C/GSA available for catalysis, thereby causing a decrease in the overall formation of NADH. The dissociation constant (K_D) is the best estimate of substrate binding affinity, however, it is difficult to estimate a K_D value for the binding of P5C/GSA to TtP5CDH because P5C/GSA are in a pH-dependent equilibrium in aqueous solution [9]. For this reason, K_m values were used as a determinant of substrate binding affinity. Table 3 reports the steady-state kinetic parameters that were determined for TtP5CDH, Put2p, and DrP5CDH. The K_m value for TtP5CDH is 42.7 μM and for Put2p, the K_m is 2-fold higher at 104 μM. The K_m value for DrP5CDH (K_m = 282.3 μM) is nearly 7-fold higher than TtP5CDH. If the inactive mutant of TtP5CDH decreases channeling simply by binding P5C/GSA, then Put2p would also be expected to have an effect on the channeling assay, albeit to a lesser extent (~ 2-fold less).

Table 3 – Steady-state kinetic parameters of monofunctional P5CDH from various species

	K_m (μM L-P5C)	k_{cat} (sec^{-1})	k_{cat}/K_m ($M^{-1}sec^{-1}$)
TtP5CDH	42.7±1.1	0.52±0.03	$1.22x10^4$
DrP5CDH	282.3±6.4	1.6±0.1	$5.67x10^3$
Put2p	104.2±4.4	1.49±0.26	$1.43x10^4$

The results shown in Figure 6, however, show that Put2p has no effect on NADH formation indicating that the effects of the inactive TtP5CDH mutant on the TtPRODH-TtP5CDH reaction are not caused by sequestration of P5C/GSA. Furthermore, the

inactive TtPRODH mutant, which does not bind P5C/GSA, also inhibited the TtPRODH-TtP5CDH reaction consistent with the inactive TtPRODH and TtP5CDH mutants lowering NADH formation by disrupting a TtPRODH:TtP5CDH complex.

Analysis of PRODH-P5CDH interactions by SPR

In order to further investigate TtPRODH-TtP5CDH substrate channeling, binding interactions between TtPRODH and TtP5CDH were investigated by SPR. In the SPR analysis, TtPRODH was used as the immobilized ligand and TtP5CDH was the analyte. The following strategy was used for biotinylating TtPRODH and immobilizing it on a BIAcore streptavidin (SA) sensor chip.

TtPRODH does not have any cysteine residues. This allowed us to specifically introduce cysteine residues on the outer surface of TtPRODH via site-directed mutagenesis. After careful analysis of the surface residues, Ser8 located near the N-terminus and Ala88 located near the top of the PRODH $\beta_8\alpha_8$ barrel were chosen for mutagenesis. These residues were strategically chosen for replacing with cysteine so that biotinylated TtPRODH could be immobilized on the SA chip in two different orientations. Figure 9 shows the predicted orientation of TtPRODH mutants S8C and Ala88C after immobilization on the SA chip. TtPRODH S8C should be immobilized near the N-terminus leaving the side and top of the PRODH $\beta_8\alpha_8$ barrel exposed to solvent (Figure 9). Conversely, TtPRODH A88C is predicted to be immobilized near the top of the PRODH $\beta_8\alpha_8$ barrel with the N-terminus region exposed to solvent. These contrasting immobilized configurations allowed us to probe two different regions of TtPRODH for binding to TtP5CDH.

Purified TtPRODH mutants S8C and A88C required the presence of the reducing agent Tris(3-hydroxypropyl)phosphine (THP) to prevent precipitation during purification. The specific activities of TtPRODH mutants S8C and A88C were 25.4 U/mg and 19.8 U/mg, respectively, which are somewhat lower than wild-type TtPRODH (34 U/mg). The engineered surface cysteine residues on TtPRODH were biotinylated using the thiol-reactive BIAM reagent and the incorporation of the biotin label was verified by Western analysis as shown in Figure 7. There was some loss of enzymatic activity during the labeling procedure. The specific activities for biotin-labeled TtPRODH mutants S8C and A88C were 15.4 U/mg and 14.6 U/mg, respectively.

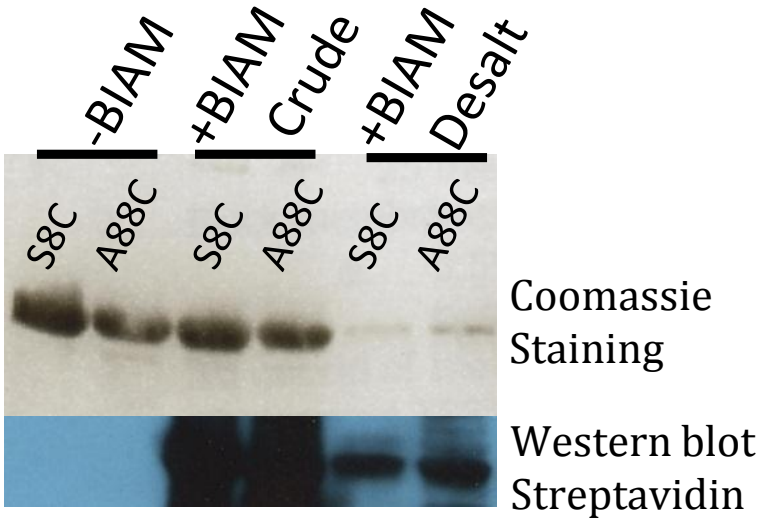

Figure 7 – Labeling of TtPRODH with Biotin. TtPRODH S8C and A88C were labeled using thiol-reactive biotinylated iodoacetamide (BIAM). Western blotting (bottom panel) using streptavidin-HRP confirms biotin labeling of TtPRODH A88C and S8C. PD-10 desalting column was used for removing excess BIAM.

Injection of TtPRODH mutants S8C and A88C elicited a response of 1900 RU and 2600 RU, respectively, upon being immobilized on the SA chip. Thus, similar amounts of both proteins were immobilized on the SA chip. After washing the immobilized surfaces, TtP5CDH (1 μM) was injected onto both surfaces. Figure 8A shows that a binding response was observed with immobilized TtPRODH A88C but not with immobilized TtPRODH S8C. This result suggests that TtP5CDH distinguishes between the two orientations of TtPRODH and specifically recognizes the configuration of immobilized TtPRODH A88C. It also indicates that the immobilized orientation of TtPRODH S8C conceals a surface on TtPRODH that is critical for TtP5CDH binding. Other analytes were also tested for binding to TtPRODH to rule out non-specific interactions. BSA and DrP5CDH did not show any binding response with either TtPRODH orientation. This further indicates that the sensorgram response observed with immobilized TtPRODH A88C is specific for TtP5CDH.

We then proceeded to measure the binding kinetics of TtP5CDH with immobilized TtPRODH A88C. Increasing concentrations of TtP5CDH were injected onto the TtPRODH A88C surface. Figure 8B shows that TtP5CDH binds to TtPRODH A88C in a concentration dependent manner. Global fitting analysis yielded a dissociation constant (K_D) of 3.03 μM and an association constant (K_A) of 3.3 x 10^5 M^{-1}. The corresponding k_{on} rate constant for binding was 1.49×10^3 $M^{-1}s^{-1}$ and k_{off} rate constant was 4.51×10^{-3} s^{-1}.

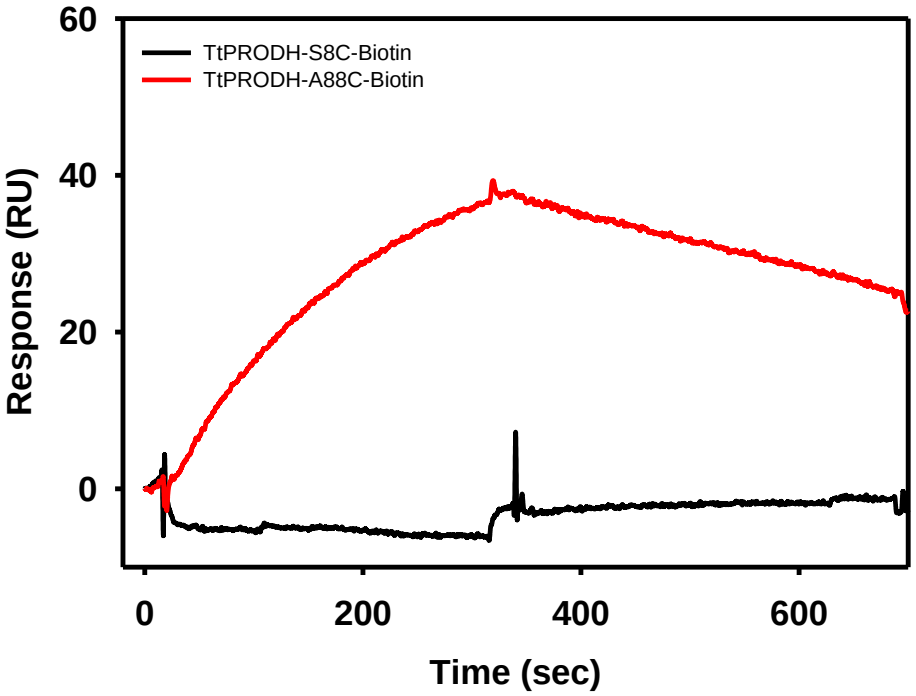

Figure 8A– TtP5CDH binds only to TtPRODH immobilized via A88C. SPR sensorgram showing binding response after injection of TtP5CDH (1 µM) to immobilized TtPRODH S8C and A88C with a flow rate of 30 µl/min (HEPES-EP buffer, pH 7.4). The association and dissociation phases were 300 sec each. The sensorgrams show that a response is only generated by injection of TtP5CDH onto immobilized TtPRODH A88C. Signals from the control flow cells have been subtracted from the sensorgrams.

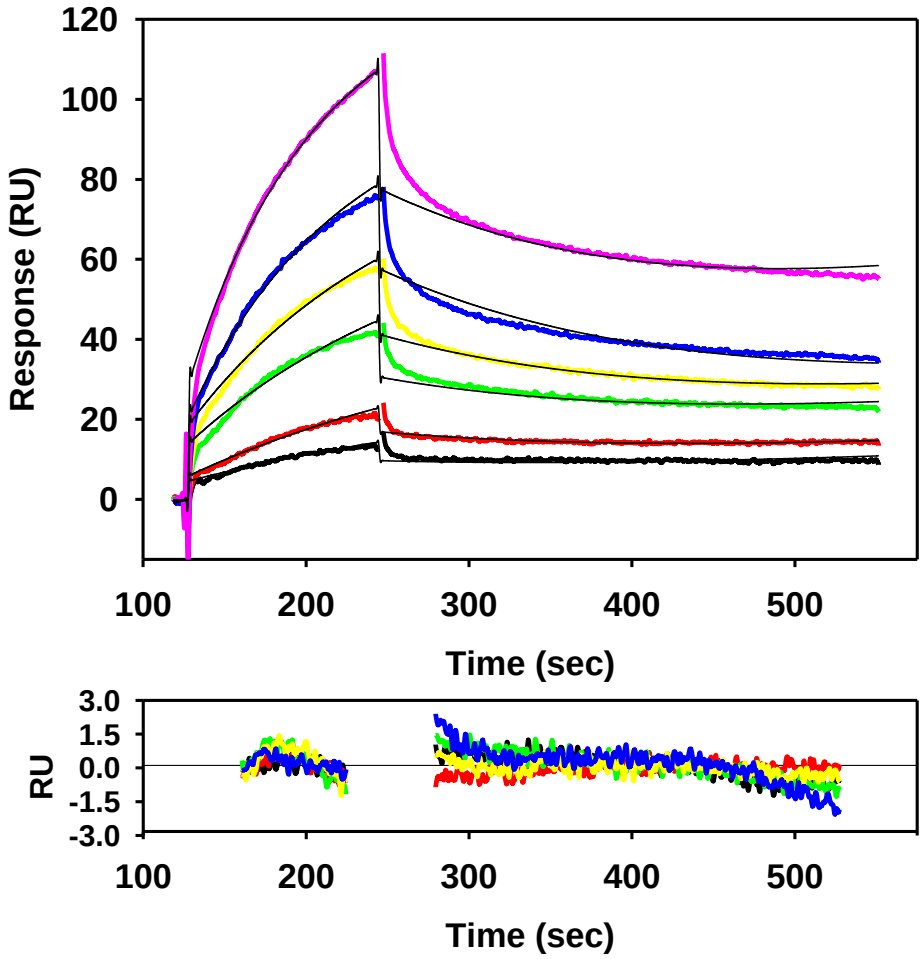

Figure 8B- SPR binding analysis of TtP5CDH and immobilized TtPRODH A88C. The concentrations of TtP5CDH injected onto the surface are 0.5 µM (black), 1 µM (red), 2 µM (green), 3 µM (yellow), 5 µM (blue), and 7.5 µM (pink). The association phase is the injection of TtP5CDH (0.5-7.5 µM) at 30 µl/min for 120 sec and the dissociation phase is the flow of HEPES-EP buffer at 30 µl/min for 300 sec. The overlapping black lines are generated from a global fit of the data to a 1:1 Langmuir binding isotherm using BIAevaluation 3.0 software. A dissociation constant, K_D, of 3.03 µM was determined for TtPRODH and TtP5CDH interaction. Bottom panel shows the plot of the residuals. The chi square value for the fit was 0.579. Signals from the control flow cells have been subtracted from the sensorgrams.

DISCUSSION

There is a growing body of evidence that suggests metabolic processes are more than just dispersed reactions occurring inside a fluidic container that is, the cell [16, 29, 45]. There appears to be mechanisms by which several intermediates of metabolism are transferred between sequential enzymes while restricting their diffusion in the cytoplasm or other cellular compartments [45]. The interactions between enzymes that lead to such channeling of intermediates range from strong interactions to weak transient interactions with binding affinities (K_D) spanning the nM to μM range [46]. In order to identify the cellular processes that limit diffusion of metabolites, there is a need to investigate substrate channeling at the molecular enzyme level. In the case of proline metabolism, Surber and Maloy first observed that PutA from *Salmonella typhimurium* catalyzed the oxidation proline to glutamate by an apparent leaky channel [47]. A more recent study from our group in conjunction with Dr. John Tanner's lab (Missouri, Columbia) confirmed this original proposal by reporting structural and kinetic evidence of an internal cavity in PutA from *B. japonicum* for transfer of P5C/GSA from the active site of PRODH to P5CDH.

The experiments discussed in this chapter were designed to explore the possibility of substrate channeling in monofunctional PRODH and P5CDH enzymes. Rate measurements for the coupled TtPRODH-TtP5CDH enzyme pair demonstrates that steady-state formation of NADH is achieved faster than the theoretical approach to steady-state by two individual enzymes. Although such rapid product formation can be explained by allosteric activation by one enzyme on the other [39], our results show that this is not the case for TtPRODH and TtP5CDH.

The results from experiments using a catalytically inactive TtP5CDH mutant and to a lesser extent the inactive TtPRODH mutant, suggests the presence of a dynamic TtPRODH-TtP5CDH interaction. In aqueous buffer, the functional enzyme pair can be disrupted by an equally compatible inactive variant of either of TtPRODH or TtP5CDH. Being structurally identical to wild-type enzymes, the inactive variants most likely form an identical complex as the wild-type enzyme but one which cannot catalyze coupled proline oxidation.

Although suggestive of a binding event between TtPRODH and TtP5CDH, the kinetic experiments do not directly provide any information on enzyme interactions. SPR was thus used to test for potential physical interactions between TtPRODH and TtP5CDH. Unexpectedly, the two orientations of TtPRODH immobilized on the SA chip revealed specific binding interactions between TtPRODH and TtP5CDH. In addition, DrP5CDH showed no evidence of binding to TtPRODH. Thus, the binding interactions observed by SPR between TtP5CDH and immobilized TtPRODH A88C appear to be specific. The K_D value estimated for the TtPRODH-TtP5CDH complex is ~ 3 μM which can be categorized as a weak transient protein-protein interaction [48].

Based on the evidence presented here and the structural data available for TtPRODH and TtP5CDH, a possible model for how TtPRODH and TtP5CDH physically interact was explored. Figure 9 shows a representation of the TtPRODH electrostatic surface. The structure of the hexameric form of TtP5CDH is shown in Figure 10. The hexamer of TtP5CDH has a hollow core along its longitudinal axis of symmetry. This hollow cylindrical core, which is approximately 12 Å in diameter and 91 Å in length, provides exclusive access to all of the six active sites in the hexamer. Apart from the two

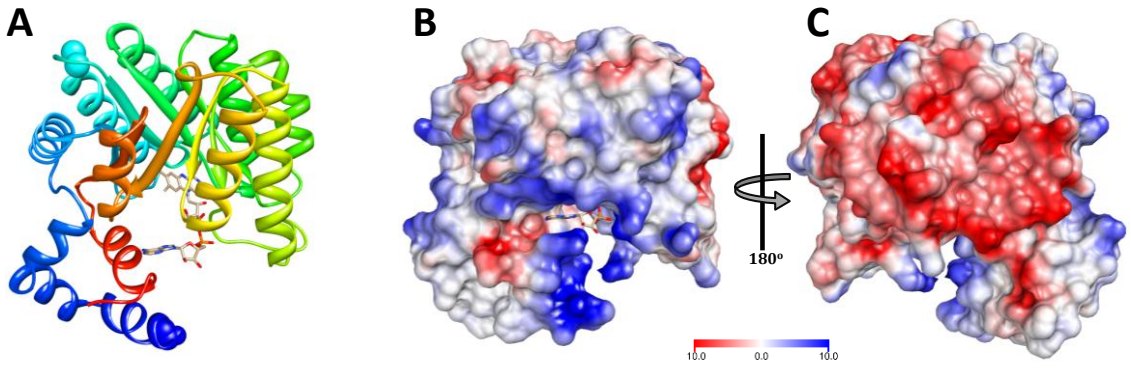

Figure 9 –Molecular and surface representation of TtPRODH. A) TtPRODH is shown as cartoon representation and colored as rainbow with N-terminus as blue and C-terminus as red (left.) Side chains of residues Ser 8 (Blue) and Ala 88 (Cyan) are displayed as spheres. B) Coulombic surface representation of TtPRODH oriented as figure A. C) View turned 180^{o} about the vertical axis. Ser 8 is in a region with basic residues whereas Ala 88 is located in a region with acidic side chains. These two residues were chosen since they are in two separate regions of TtPRODH with the most noticeable surface electrostatics. The coulombic representation used blue color for electropositive charge and red color for electronegative charge. Either of these two regions can serve as a possible interface with TtP5CDH. Figures were created using monomeric TtPRODH structure (PDB ID:2G37) and UCSF Chimera [49].

ends of the hexamer, there are no other major paths into the core. Access to the P5CDH active site is not possible from outside the hexmeric core. TtP5CDH shares considerable sequence similarity (similarity 51%, Iidentity 37%) and structural homology with the P5CDH domain of *B. japonicum* PutA If we use the P5CDH active site orientation from the BjPutA structure (PDB ID:3HAZ), we will notice that the substrate P5C/GSA must enter the core region of TtP5CDH to reach the active site Cys322 and the NAD^{+} cofactor. Once GSA is oxidized to glutamate, it appears that glutamate can exit the active site on the exterior side of the hexamer. It is possible then, that the inner core of the hexamer facilitates capture of P5C/GSA, thus generating a conduit for channeling P5C/GSA.

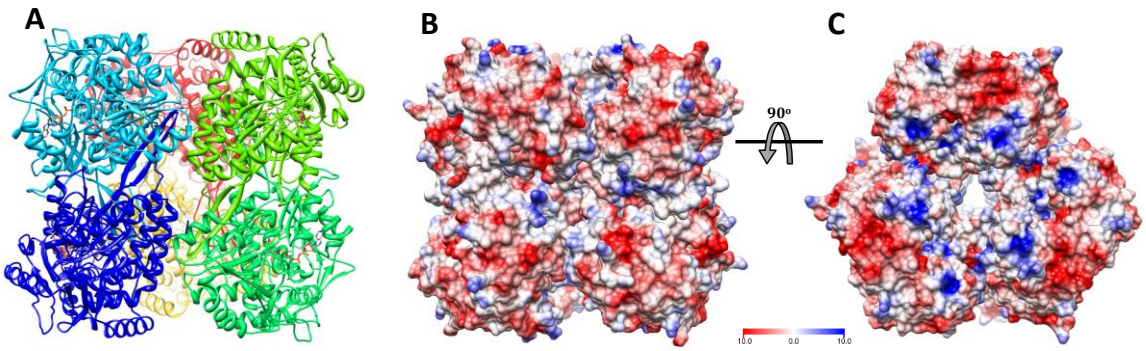

Figure 10 –Molecular and surface representation of TtP5CDH. A) Each chain of TtP5CDH hexamer is represented as cartoon and with different color. B) Coulombic surface representation of TtP5CDH oriented as left figure A and C) turned 90^{o} about the horizontal axis. The Right figure is looking down the inner core of TtP5CDH through which all the six active site gain access to substrate glutamate semialdehyde. The coulombic representation used blue color for electropositive charge and red color for electronegative charge. Figures were created using hexameric structure of TtP5CDH (PDB ID:2J40) and UCSF Chimera [49].

Based on the considerations above, a docking model of TtPRODH and TtP5CDH was made using ClusPro [50]. The docking parameters were based on electrostatic interactions without any constraints on TtPRODH or TtP5CDH orientation. The model predicts favorable docking interactions between the regions of complementary charged surfaces of TtPRODH and TtP5CDH. The electropositive N-terminal region of TtPRODH (blue surface, Figure 9B) appears to dock in close proximity to an electronegative region (red surface, Figure 10C) of TtP5CDH. Interestingly, the proposed docking model (Figure 11) is consistent with our results from SPR showing TtP5CDH only binds to immobilized TtPRODH A88C. The orientation of TtPRODH A88C would allow for the interactions in the docking model whereas the orientation of TtPRODH S8C would block the predicted docking interactions. Further analysis is required to

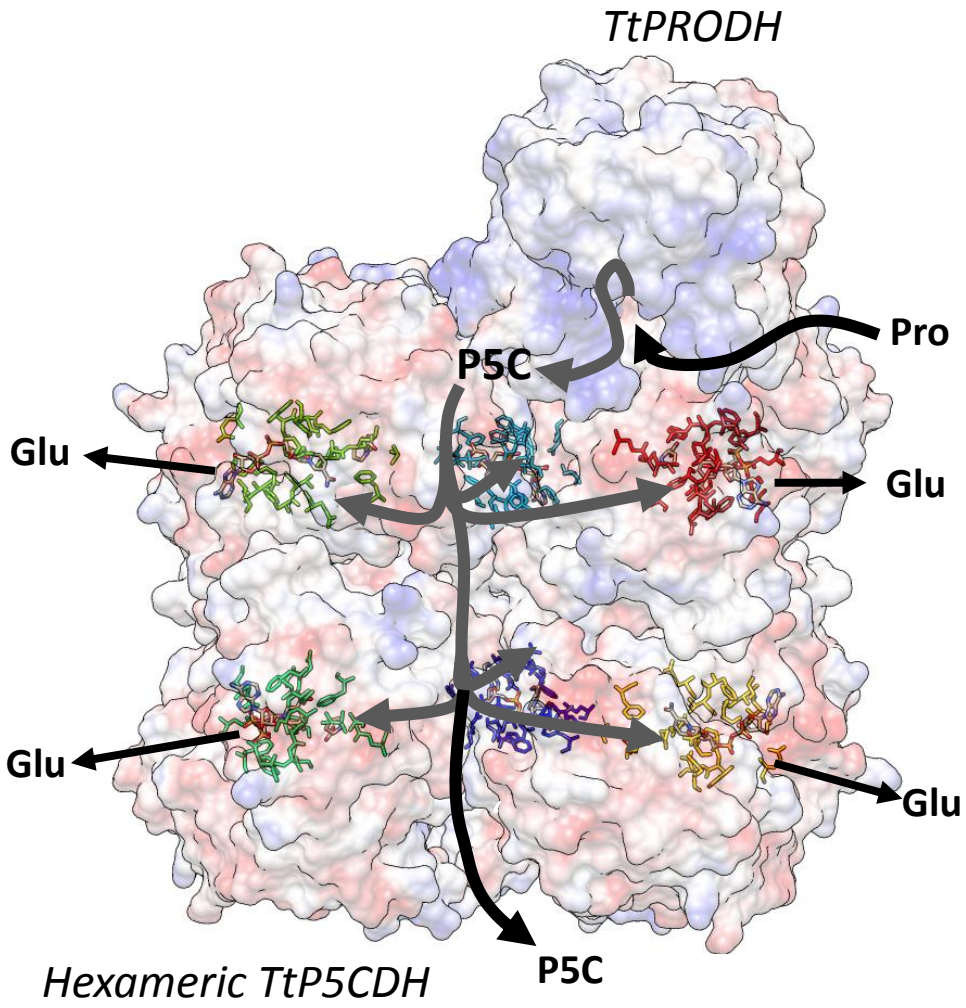

Figure 11- A scheme for substrate channeling overlaid on the predicted docking model of TtPRODH-TtP5CDH - TtPRODH and TtP5CDH are shown as transparent surfaces with coulombic charge. The orientation of TtP5CDH is identical to that shown in Figure 10 B. TtPRODH is shown docked on top of TtP5CDH as predicted by ClusPro [50]. NAD^+ and active residues for each of the six active sites of TtP5CDH are shown as colored sticks. The proposed channeling steps are indicated by grey arrows. The docking model suggests that after P5C/GSA exits TtPRODH, P5C/GSA is directed toward the inner core of the TtP5CDH hexamer. Hexameric assembly of TtP5CDH could facilitate the channeling process by sequestering P5C near the six TtP5CDH active sites. The surface representation was created using UCSF Chimera [49].

understand the stoichiometry of a putative TtPRODH-TtP5CDH complex considering that the TtP5CDH hexamer has a 3-fold symmetry. In addition, a residue conservation map of the TtP5CDH surface shows a high degree of variability in residues in the region where TtPRODH-TtP5CDH binding is predicted. This could explain why only TtP5CDH binds TtPRODH whereas the closely related DrP5CDH does not (sequence similarity 69%, identity 51%).

According to a trend observed by Nooren and Thornton, a transient heterodimer with a dissociation constant of ~ 3 μM can be expected to have an interface contact area of approximately 500 $Å^2$ [48]. In order to calculate the interface area between TtPRODH and TtP5CDH, a more thorough docking analysis is required that takes into account the solvent water molecules which may affect the TtPRODH-TtP5CDH interface. Overall, our results provide evidence that the two-step oxidation of proline to glutamate catalyzed by PRODH and P5CDH from *Thermus thermophilus* involves a channeling mechanism. This study lays the groundwork for testing substrate channeling in other monofunctional PRODH and P5CDH such as the human enzymes. TtPRODH and TtP5CDH will also serve as a model for investigating substrate channeling between other individual enzymes that catalyze consecutive reactions.

REFERENCES

1. Phang, J.M., J. Pandhare, and Y. Liu, *The metabolism of proline as microenvironmental stress substrate.* J Nutr, 2008. **138**(10): p. 2008S-2015S.
2. Takagi, H., *Proline as a stress protectant in yeast: physiological functions, metabolic regulations, and biotechnological applications.* Appl Microbiol Biotechnol, 2008. **81**(2): p. 211-23.
3. Krishnan, N., et al., *Characterization of a Helicobacter hepaticus putA mutant strain in host colonization and oxidative stress.* Infect Immun, 2008. **76**(7): p. 3037-44.
4. Curtis, J., G. Shearer, and D.H. Kohl, *Bacteriod proline catabolism affects N_2 fixation rate of drought-stressed soybeans.* Plant Physiol., 2004. **136**: p. 3313-3318.
5. Kohl, D.H., et al., *Proline metabolism in N_2-fixing root nodules: Energy transfer and regulation of purine synthesis.* Proc. Natl. Acad. Sci. USA, 1988. **85**: p. 2036-2040.
6. Lamour, N., et al., *Proline metabolism in procyclic Trypanosoma brucei is down-regulated in the presence of glucose.* J. Biol. Chem., 2005. **280**(12): p. 11902-10.
7. Tanner, J.J., *Structural biology of proline catabolism.* Amino Acids, 2008. **35**(4): p. 719-30.
8. Arentson, B.W., N. Sanyal, and D.F. Becker, *Substrate channeling in proline metabolism.* Front Biosci, 2012. **17**: p. 375-88.
9. Bearne, S.L. and R. Wolfenden, *Glutamate gamma-semialdehyde as a natural transition state analogue inhibitor of Escherichia coli glucosamine-6-phosphate synthase.* Biochemistry, 1995. **34**(36): p. 11515-20.
10. Bearne, S.L., O. Hekmat, and J.E. Macdonnell, *Inhibition of Escherichia coli CTP synthase by glutamate gamma-semialdehyde and the role of the allosteric effector GTP in glutamine hydrolysis.* Biochem J, 2001. **356**(Pt 1): p. 223-32.
11. Thoden, J.B., et al., *The small subunit of carbamoyl phosphate synthetase: snapshots along the reaction pathway.* Biochemistry, 1999. **38**(49): p. 16158-66.
12. Farrant, R.D., et al., *Pyridoxal phosphate de-activation by pyrroline-5-carboxylic acid. Increased risk of vitamin B6 deficiency and seizures in hyperprolinemia type II.* J Biol Chem, 2001. **276**(18): p. 15107-16.
13. Nomura, M. and H. Takagi, *Role of the yeast acetyltransferase Mpr1 in oxidative stress: regulation of oxygen reactive species caused by a toxic proline catabolism intermediate.* Proc Natl Acad Sci U S A, 2004. **101**(34): p. 12616-21.
14. Maxwell, S.A. and G.E. Davis, *Differential gene expression in p53-mediated apoptosis-resistant vs. apoptosis-sensitive tumor cell lines.* Proc Natl Acad Sci U S A, 2000. **97**(24): p. 13009-14.

15. Srivastava, D., et al., *Crystal structure of the bifunctional proline utilization A flavoenzyme from Bradyrhizobium japonicum.* Proceedings of the National Academy of Sciences, 2010. **107**(7): p. 2878-2883.
16. Ovadi, J., *Physiological significance of metabolic channelling.* J Theor Biol, 1991. **152**(1): p. 1-22.
17. Singh, R.K., et al., *Small-angle X-ray scattering studies of the oligomeric state and quaternary structure of the trifunctional proline utilization A (PutA) flavoprotein from Escherichia coli.* J Biol Chem, 2011. **286**(50): p. 43144-53.
18. White, T.A., et al., *Structure and kinetics of monofunctional proline dehydrogenase from Thermus thermophilus.* J Biol Chem, 2007. **282**(19): p. 14316-27.
19. Inagaki, E., et al., *Crystal structure of Thermus thermophilus Delta1-pyrroline-5-carboxylate dehydrogenase.* J Mol Biol, 2006. **362**(3): p. 490-501.
20. Geck, M.K. and J.F. Kirsch, *A novel, definitive test for substrate channeling illustrated with the aspartate aminotransferase/malate dehydrogenase system.* Biochemistry, 1999. **38**(25): p. 8032-7.
21. Rakus, D., et al., *Interaction between muscle aldolase and muscle fructose 1,6-bisphosphatase results in the substrate channeling.* Biochemistry, 2004. **43**(47): p. 14948-57.
22. James, C.L. and R.E. Viola, *Production and characterization of bifunctional enzymes. Substrate channeling in the aspartate pathway.* Biochemistry, 2002. **41**(11): p. 3726-31.
23. Lherbet, C., et al., *Absence of substrate channeling between active sites in the Agrobacterium tumefaciens IspDF and IspE enzymes of the methyl erythritol phosphate pathway.* Biochemistry, 2006. **45**(11): p. 3548-53.
24. Szabo, A., L. Stolz, and R. Granzow, *Surface plasmon resonance and its use in biomolecular interaction analysis (BIA).* Curr Opin Struct Biol, 1995. **5**(5): p. 699-705.
25. Dunn, M.F., et al., *The tryptophan synthase bienzyme complex transfers indole between the alpha- and beta-sites via a 25-30 A long tunnel.* Biochemistry, 1990. **29**(37): p. 8598-607.
26. Zhang, S., et al., *Chorismate mutase-prephenate dehydratase from Escherichia coli. Study of catalytic and regulatory domains using genetically engineered proteins.* J Biol Chem, 1998. **273**(11): p. 6248-53.
27. Thoden, J.B., et al., *Structure of carbamoyl phosphate synthetase: a journey of 96 A from substrate to product.* Biochemistry, 1997. **36**(21): p. 6305-16.
28. Lu, Y., Y.H. Zhang, and L.R. Lynd, *Enzyme-microbe synergy during cellulose hydrolysis by Clostridium thermocellum.* Proc Natl Acad Sci U S A, 2006. **103**(44): p. 16165-9.

29. Srere, P.A. and J. Ovadi, *Enzyme-enzyme interactions and their metabolic role.* FEBS Lett, 1990. **268**(2): p. 360-4.
30. Williams, I. and L. Frank, *Improved chemical synthesis and enzymatic assay of delta-1-pyrroline-5-carboxylic acid.* Anal Biochem, 1975. **64**(1): p. 85-97.
31. Grauschopf, U., A. Fritz, and R. Glockshuber, *Mechanism of the electron transfer catalyst DsbB from Escherichia coli.* Embo J, 2003. **22**(14): p. 3503-13.
32. Lineweaver, H. and D. Burk, *The determination of enzyme dissociation constants.* J. Am. Chem. Soc., 1934. **56**: p. 658-666.
33. Becker, D.F. and E.A. Thomas, *Redox properties of the PutA protein from Escherichia coli and the influence of the flavin redox state on PutA-DNA interactions.* Biochemistry, 2001. **40**: p. 4714-4722.
34. Srivastava, D., et al., *The three-dimensional structural basis of type II hyperprolinemia.* J Mol Biol, 2012. **420**(3): p. 176-89.
35. Meek, T.D., E.P. Garvey, and D.V. Santi, *Purification and characterization of the bifunctional thymidylate synthetase-dihydrofolate reductase from methotrexate-resistant Leishmania tropica.* Biochemistry, 1985. **24**(3): p. 678-86.
36. Xu, D., C.J. Tsai, and R. Nussinov, *Hydrogen bonds and salt bridges across protein-protein interfaces.* Protein Eng, 1997. **10**(9): p. 999-1012.
37. DeLano, W.L., *The PyMOL Molecular Graphics System.* DeLano Scientific, San Carlos, CA, USA., 2002.
38. Szabados, E. and R.I. Christopherson, *Relationship between the catalytic sites of human bifunctional IMP synthase.* The International Journal of Biochemistry & Cell Biology, 1998. **30**(8): p. 933-942.
39. Baker, P., J. Carere, and S.Y. Seah, *Substrate specificity, substrate channeling, and allostery in BphJ: an acylating aldehyde dehydrogenase associated with the pyruvate aldolase BphI.* Biochemistry, 2012. **51**(22): p. 4558-67.
40. Zhang, M., et al., *Structures of the Escherichia coli PutA proline dehydrogenase domain in complex with competitive inhibitors.* Biochemistry, 2004. **43**(39): p. 12539-48.
41. Gonzalez, N., J. Wiggs, and M.J. Chamberlin, *A simple procedure for resolution of Escherichia coli RNA polymerase holoenzyme from core polymerase.* Arch Biochem Biophys, 1977. **182**(2): p. 404-8.
42. Ray Williams, M.K.a.R.S., *BSA and Restriction Enzyme Digestions* Promega Notes, 1996. **59**.
43. Manevski, N., et al., *Albumin stimulates the activity of the human UDP-glucuronosyltransferases 1A7, 1A8, 1A10, 2A1 and 2B15, but the effects are enzyme and substrate dependent.* PLoS One, 2013. **8**(1): p. e54767.
44. Yang, B. and C.E. Wyman, *BSA treatment to enhance enzymatic hydrolysis of cellulose in lignin containing substrates.* Biotechnol Bioeng, 2006. **94**(4): p. 611-7.

45. Huang, X., H.M. Holden, and F.M. Raushel, *Channeling of substrates and intermediates in enzyme-catalyzed reactions.* Annu Rev Biochem, 2001. **70**: p. 149-80.
46. Perkins, J.R., et al., *Transient protein-protein interactions: structural, functional, and network properties.* Structure, 2010. **18**(10): p. 1233-43.
47. Surber, M.W. and S. Maloy, *The PutA protein of Salmonella typhimurium catalyzes the two steps of proline degradation via a leaky channel.* Arch Biochem Biophys, 1998. **354**(2): p. 281-7.
48. Nooren, I.M. and J.M. Thornton, *Structural characterisation and functional significance of transient protein-protein interactions.* J Mol Biol, 2003. **325**(5): p. 991-1018.
49. Pettersen, E.F., et al., *UCSF Chimera--a visualization system for exploratory research and analysis.* J Comput Chem, 2004. **25**(13): p. 1605-12.
50. Comeau, S.R., et al., *ClusPro: an automated docking and discrimination method for the prediction of protein complexes.* Bioinformatics, 2004. **20**(1): p. 45-50.
51. Chen, M., et al., *Directed evolution of an artificial bifunctional enzyme, gamma-glutamyl kinase/gamma-glutamyl phosphate reductase, for improved osmotic tolerance of Escherichia coli transformants.* FEMS Microbiol Lett, 2006. **263**(1): p. 41-7.
52. Bennett, B.D., et al., *Absolute metabolite concentrations and implied enzyme active site occupancy in Escherichia coli.* Nat Chem Biol, 2009. **5**(8): p. 593-9.
53. Csonka, L.N., *Regulation of cytoplasmic proline levels in Salmonella typhimurium: effect of osmotic stress on synthesis, degradation, and cellular retention of proline.* J Bacteriol, 1988. **170**(5): p. 2374-8.
54. Roesser, M. and V. Muller, *Osmoadaptation in bacteria and archaea: common principles and differences.* Environ Microbiol, 2001. **3**(12): p. 743-54.
55. Whatmore, A.M., J.A. Chudek, and R.H. Reed, *The effects of osmotic upshock on the intracellular solute pools of Bacillus subtilis.* J Gen Microbiol, 1990. **136**(12): p. 2527-35.
56. Kosuge, T. and T. Hoshino, *Construction of a proline-producing mutant of the extremely thermophilic eubacterium Thermus thermophilus HB27.* Appl Environ Microbiol, 1998. **64**(11): p. 4328-32.
57. Chen, C., et al., *Tomato QM-like protein protects Saccharomyces cerevisiae cells against oxidative stress by regulating intracellular proline levels.* Appl Environ Microbiol, 2006. **72**(6): p. 4001-6.
58. Morita, Y., S. Nakamori, and H. Takagi, *L-proline accumulation and freeze tolerance of Saccharomyces cerevisiae are caused by a mutation in the PRO1 gene encoding gamma-glutamyl kinase.* Appl Environ Microbiol, 2003. **69**(1): p. 212-9.

59. Jaksic, T., D.A. Wagner, and V.R. Young, *Plasma proline kinetics and concentrations in young men in response to dietary proline deprivation.* Am J Clin Nutr, 1990. **52**(2): p. 307-12

CHAPTER 3

Purification and Characterization of Put1p and Put2p from *Saccharomyces cerevisiae*

Note: This chapter contains results published in the research article: "Purification and characterization of Put1p from Saccharomyces cerevisiae." Wanduragala S*, Sanyal N*, Liang X, Becker DF. Arch Biochem Biophys. 2010 Jun 15;498(2):136-42. (*Equal contribution). Permission for usage in thesis obtained from Elsevier B.V.

INTRODUCTION

The oxidative conversion of proline to glutamate involves two enzymes, a flavin dependent proline dehydrogenase (PRODH) and a NAD^+-dependent Δ^1-pyrroline-5-carboxylate (P5C) dehydrogenase (P5CDH). PRODH and P5CDH help organisms respond to changes in the nutritional environment by initiating the breakdown of proline as a source for nitrogen, carbon, and energy [1-6]. In *Saccharomyces cerevisiae*, Put1p and Put2p are the corresponding PRODH and P5CDH enzymes, respectively (Scheme 1) [7]. In yeast and other eukaryotes, PRODH and P5CDH are localized in the mitochondria [8, 9]. PRODH catalyzes the first step of proline oxidation by generating P5C, an intermediate in the proline catabolic pathway (see Scheme 1). The reaction involves two phases or two half-reactions. In the reductive half-reaction electrons are transferred from proline to the flavin adenine dinucleotide cofactor to form P5C. The second phase (i.e., oxidative half-reaction) of the catalytic cycle involves oxidation of reduced flavin ($FADH_2$) to regenerate FAD. P5C is then hydrolyzed to γ-glutamic acid semialdehyde (GSA) which is subsequently oxidized by P5CDH to form glutamate and NADH.

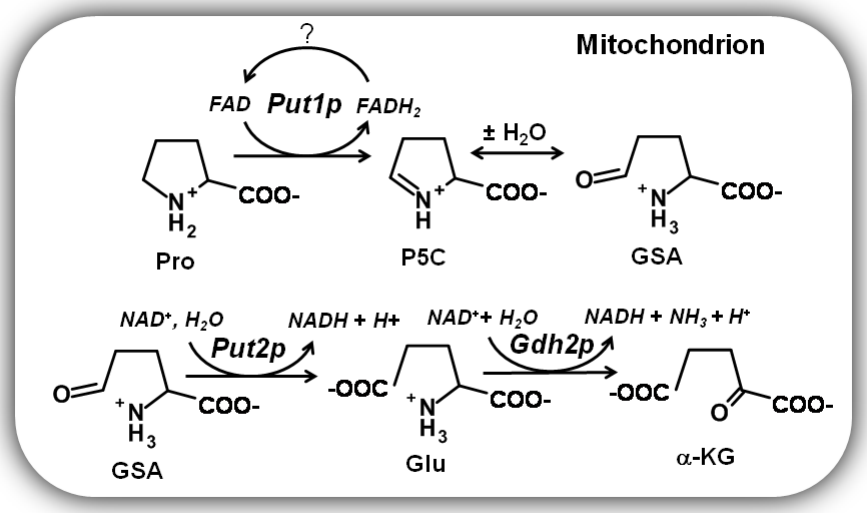

Scheme 1- Overview of proline catabolism in *S. cerevisiae*.

Expression of the *PUT1* and *PUT2* genes in yeast is sensitive to proline levels and nitrogen quality. In the presence of preferred nitrogen sources such as glutamine and ammonia, *PUT* gene expression is repressed [10]. In nitrogen limiting environments, *PUT1* and *PUT2* expression is upregulated coinciding with derepression of the *PUT4* gene which encodes a proline specific transporter [10]. Activation of the *PUT1 and PUT2* genes is regulated by Put3p, a transcriptional regulator which directly senses proline and belongs to the $Zn(II)_2Cys_6$ protein family [11-13]. Binding of proline to Put3p leads to a 20-fold activation of the *PUT* genes [12]. Put3p also induces small increases in *PUT* gene expression independently of proline in response to poor nitrogen sources [13]. The resulting Put3p activation of the *PUT1* and *PUT2* genes enables yeast to utilize proline as a nitrogen source in coordination with glutamate dehydrogenase (Gdh2p) which oxidatively deaminates glutamate to generate ammonia and α-ketoglutarate (Scheme 1) [10, 14].

Human PRODH (*PRODH1*), also known as proline oxidase (POX1), is of particular importance as it has been shown to have unique roles in regulating cell survival and apoptotic pathways [1, 15]. Expression of human PRODH is upregulated by the tumor suppressor p53 protein with increased PRODH activity leading to induction of cell death pathways and helping to prevent cancer progression [16, 17]. Using a mouse xenograft tumor model, Phang and colleagues recently showed that PRODH activity significantly reduces tumor formation [18]. The mechanism by which human PRODH contributes to apoptosis involves the generation of reactive oxygen species such as superoxide anions either directly at the enzyme active site or indirectly due to increased electron flux in the mitochondrial electron pathway.

Although PRODH has important roles in energy metabolism, nitrogen utilization, and in mammals, the programmed cell death pathway, detailed information about the biochemical and structural properties of PRODH from a eukaryotic organism are still lacking. In bacteria, the best characterized PRODH enzymes from bacteria are the bifunctional PutA enzymes which encode PRODH and P5CDH on a single polypeptide and the monofunctional PRODH enzyme from *Thermus thermophilus* (TtPRODH) [19, 20]. X-ray crystal structures of the PRODH domain of PutA from *Escherichia coli* (EcPutA) and TtPRODH show a common $(\beta\alpha)_8$ barrel fold with a noncovalently bound FAD cofactor [19-21]. Human PRODH and Put1p most likely share the same $(\beta\alpha)_8$ barrel fold and sequence alignments with the bacterial enzymes show human PRODH and Put1p also share important residues for substrate and FAD binding [19].

To better understand PRODH and P5CDH enzymes from eukaryotic organisms, we sought to purify and characterize Put1p and Put2p from *S. cerevisiae*. Particular focus was given to the oxidative half-reaction of Put1p and its reactivity with molecular oxygen as it may provide insight into the physiological role of human PRODH in superoxide production and apoptotic signaling pathways. The direct electron acceptor for Put1p in the oxidative half-reaction has not been demonstrated but a functional mitochondrial respiratory chain is necessary for *S. cerevisiae* to utilize proline as a nitrogen source [8]. Based on steady state kinetics, we propose that Put1p directly couples proline oxidation to ubiquinone reduction in the electron transport chain.

EXPERIMENTAL PROCEDURES

Materials

Ubiquinone-1 (CoQ_1), flavin adenine dinucleotide (FAD), nicotinamide adenine dinucleotide (NAD^+), L-tetrahydro-2-furoic acid (L-THFA), succinic semialdehyde, phenazine methosulfate, guanidium hydrochloride, antibiotics and buffers were purchased from Sigma-Aldrich. 2,6-dichlorophenolindophenol (DCPIP), *o*-aminobenzaldehyde (*o*-AB), isopropyl β-D-1-thiogalactopyranoside (IPTG), sodium chloride and Tris-HCl were purchased from Fisher Scientific Inc. L-proline was purchased from Acros Organics Ltd. All other chemicals and buffers were purchased from Sigma-Aldrich, Inc. Molecular size standards used for calibrating size exclusion columns were purchased from Sigma. Bicinchoninic acid (BCA) reagent used for protein quantitation was obtained from Pierce. All experiments used Nanopure water. D,L-P5C was chemically synthesized from DL-hydroxylysine as described previously by Williams and Frank and stored in 1M HCl at 4^{o}C [22]. D,L-P5C contains equimolar concentration of D-P5C and L-P5C.

Constructs

The *PUT1* and *PUT2* clones were a generous gift from Dr. Marjorie Brandriss at the University of Medicine and Dentistry of New Jersey-New Jersey Medical School [23]. The genes were expressed from a pET14b expression vector containing N-terminal 6x his tag. Put1p protein lacked the 18 residue mitochondrial signaling peptide (Put1pΔ18). Put2p was expressed as a full-length protein.

Purification and characterization of Put1p and Put2p

Put1pΔ18 and Put2p were expressed and purified from *E. coli* strain BL21(DE3) pLysS with a N-terminal 6xHis tag using the pET14b expression vector as described here. The pET14b-PUT1Δ18 and pET14b-PUT2 constructs were transformed into *E. coli* BL21(DE3) pLysS. Transformed cells were plated onto Luria-Bertani (LB) agar containing chloramphenicol (34 μg/ml) and ampicillin (50 μg/ml). Resulting colonies were inoculated in 5 ml of LB broth containing the necessary antibiotics and grown to an optical density at 600 nm (OD_{600}) of 1.0. 1 ml of the LB culture was then used to inoculate 1 L of Terrific Broth media containing chloramphenicol (34 μg/ml) and ampicillin (50 μg/ml). The 1 L cultures were incubated at 37^{o}C with shaking (250 rpm) until OD_{600} of 0.8 at which point Put1p expression was induced with 0.5 mM IPTG overnight at 20^{o}C.

The overnight cultures were centrifuged at 6000 rpm for 20 min at 4^{o}C. The resulting pellets were resuspended in a final 50 ml volume of binding buffer (20 mM Tris, 5 mM imidazole, 0.5 M NaCl, 10% glycerol, pH 7.9) supplemented with protease inhibitors (3 mM ε-amino-N-caproic acid, 0.3 mM phenyl methyl sulfonyl chloride, 1.2 μM leupeptin, 48 μM N-*p*-tosyl-L-phenyl alanine chloromethyl ketone, 78 μM N-α-tosyl-L-lysine chloromethylketone). Additionally, 1 mM FAD and 0.5% *n*-octyl-β-D-glucoside was supplemented for Put1p purification. The cell suspension was disrupted by sonication at 4^{o}C for a total of 5 min (5 sec pulse on, 15 sec pulse off, 40% power). The cell extract was centrifuged at 16000 rpm (4^{o}C) for 60 min. The supernatant (50 ml) was passed through a 0.8 μm filter (VWR) and applied to a Ni-NTA superflow (Qiagen) resin (25 ml bed volume in a 2.8 cm x 30 cm column) equilibrated with 1X binding buffer. Wash

buffer (125 ml, 20 mM Tris, 60 mM imidazole, 0.5 M NaCl, 10% glycerol, pH 7.9) was then applied to the column followed by elution buffer (20 mM Tris, 500 mM imidazole, 0.5 M NaCl, 10% glycerol, pH 7.9) with a flow rate of 3 ml/min to elute protein fractions. Fractions from the elution step were then analyzed by SDS-PAGE and pooled. Pooled Put1p was then dialyzed into 50 mM Tris buffer (pH 8.1) containing 10% glycerol and concentrated using an Amicon 30-kDa cutoff filter (Millipore). Put2p was dialyzed into 50 mM Tris buffer (pH 7.9) containing 25% glycerol.

The molar ratio of flavin to Put1p polypeptide was estimated by denaturing Put1p in 6 M guanidinium chloride. The spectrum was recorded from 600 to 250 nm. The total amount of polypeptide was determined using the molar extinction coefficient of denatured Put1p at 280 nm (A_{280}= 45060 $M^{-1}cm^{-1}$) estimated by the ProtParam tool (ExPASy Proteomics Server). The amount of flavin was determined using the molar extinction coefficient for free FAD at 450 nm (A_{450}= 11700 M^{-1} cm^{-1}) in guanidinium chloride [24]. The molar extinction coefficient of flavin bound to Put1p was estimated to be 10800 M^{-1} cm^{-1} at 451 nm. The concentration of total Put1p protein was determined using the BCA method [25] while the concentration of flavin-bound Put1p was determined using the molar extinction coefficient for bound FAD (A_{451} = 10800 M^{-1} cm^{-1}).

The oligomeric size of Put1p and Put2p were estimated using gel filtration chromatography. Superdex-200 10/300 GL prepacked column (GE Healthcare) was equilibrated with running buffer (50 mM Tris, pH 8, 150 mM NaCl). Purified Put1p and Put2p were diluted to a concentration of 2 mg/ml in a volume of 250 µL in running buffer. All samples and standards were spun at 10,000 rpm for 5 min prior to applying on

column. The proteins were individually applied on the Superdex-200 column with a flow rate of 0.5 ml/min at 4^{o}C on a BioRad Biologic purification system (Lab of Dr. Joseph Barycki, University of Nebraska-Lincoln). Elution of fractions was analyzed using A_{280} nm detection.

Steady-state kinetic measurements

Put1p kinetics

Put1p activity was measured at 25^{o}C using terminal electron acceptors DCPIP, oxygen and CoQ_1. The concentrations of Put1p used for all of the kinetic assays are based on the amount of flavin-bound Put1p. Proline:DCPIP oxidoreductase assay was performed as described in a 1-ml reaction volume using Cary 100 and Cary 50 UV-visible spectrophotometers [26]. The DCPIP assay mixture contained 0.05 μM of Put1p enzyme, 0.27 mM phenazine methosulfate, 75 μM DCPIP and proline concentrations ranging from 0 to 300 mM in 20 mM Tris at pH 8.0. The rate of DCPIP reduction was measured at 595 nm (ε = 16100 cm^{-1} M^{-1}) [26]. Proline:O_2 oxidoreductase activity (1 ml assay volume) was measured in air saturated potassium phosphate buffer (50 mM, pH 8.0) using 1 μM Put1p, 4 mM *o*-AB and 0-300 mM proline at 443 nm by following the formation of the *o*-AB-P5C yellow complex (ε = 2590 cm^{-1} M^{-1}) [27]. Oxygen utilization by Put1p was also measured using a Clark type Pt,Ag/AgCl-electrode. The reaction mixture contained 2.2 μM Put1p and 300 mM proline in 50 mM phosphate buffer at pH 8.0 (25 °C).

CoQ_1 reduction was measured using 0.1 μM Put1p in 50 mM phosphate buffer at pH 8.0 with 0-300 mM proline and 0-100 μM CoQ_1. Reduction of CoQ_1 was followed at 275 nm (ε= 13700 cm^{-1} M^{-1}) using a 0.15 cm path length on a Hi-Tech Scientific SF-61DX2

stopped-flow instrument at 25°C [28]. The kinetic parameters K_m and k_{cat} were estimated by regression analysis of the initial reaction velocity versus proline concentration using the Michaelis-Menten equation and Lineweaver-Burk plot analysis [29]. The binding order of the Put1p proline:CoQ_1 oxidoreductase reaction was evaluated using double reciprocal plots of reaction velocity versus variable substrate concentrations. Assays were performed in 50 mM potassium phosphate (pH 8.0) using 0. 2 µM Put1p and with proline concentrations varied from 5-150 mM and CoQ_1 concentrations varied 5-60 µM. Using global curve fit analysis in SigmaPlot 11 software, data was fitted to a classical ping-pong mechanism (Equation 3.1).

$$v = \frac{V_{max}[A][B]}{K_{mB}[A] + K_{mA}[B] + [A][B]} \qquad (3.1)$$

Inhibition studies with L-THFA were performed using the DCPIP assay as described previously [30]. For these assays, proline concentrations were varied from 0 – 200 mM and the final L-THFA concentrations were varied from 0 – 6 mM using 100X stock solutions of L-THFA in 50 mM Tris buffer (pH 8.0). The inhibition constant (K_i) for L-THFA was estimated by Dixon plot analysis [31]. For all of the above experiments, the initial velocity values were the average from assays performed in duplicate or triplicate.

Proline titration of Put1p

Proline titrations of Put1p were performed at 20 °C in 50 mM Tris buffer (pH 8.0) containing 50 mM NaCl and 10% glycerol under anaerobic conditions. The Put1p-proline mixtures were equilibrated 5 min after each addition of proline prior to recording each spectrum on a Cary 100 spectrophotometer. A correction for turbidity that occurred

during the experiment was applied by subtracting a light scattering spectrum. The amount of turbidity in each spectrum was determined by measuring the increase in absorbance at 700 nm due to scattering. The titration data were analyzed as previously described assuming the formation of a reduced PutA-P5C complex [26, 32]. Although P5C is hydrolyzed to the open GSA form, the ring and open chain forms are rapidly reversible with P5C favored at pH > 7.0, indicating that P5C will be the predominant form at pH 8.0 [33].

Put2p kinetics

Put2p activity was measured by monitoring the formation of NADH at 340 nm (ε = 6400 cm^{-1} M^{-1}[34]) at 25 °C. The assay buffer contained 50 mM potassium phosphate (pH 7.5) and 25 mM NaCl. Put2p enzyme concentration was 0.4 μM (25.6 μg/ml) and NAD^+ concentration was 0.2 mM. Varying concentrations of L-P5C ranging from 1 to 300 μM were used. Steady-state kinetics was also performed using 2-100 mM succinic semialdehyde as an alternative substrate. Initial rates were fitted to a Michaelis-Menten equation (equation 3.2).

$$v = \frac{V_{max}[S]}{K_m + [S]} \qquad (3.2)$$

pH dependence of Put1p and Put2p activity

The pH optimum for Put1p and Put2p activity was determined using a mixed buffer system from pH 6.0–9.0 comprised of 20 mM each HEPES, MES, MOPS and TAB (80 mM total). Put1p activity was measured by Proline:DCPIP oxidoreductase assay using 0.1 μM Put1p and 220 mM proline. Put2p activity was measured by monitoring NADH

formation as described above except using 0.27 µM Put2p and 70 µM L-P5C. Data were fit to the equation :

$$vel = \frac{v_{lim}}{1 + 10^{\mathrm{p}Ka1 - pH} + 10^{pH - \mathrm{p}Ka2}} \qquad (3.3)$$

where v_{lim} is the limiting velocity (µmol/min) and pK_{a1} and pK_{a2} represent the acidic and alkaline ionizations that contribute to the pH dependent curve of the reaction velocity.

RESULTS

Molecular properties of Put1p and Put2p

Purified Put1p lacking the N-terminal residues 1-18 (Put1pΔ18) was shown by SDS-PAGE to have an apparent molecular weight of 50 kDa (Figure 1A) which nearly matches the predicted molecular weight of 53665 Da for the product of the N-terminal 6xHis Put1pΔ18 construct. SDS-PAGE analysis showed that purified Put2p had an apparent molecular weight of 64 kDa which is similar to its predicted molecular weight of 64304 Da (Figure 1B). The oligomeric states of Put1p and Put2p were studied using gel filtration chromatography. Figure 1C shows the elution profile of the two proteins. Calculated molecular weight of Put1p in solution is 1,229,316 Da. Such a high molecular weight is suggestive of aggregate formation in solution. The molecular weight of Put2p was estimated to be 265,292 Da and is indicative of a tetramer in solution.

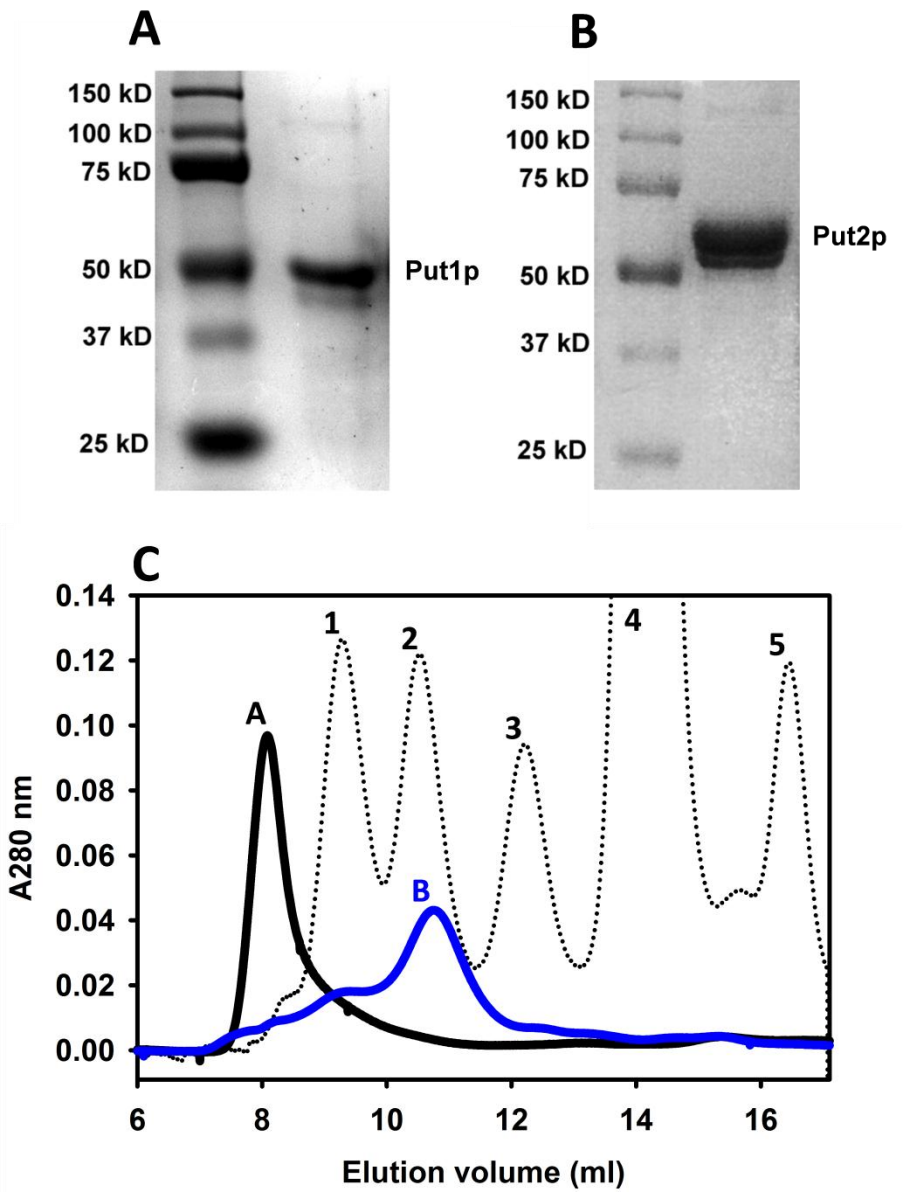

Figure 1- Analysis of molecular weight of purified Put1p and Put2p. SDS-PAGE analysis of A) Put1p (3 µg) and B) Put2p (15 µg) each purified from *E. coli*. Predicted molecular weights of Put1p and Put2p are 53665 Da and 64304 Da, respectively. C) Analysis of the oligomeric size of Put1p (solid black trace) and Put2p (solid blue trace) by gel filtration chromatography. Using a plot of $\log_{10}$[molecular weight] versus elution volume of molecular weight standards, the estimated oligomeric size of Put1p and Put2p were 1,229,316 Da and 265,292 Da. For the molecular weight, Put1p is expected to be aggregated in solution and Put2p is expected to be a homotetramer. Molecular size standards are indicated as dotted curve. 1-thyroglobulin (M_r 669,000 Da), 2-ferritin (M_r 440,000 Da), 3-bovine serum albumin (M_r 67,000 Da), 4-carbonic anhydrase (M_r 29,000 Da) and 5-RNase A (M_r 13,700 Da).

Kinetic characterization

The UV-visible spectrum of Put1p is shown in Figure 2. Absorption maxima are at 355 and 450 nm with a shoulder at 478 nm and are indicative of a bound FAD cofactor to the Put1p protein. (Figure 2, Inset A). Quantitation of the polypeptide at 280 nm and the flavin at 451 nm indicates a flavin/polypeptide ratio of 0.43. The flavin/polypeptide ratios varied from 0.3–0.45 between different preparations. Thus, recombinant Put1p contains a significant amount of the apo-form. Addition of proline to Put1p resulted in reduction of the flavin cofactor in a concentration dependent manner (Figure 2, Inset B). No anionic semiquinone was observed indicating flavin semiquinone is not stabilized during proline

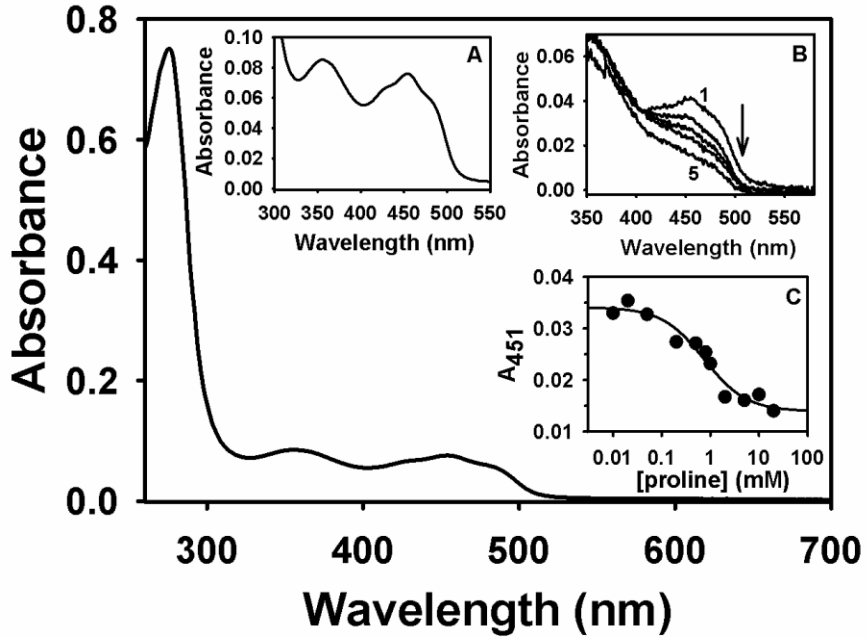

Figure 2- Spectral properties of purified Put1p. Put1p in 20 mM Tris–HCl buffer (pH 8.0) containing 100 mM NaCl and 0.25% octyl-glucoside. Concentrations of total and flavin-bound Put1p protein are 16.1 and 7 μM, respectively. Inset A, flavin spectrum from 550 to 300 nm of the same Put1p protein shown below. Inset B, titration of Put1p (3.8 μM flavin-bound form) with proline in 50 mM Tris–NaCl buffer (pH 8.0). Curves 1–5 are selected spectra from the titration at 0, 0.01, 0.200, 1.0, and 5 mM proline. Inset C, best fit analysis of the absorbance decrease at 451 nm during the titration with proline assuming the formation of a Put1p–P5C complex from which a K_{eq} of 1.4 mM^{-1} proline was estimated.

reduction. 50% of the FAD in Put1p was reduced at 0.7 mM proline as estimated from the plot shown in Figure 2 (Inset C).

Kinetic parameters for Put1p using the proline:DCPIP oxidoreductase assay were K_m = 36 ± 5 mM proline and k_{cat} = 27 s^{-1}. The K_m value is similar to that reported for the monofunctional TtPRODH enzyme (K_m = 27 mM proline, k_{cat} = 13 s^{-1}) but the turnover number is about 2-fold higher [20]. For PutA enzymes, K_m values range from 100-150 mM proline with turnover numbers around 5-12 s^{-1} [35]. The kinetic parameters for Put1p along with TtPRODH may indicate that monofunctional enzymes generally exhibit higher turnover numbers and a lower K_m values for proline than bifunctional PutA enzymes.

Put2p kinetic parameters measured by NADH reduction indicate a K_m of 104.2 ± 4.4 µM L-P5C and a turnover number (k_{cat}) of 1.49 ± 0.26 sec^{-1}. In comparison *Thermus thermophilus* P5CDH has a K_m of 42.7 ± 1.1 µM L-P5C and k_{cat} of 0.52 ± 0.03 sec^{-1} (Chapter 2) and Human P5CDH has a K_m of 31.6 ± 7.9 µM L-P5C and k_{cat} of 10.0 ± 0.9 sec^{-1} [34].

pH dependence of Put1p and Put2p activity

The pH optimum for the Put1p reaction was determined by following proline:DCPIP oxidoreductase activity over the pH range 6–9. Figure 3 shows a symmetrical and bell-shaped curve for Put1p activity with a pH optimum of 8.25. By fitting the data to equation 3.3, pK_a values of 7.54±0.09 (pK_{a1}) and 9.18±0.13 (pK_{a2}) were estimated for the two ionization events observed in the pH dependence of Put1p activity. Over a pH range of 6-9, activity of Put2p also exhibited a symmetrical bell-shaped curve. However, a more acidic pH optimum for Put2p activity was observed. The peak activity was seen at 7.15 and pK_a values of 6.03±0.13 (pK_{a1}) and 8.31±0.11 (pK_{a2}) were estimated for the ascending and descending limbs of the curve, respectively.

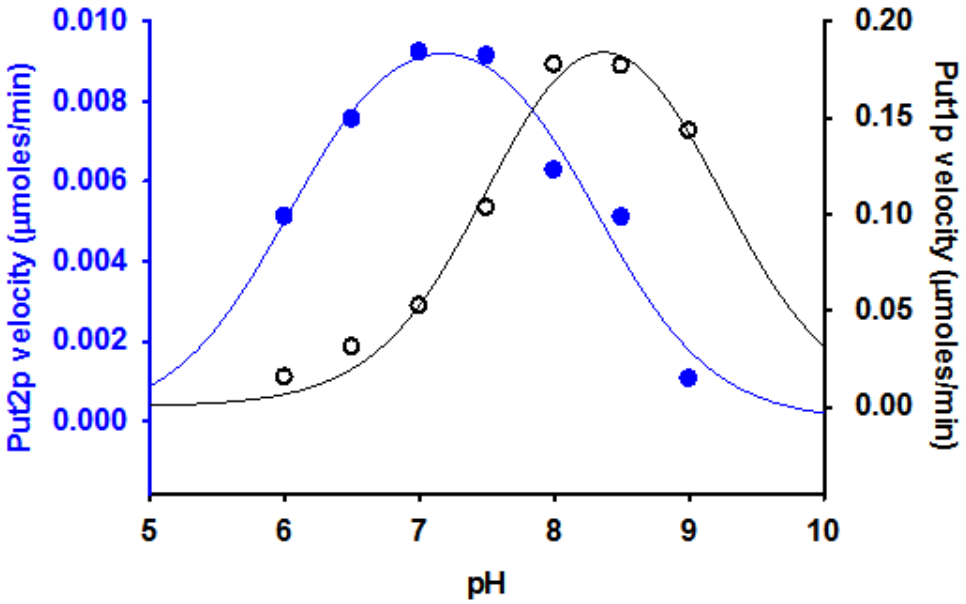

Figure 3- pH profiles of Put1p and Put2p enzymatic activity. The pH profile for the Put1p reaction (black open circles) was determined by following proline:DCPIP oxidoreductase activity using 0.1 µM Put1p and 220 mM proline over the pH range 6–9 at 25°C. Put2p activity was measured by NADH formation assay using 0.27 µM Put2p and 70 µM L-P5C (blue closed circles). The pK_a values for Put1p and Put2p were estimated by fitting the data to equation 3.3. pK_a values of 7.54±0.09 (pK_{a1}) and 9.18±0.13 (pK_{a2}) with a pH optimum of 8.25 were estimated for Put1p (black curve). Put2p was estimated to have peak activity at 7.15 and pK_a values of 6.03±0.13 (pK_{a1}) and 8.31±0.11 (pK_{a2}) (blue curve). pK_{a1} and pK_{a2} are the ionization constants for two ionizable groups that influence the observed pH dependence of Put1p and Put2p activity.

Substrate specificity and inhibition

The ability of Put1p to use alternative substrate *trans*-4-hydroxy-L-proline and was tested. Only very low activity (0.008 U/mg) was observed with 4-hydroxy-L-proline which is more than 2000-fold lower than the specific activity of Put1p with proline (18 U/mg).). Put1p also exhibited very low activity (0.004 U/mg) with L-pipecolic acid and no activity with D-proline. Thus Put1p has strong substrate specificity for L-proline.

A potent inhibitor of PRODH activity is L-THFA, an isostructural analog of proline. Previously, TtPRODH was shown to be inhibited by L-THFA with a K_i of 1 mM [20].

Figure 4 shows a Dixon plot analysis of the inhibition of Put1p activity by L-THFA. The plot is consistent with L-THFA acting as a competitive inhibitor of Put1p with a K_i of 5.5 mM. Most likely L-THFA binds to the active site of Put1p similarly to that observed in the X-ray crystal structures of the *E. coli* PRODH domain complexed with L-THFA [36].

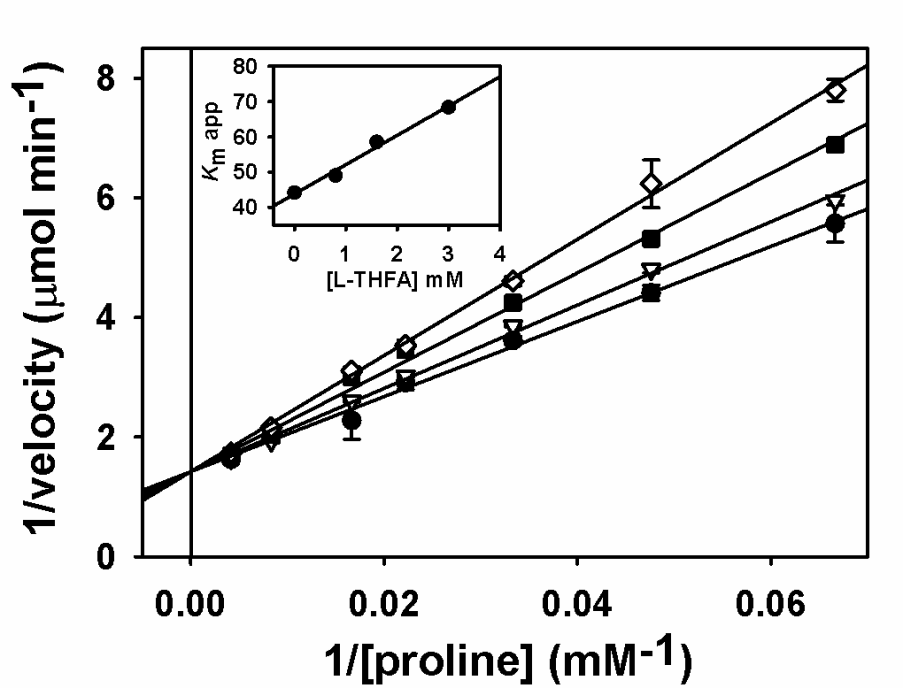

Figure 4- Inhibition of Put1p activity by L-THFA. A K_i value of 5.5 mM THFA was estimated by Dixon plot analysis of the reaction velocity versus L-THFA at various proline concentrations (0-200 mM).

The substrate for Put2p is open-chained GSA which is in a non-enzymatic equilibrium with cyclic P5C. We wanted to test Put2p activity using an obligate open-chain substrate such as succinic semialdehyde. Put2p exhibits a 15000-fold lower k_{cat}/K_m with succinic semialdehyde (k_{cat}/K_m = 0.974 M^{-1} s^{-1}) relative to P5C/GSA (k_{cat}/K_m = 14900 M^{-1} s^{-1}) Thus, succinic semialdehyde is a relatively poor substrate for Put2p.

Oxidative half-reaction

Because upregulation of human PRODH1 (or POX) activity leads to the formation of reactive oxygen species and has important roles in apoptosis, we sought to characterize the reactivity of Put1p with oxygen. The reactivity of Put1p with molecular oxygen or oxidase activity was evaluated at different proline concentrations in air-saturated buffer by monitoring P5C production with *o*-AB. Kinetic parameters for Put1p oxidase activity were k_{cat} = 0.8 min^{-1} and K_m = 50 mM proline (Figure 5).

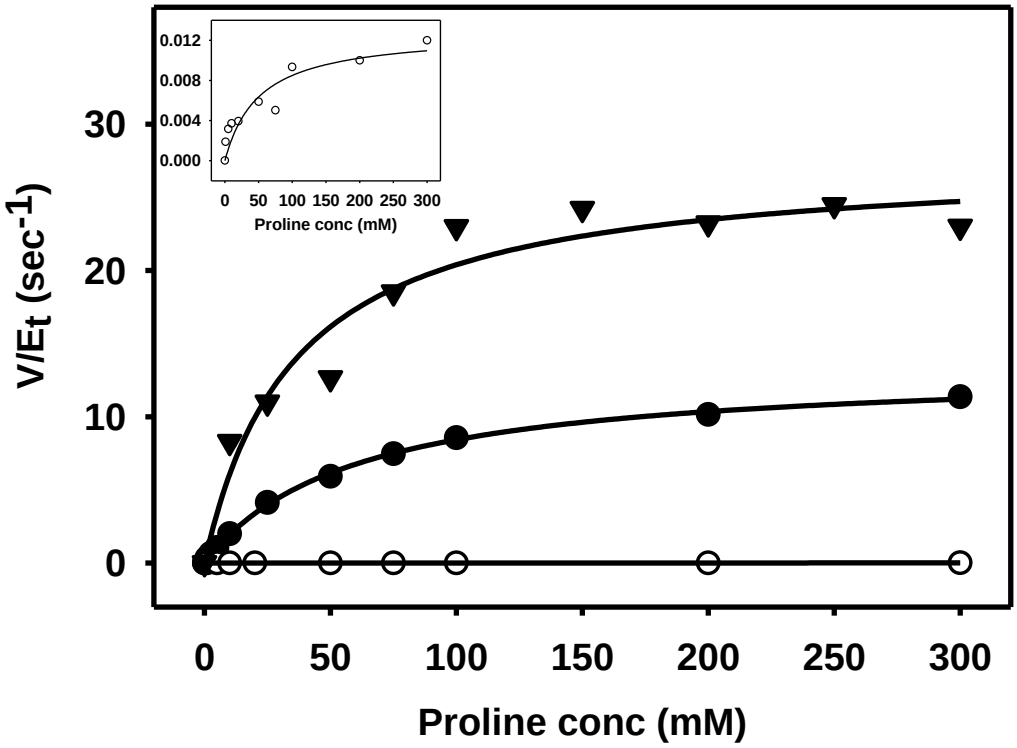

Figure 5- Estimation of kinetic parameters using different electron acceptors. The electron acceptors considered for catalytic turnover of Put1p were DCPIP, CoQ_1 and oxygen. Kinetic parameters for proline as substrate were measured using 75 µM DCPIP (▼), 100 µM CoQ_1(●) or air-saturated reaction buffer (○, Inset). The initial rates were fitted to a Michaelis-Menten equation. The K_m for proline using these electron acceptors was comparable (36 mM, 59 mM and 50 mM for DCPIP, CoQ_1, and oxygen respectively). k_{cat} for Put1p using artificial electron acceptor DCPIP and CoQ_1were 27.6 sec^{-1} and 13.4 sec^{-1}. Put1p exhibited negligible turnover using molecular oxygen (k_{cat} = 0.013 sec^{-1}).

Put1p displayed similar activity in assays using an O_2 electrode in which Put1p depleted oxygen at a rate of 0.54 min^{-1}. The turnover number with molecular oxygen is 15-fold lower for Put1p than TtPRODH (12 min^{-1}) [20].

The Put1p oxidative half-reaction was then characterized using CoQ_1 as the electron acceptor. The k_{cat} and K_m values determined with CoQ_1 were 20 ± 1 s^{-1} and 57 ± 6 μM, respectively. The kinetic parameters for proline with CoQ_1 concentration held constant (100 μM) were estimated to be k_{cat} = 13.4 ± 0.2 s^{-1} and K_m = 59 ± 3 mM proline. The high turnover rate of Put1p with CoQ_1 suggests ubiquinone is the most likely the physiological electron acceptor for Put1p. The order of the reaction was then analyzed by varying proline concentration at different CoQ_1 concentrations. Figure 6 shows double reciprocal plots of the reaction velocity versus proline (Figure 6A) and CoQ_1 (Figure 6B). The data in both plots could be fit with parallel slopes indicating a ping-pong mechanism (Scheme 2) in which no ternary complex is required during catalytic turnover with proline and ubiquinone.

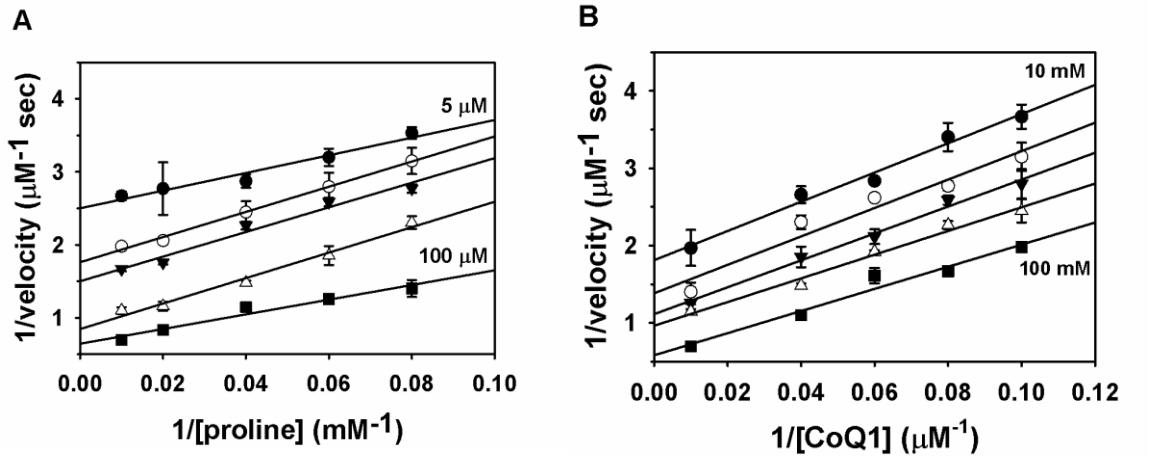

Figure 6- Binding order analysis of Put1p with proline and CoQ_1. Panel A shows a double reciprocal plot of velocity versus proline at four different CoQ_1 concentrations (5, 10, 20, and 60 μM). Panel B shows a double reciprocal plot of velocity versus CoQ_1 at four different proline concentrations (5, 20, 50, and 150 mM). Assays were performed in 50 mM potassium phosphate (pH 8.0) at 25°C. Data were fit by global curve fitting to a linear polynomial equation with a shared slope parameter (R^2 values of 0.95 and 0.97).

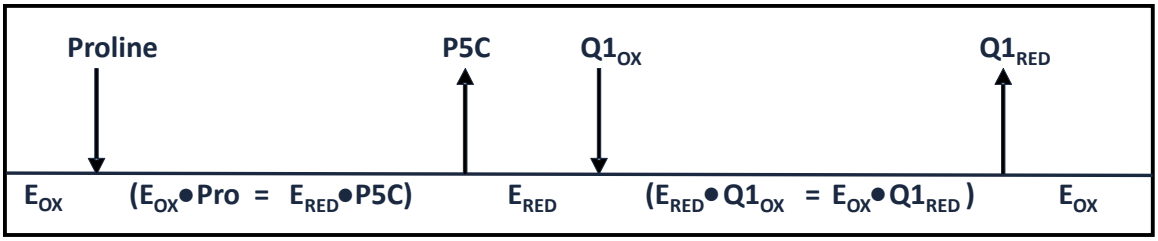

Scheme 2- Schematic representation of binding order of CoQ_1 and proline with Put1p

DISCUSSION

Sequence comparisons among bacterial PutA/PRODHs, Put1p, and human PRODH predict that a number of residues important for substrate and FAD binding in the PRODH catalytic core are conserved [20]. The sequence similarity between Put1p (476 amino acids) and the PRODH domain of EcPutA (1-669 residues) is 39%. Put1p and human PRODH1 have 25% sequence identity and 41% similarity consistent with a shared PRODH domain and a catalytic core structure. Nine conserved motifs important for substrate (1-3, 7-9) and FAD binding (4-6) have been identified in the PRODH domain of bacterial PutA and monofunctional PRODH enzymes [20]. Of these, motifs 3, 8, and 9 are strongly conserved in Put1p. Figure 7 shows a sequence alignment of motifs 3, 8 and 9 in Put1p and EcPutA. Conserved residues in these motifs which are critical for proline binding in EcPutA include Asp370, Tyr540, Arg555, and Arg556 (Asp257, Tyr430, Arg445, and Arg446 in Put1p). Important residues for FAD binding are also conserved in Put1p. These residues are found in motifs 4-6 and in EcPutA include Gln404 (Gln 294, Put1p) that forms a hydrogen bond with the FAD O(2), Arg431 which hydrogen bonds to the N(5) of FAD (K321, Put1p), and His487 (His377, Put1p) that interacts with the FAD pyrophosphate [20]. Another important residue for FAD binding in EcPutA is Glu559

(motif 9) which hydrogen bonds to the ribityl 3′ -OH and is conserved in Put1p (Glu449). Lastly, Put1p is predicted to have the α5a helix that is a unique feature of the $(\beta\alpha)_8$ barrel in EcPutA. In EcPutA, Trp438 (motif 5) from the α5a helix stacks against the adenine ring of the FAD. The corresponding residue in Put1p is Ile328 which would serve a similar purpose of providing non-polar interactions with the adenine ring.

Proline Binding

	Motif 3	Motif 8	Motif 9
EcPutA	IDAEE (369-373)	IYAPVG (539-544)	LLAYLVRRLLENG (549-561)
hPRODH1	VDAEQ (295-299)	KYVPYG (463-468)	VLPYLSRRALENS (473-485)
Put1p	IDAEK (256-260)	KYVPWG (429-434)	TKDYLLRRLQENG (439-451)

FAD Binding

	Motif 4	Motif 5	Motif 6	
EcPutA	GFVIQAYQKR (400-409)	RLVKGAYWDSEIK (431-443)	FATHN (484-488)	
hPRODH1	FNTYQCYLKD (325-334)	KLVRGAYLAQERA (356-368)	VASHN (411-415)	
Put1p	VGTWQLYLRD (290-229)	KLVRGAYIHSEKN (321-333)	VASHN (374-378)	

Figure 7- Alignment of PRODH domain sequence motifs between *E. coli* PutA (EcPutA), Human PRODH (hPRODH1) and Put1p. Conserved residues with critical roles in proline and FAD interactions as mentioned in the text are underlined. Alignment was performed using GeneDoc software and the EcPutA (AAB59985), hPRODH1 (NP_057419.4), and Put1p (NP_013243) sequences.

Put1p activity with other secondary amine compounds was tested to explore how strongly L-proline is the preferred substrate. Humans have two PRODH enzyme forms that share 45% sequence identity, PRODH1 (NM_016335) which is specific for L-proline, and PRODH2, (NM_021232) which is specific for *trans*-4-hydroxy-L-proline. PRODH2 (OH-PRODH) catalyzes the oxidation of *trans*-4-hydroxy-L-proline to Δ^1-pyrroline-3-hydroxy-5-carboxylate [37, 38].]. Humans also have the enzyme, L-pipecolic acid oxidase, which converts L-pipecolic acid to Δ^1-piperideine-6-carboxylic

acid. Because *S. cerevisiae* encodes only one PRODH gene, we were interested to see whether Put1p exhibited a broad substrate specificity that could accommodate variations in the five-membered pyrrolidine ring.

Conserved among all bacterial PutA/PRODH enzymes is an active site Tyr residue (Tyr540 in EcPutA) that helps shape the proline binding site [37]. Interestingly, human PRODH1 and HO-PRODH differ at this corresponding residue with the Tyr replaced by a smaller Ser residue in HO-PRODH [37]. Recently, Ostrander et al. provided evidence that Tyr540 in EcPutA imposes spatial constraints in the active site that determines the preference for proline over hydroxyproline [37]. Substitution of Tyr540 with Ser or Ala in EcPutA decreased the preference for proline by > 20-fold suggesting the corresponding Ser residue in HO-PRODH allows utilization of both proline and hydroxyproline [37]. As noted above Put1p is predicted to share the corresponding Tyr residue (Tyr430, motif 8) found in bacterial PutA/PRODH enzymes and human PRODH1. Accordingly, Put1p exhibits a strict preference for proline over hydroxyproline (2000-fold) consistent with the active site Tyr residue helping to define substrate specificity. Other lower organisms that lack a specific OH-PRODH enzyme, have hydroxyproline epimerases that catalyze the conversion of hydroxy-L-proline to hydroxy-D-proline [38-40]. Hydroxy-D-proline is then oxidized to Δ^1- pyrroline-4-hydroxy-2-carboxylate by hydroxy-D-proline oxidase [38-40]. *S. cerevisiae* does not contain this pathway for hydroxyproline. The ability of microorganisms to utilize hydroxy-L-proline can provide important metabolic advantages in pathogen- and symbiotic-host interactions in mammals and plants [38-41]. Recently, a hydroxyproline transport system was identified in the soil microbe *Sinorhizobium meliloti,* the first to be described in a prokaryote [41].

Succinic semialdehyde is four-carbon aldehyde that lacks an α–amino group. Upon testing the possibility of succinic semialdehyde as a substrate for Put2p, we found that Put2p exhibits a 15000-fold lower catalytic efficiency relative to P5C/GSA. Analysis of *T.thermophilus* P5CDH structure with glutamate bound to the active site (PDB ID: 2BHQ) reveals several possible ionic interactions of the α-carboxylate and amine groups of glutamate with residues in the TtP5CDH active site. The α-carboxylate group of glutamate is 3 Å from the backbone amide nitrogen of Gly 477 and Ala 488. The α-carboxylate moiety is also within hydrogen bonding distance (2.7 Å) to Ser 323. These active site residues appear to be well conserved in Put2p and other P5CDH's including human P5CDH and bifunctional PutA from *Bradyrhizobium japonicum*. Similar interactions might be possible in the Put2p active site. Shortage of one carbon atom in the aliphatic succinic semialdehyde may lead to lack of stabilizing interactions in the active site, thereby allowing Put2p to select appropriate substrate for the proline oxidative pathway.

The oxidative half-reaction of Put1p was investigated to provide molecular insights into the mitochondrial functions of human PRODH. A comparison of the Put1p and human PRODH1 sequences reveals a 25% sequence identity (41% similarity) consistent with a shared $(\beta\alpha)_8$ PRODH domain and a catalytic core structure. Put1p exhibited low reactivity with molecular oxygen and high activity with ubiquinone during catalytic turnover with proline. How adequately these results address the properties of human PRODH are not yet clear. Despite a high degree of similarity, Put1p and human PRODH may have fundamental differences in the oxidative half-reaction step. The ability of human PRODH to contribute to both mitochondrial energetics and apoptosis may be a

key distinctive feature of this enzyme. Human PRODH may have significant reactivity with molecular oxygen which would explain its role in generating mitochondrial reactive oxygen species and apoptosis. A useful comparison that has been used to describe PRODH reactivity in air is the ratio of the turnover numbers from the proline oxidoreductase assays using DCPIP and oxygen as electron acceptors (DCPIP/O_2). The DCPIP/O_2 activity ratio for Put1p is > 2000 and is similar to the value for EcPutA (> 2500). In contrast, TtPRODH has a DCPIP/O_2 activity ratio of 61 indicating less preference for DCPIP over oxygen. Also, PutA from *Helicobacter pylori* was reported to have a DCPIP/O_2 activity ratio of 16 [42]. Structural insights into the variation of oxygen reactivity among PutA/PRODH enzymes are still lacking but the differences in oxygen reactivity observed among PRODH enzymes is likely a consequence of diverse environmental niches and unique physiological roles for proline metabolism such as the programmed cell death pathway in mammals.

REFERENCES

1. Phang, J.M., J. Pandhare, and Y. Liu, *The metabolism of proline as microenvironmental stress substrate.* J Nutr, 2008. **138**(10): p. 2008S-2015S.
2. Takagi, H., *Proline as a stress protectant in yeast: physiological functions, metabolic regulations, and biotechnological applications.* Appl Microbiol Biotechnol, 2008. **81**(2): p. 211-23.
3. Krishnan, N., et al., *Characterization of a Helicobacter hepaticus putA mutant strain in host colonization and oxidative stress.* Infect Immun, 2008. **76**(7): p. 3037-44.
4. Curtis, J., G. Shearer, and D.H. Kohl, *Bacteriod proline catabolism affects N_2 fixation rate of drought-stressed soybeans.* Plant Physiol., 2004. **136**: p. 3313-3318.
5. Kohl, D.H., et al., *Proline metabolism in N_2-fixing root nodules: Energy transfer and regulation of purine synthesis.* Proc. Natl. Acad. Sci. USA, 1988. **85**: p. 2036-2040.
6. Lamour, N., et al., *Proline metabolism in procyclic Trypanosoma brucei is down-regulated in the presence of glucose.* J. Biol. Chem., 2005. **280**(12): p. 11902-10.
7. Brandriss, M.C. and B. Magasanik, *Genetics and physiology of proline utilization in Saccharomyces cerevisiae: enzyme induction by proline.* J Bacteriol, 1979. **140**(2): p. 498-503.
8. Wang, S.-S. and M.C. Brandriss, *Proline utilization in Saccharomyces cerevisiae: sequence, regulation, and mitochondrial localization of the PUT1 gene product.* Mol. Cell. Biol., 1987. **7**(12): p. 4431-4440.
9. Reinders, J., et al., *Toward the complete yeast mitochondrial proteome: multidimensional separation techniques for mitochondrial proteomics.* J Proteome Res, 2006. **5**(7): p. 1543-54.
10. Magasanik, B. and C.A. Kaiser, *Nitrogen regulation in Saccharomyces cerevisiae.* Gene, 2002. **290**(1-2): p. 1-18.
11. Brandriss, M.C. and B. Magasanik, *Genetics and physiology of proline utilization in Saccharomyces cerevisiae: mutation causing constitutive enzyme expression.* J Bacteriol, 1979. **140**(2): p. 504-7.
12. Sellick, C.A. and R.J. Reece, *Modulation of transcription factor function by an amino acid: activation of Put3p by proline.* Embo J, 2003. **22**(19): p. 5147-53.
13. Leverentz, M.K., et al., *Mutation of a phosphorylatable residue in Put3p affects the magnitude of rapamycin-induced PUT1 activation in a Gat1p-dependent manner.* J Biol Chem, 2009. **284**(36): p. 24115-22.
14. Miller, S.M. and B. Magasanik, *Role of NAD-linked glutamate dehydrogenase in nitrogen metabolism in Saccharomyces cerevisiae.* J Bacteriol, 1990. **172**(9): p. 4927-35.
15. Liu, Y., et al., *Proline oxidase activates both intrinsic and extrinsic pathways for apoptosis: the role of ROS/superoxides, NFAT and MEK/ERK signaling.* Oncogene, 2006. **25**: p. 5640-5647.
16. Donald, S.P., et al., *Proline oxidase, encoded by p53-induced gene-6, catalyzes the generation of proline-dependent reactive oxygen species.* Cancer Res., 2001. **61**(5): p. 1810-5.

17. Polyak, K., et al., *A model for p53-induced apoptosis.* Nature, 1997. **389**(6648): p. 300-5.
18. Liu, Y., et al., *Proline oxidase functions as a mitochondrial tumor suppressor in human cancers.* Cancer Res, 2009. **69**(16): p. 6414-22.
19. Tanner, J.J., *Structural biology of proline catabolism.* Amino Acids, 2008. **35**(4): p. 719-30.
20. White, T.A., et al., *Structure and kinetics of monofunctional proline dehydrogenase from Thermus thermophilus.* J. Biol. Chem, 2007. **282**: p. 14316-14327.
21. Lee, Y.H., et al., *Structure of the proline dehydrogenase domain of the multifunctional PutA flavoprotein.* Nat. Struct. Biol., 2003. **10**(2): p. 109-114.
22. Williams, I. and L. Frank, *Improved chemical synthesis and enzymatic assay of delta-1-pyrroline-5-carboxylic acid.* Anal Biochem, 1975. **64**(1): p. 85-97.
23. Wang, S.-S. and M.C. Brandriss, *Proline utilization in Saccharomyces cerevisiae: analysis of the cloned PUT1 gene.* Mol. Cell. Biol., 1986. **6**: p. 2638-2645.
24. Thorpe, C., R.G. Matthews, and C.H. Williams, Jr., *Acyl-coenzyme A dehydrogenase from pig kidney. Purification and properties.* Biochemistry, 1979. **18**(2): p. 331-7.
25. Brown, R.E., K.L. Jarvis, and K.J. Hyland, *Protein measurement using bicinchoninic acid: elimination of interfering substances.* Anal Biochem, 1989. **180**(1): p. 136-9.
26. Becker, D.F. and E.A. Thomas, *Redox properties of the PutA protein from Escherichia coli and the influence of the flavin redox state on PutA-DNA interactions.* Biochemistry, 2001. **40**: p. 4714-4722.
27. Mezel, V.A. and W.E. Knox, *Properties and analysis of a stable derivative of pyrroline-5-carboxylic acid for use in metabolic studies.* Anal. Biochem., 1976. **74**: p. 430-440.
28. Grauschopf, U., A. Fritz, and R. Glockshuber, *Mechanism of the electron transfer catalyst DsbB from Escherichia coli.* Embo J, 2003. **22**(14): p. 3503-13.
29. Lineweaver, H. and D. Burk, *The determination of enzyme dissociation constants.* J. Am. Chem. Soc., 1934. **56**: p. 658-666.
30. Zhu, W., et al., *Effects of proline analog binding on the spectroscopic and redox properties of PutA.* Arch. Biochem. Biophys., 2002. **408**(1): p. 131-6.
31. Dixon, M., *The Determination of Enzyme Inhibitor Constants.* Biochemical Journal, 1953. **55**: p. 170-171.
32. Brown, E.D. and J.M. Wood, *Conformational change and membrane association of the PutA protein are coincident with reduction of its FAD cofactor by proline.* J. Biol. Chem., 1993. **268**: p. 8972-8979.
33. Bearne, S.L. and R. Wolfenden, *Glutamate gamma-semialdehyde as a natural transition state analogue inhibitor of Escherichia coli glucosamine-6-phosphate synthase.* Biochemistry, 1995. **34**(36): p. 11515-20.
34. Srivastava, D., et al., *The three-dimensional structural basis of type II hyperprolinemia.* J Mol Biol, 2012. **420**(3): p. 176-89.
35. Krishnan, N. and D.F. Becker, *Characterization of a bifunctional PutA homologue from Bradyrhizobium japonicum and identification of an active site*

residue that modulates proline reduction of the flavin adenine dinucleotide cofactor. Biochemistry, 2005. **44**(25): p. 9130-9.

36. Zhang, M., et al., *Structures of the Escherichia coli PutA proline dehydrogenase domain in complex with competitive inhibitors.* Biochemistry, 2004. **43**: p. 12539-12548.
37. Ostrander, E.L., et al., *A conserved active site tyrosine residue of proline dehydrogenase helps enforce the preference for proline over hydroxyproline as the substrate.* Biochemistry, 2009. **48**(5): p. 951-9.
38. Adams, E. and L. Frank, *Metabolism of proline and the hydroxyprolines.* Annu Rev Biochem, 1980. **49**: p. 1005-61.
39. Goytia, M., et al., *Molecular and structural discrimination of proline racemase and hydroxyproline-2-epimerase from nosocomial and bacterial pathogens.* PLoS One, 2007. **2**(9): p. e885.
40. Chamond, N., et al., *Proline racemases are conserved mitogens: characterization of a Trypanosoma vivax proline racemase.* Mol Biochem Parasitol, 2009. **165**(2): p. 170-9.
41. Maclean, A.M., et al., *Identification of a hydroxyproline transport system in the legume endosymbiont Sinorhizobium meliloti.* Mol Plant Microbe Interact, 2009. **22**(9): p. 1116-27.
42. Krishnan, N. and D.F. Becker, *Oxygen reactivity of PutA from Helicobacter species and proline-linked oxidative stress.* J. Bacteriol., 2006. **188**(4): p. 1227-35.

CHAPTER 4

Studying the effect of solvent pH on channeling of intermediate Δ^1–pyrroline-5-carboxylate in PutA from *Bradyrhizobium japonicum*

Note: This chapter contains methodology published in the research article: "Crystal structure of the bifunctional proline utilization A, flavoenzyme from Bradyrhizobium japonicum." Srivastava D, Schuermann JP, White TA, Krishnan N, Sanyal N, Hura GL, Tan A, Henzl MT, Becker DF, Tanner JJ. Proc Natl Acad Sci U S A. 2010 Feb 16;107(7):2878-83.

INTRODUCTION

Proline utilization A (PutA) from *Bradyrhizobium japonicum* (BjPutA) is a bifunctional enzyme containing two catalytic domains- proline dehydrogenase (PRODH) and Δ^1-pyrroline-5-carboxylate dehydrogenase (P5CDH) [1]. This type of multi-domain organization of proline catabolic enzymes in *B. japonicum* is also observed in other Gram-negative bacteria [2]. The oxidation of proline to glutamate is catalyzed in consecutive reactions by PRODH and P5CDH (Scheme 1). In the first step, proline dehydrogenase (PRODH; EC 1.5.99.8) uses a flavin adenine dinucleotide (FAD) cofactor as an electron acceptor to remove two electrons from proline, rendering the intermediate Δ^1-pyrroline-5-carboxylate (P5C). P5C then undergoes a non-enzymatic hydrolysis, which opens the ring structure and generates γ-glutamate semialdehyde (GSA). P5C dehydrogenase (P5CDH; EC 1.5.1.12) next pulls off two additional electrons from GSA using nicotinamide adenine dinucleotide (NAD^+) to complete the conversion of proline to glutamate [3]. Avoiding release of P5C/GSA into bulk solvent during proline oxidation may be beneficial due to the chemical properties of P5C/GSA as discussed in Chapter 1.

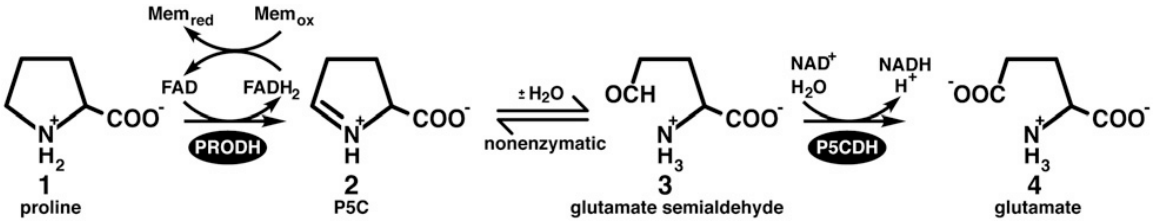

Scheme 1 – Reactions catalyzed by the PRODH and P5CDH domains of BjPutA

Recently, Srivastava *et al* reported a 2.1 Å resolution crystal structure of BjPutA (999-residue polypeptide) that reveals an interior channel connecting the PRODH and P5CDH active sites [4] (PDB ID: 3HAZ) (Figure 1A). Supporting kinetic studies have

demonstrated that BjPutA transfers the intermediate P5C/GSA from the PRODH active site to the P5CDH active site. The dimeric structure of BjPutA seems to be critical for sealing the channel and minimizing access to bulk solvent. A β-flap protrudes from the P5CDH domain (β-strands, residues 628-646 and 977-989) from one protomer and forms intermolecular interactions with the P5CDH domain of the second protomer (Figure 1B).

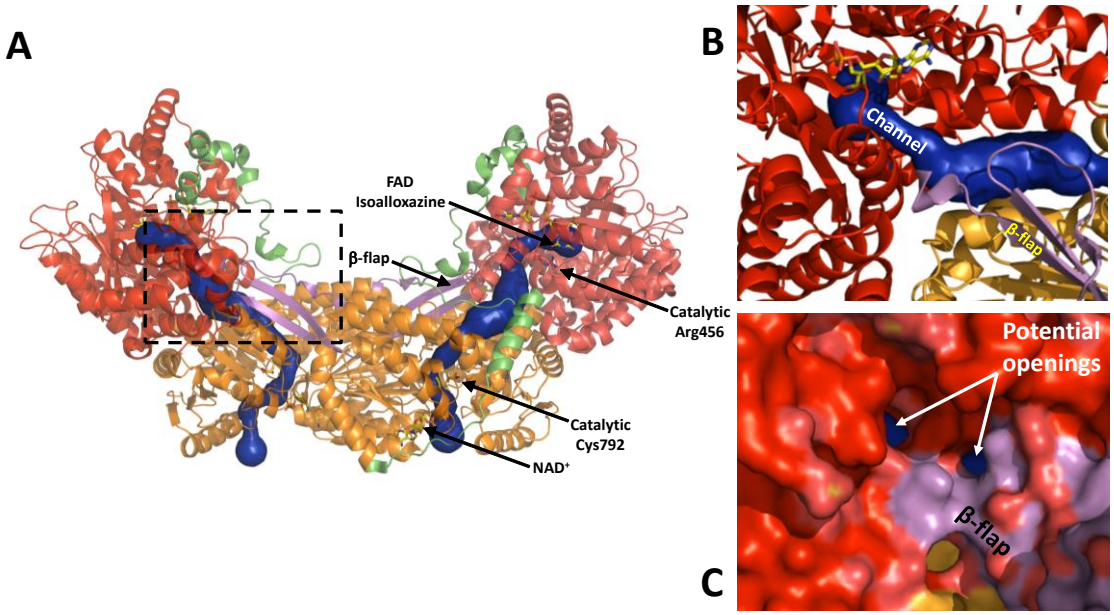

Figure 1- Overall structure of dimeric BjPutA and structural role of the C-terminal β-flap region. A) Ribbon representation of dimeric BjPutA. The PRODH domain (red) and the P5CDH domain (orange) of each protomer are connected by a linker region (green). Active site residues (Arg456, Cys792), FAD and NAD^+ are displayed as sticks. β-flap of each protomer is colored as magenta. The substrate channel of each BjPutA protomer is shown as a blue surface. B) Close-up view of the dotted section of the dimer showing the C-terminal region of the β-flap. C) Surface representation of the β-flap region showing potential openings that lead to the internal channel of BjPutA. The figures were made using PyMol [5] and PDB ID: 3HAZ.

Figure 1C shows that in BjPutA the β-flap not only helps stabilize dimer formation but is also important for sealing the central cavity. There appears to be two adjacent openings near the β-flap that may allow access between external solvent and the internal channel. To study the extent to which the substrate channel is closed off from

bulk solvent for transfer of P5C and its hydrolysis to GSA, we used a truncated variant of BjPutA. Residues 987-999 of the C-terminal region of the β-flap were deleted to test whether bulk solvent access to the channel could be increased (Scheme 2). The truncated BjPutA 1-986 mutant is expected to exhibit less channeling of P5C/GSA due to potentially increased exposure of the channel cavity to bulk solvent. The overall PRODH/P5CDH coupled reaction in the BjPutA 1-986 mutant may also become more sensitive to the bulk solvent environment (e.g., pH) relative to wild-type BjPutA.

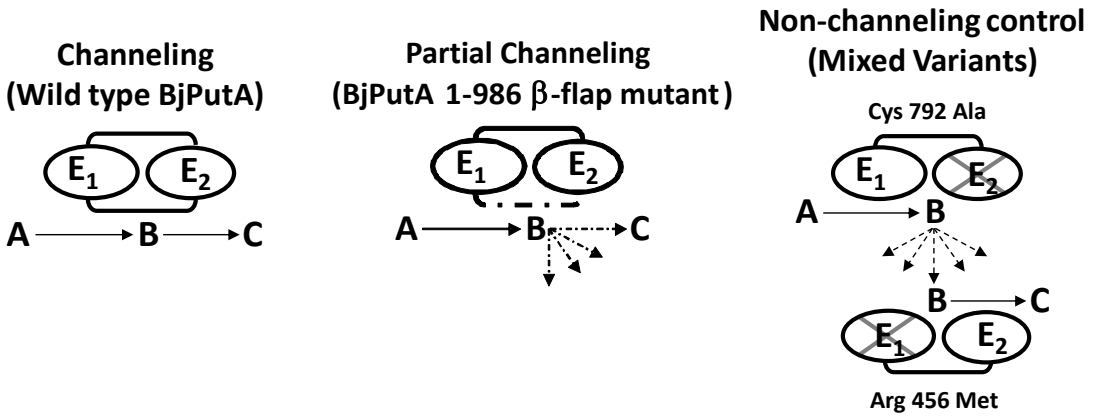

Scheme 2- Schematic representation of enzymes used for comparing substrate channeling in bifunctional enzymes. E1 and E2 represent PRODH and P5CDH respectively. A, B and C represent proline, P5C/GSA and glutamate respectively.

In the proline catabolic pathway, channeling of P5C/GSA may be important for making the hydrolysis of P5C to GSA more favorable at physiological pH values. The P5C/GSA equilibrium is highly pH dependent. Bearne and Wolfenden have demonstrated by nuclear magnetic resonance that GSA is favored at pH < 6.6 due to protonation of the pyrrolinium ring, which facilitates the hydrolysis of P5C to GSA (Figure 2). Thus, one benefit of channeling between PRODH and P5CDH would be to increase the pK_a of the pyrrolinium species above pH 6.6, making the hydrolysis of P5C

to GSA more favorable at physiological pH conditions. If we only consider the P5C/GSA hydrolysis step, substrate channeling is likely more critical for the proline catabolic pathway than for proline biosynthesis, since P5C formation is favored at physiological pH.

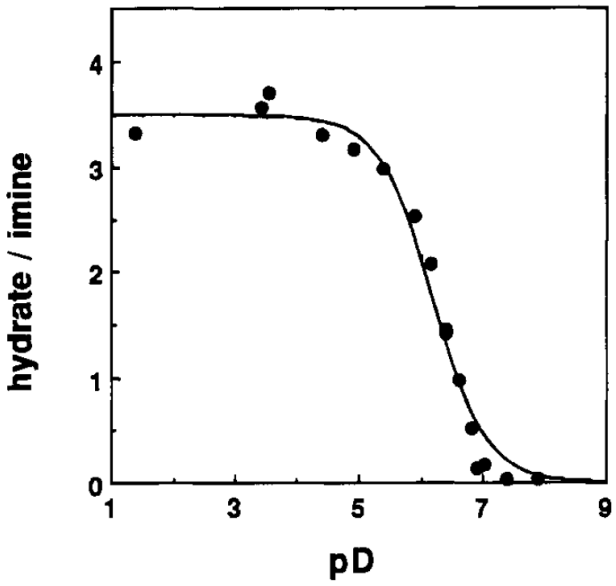

Figure 2- pH dependent hydrolysis of Δ^1-pyrroline-5-carboxylate (P5C) to γ-glutamate semialdehyde (GSA). Ratio of the hydrate of GSA to the imine of P5C as a function of pD obtained from a proton NMR spectra [6]. The pK_a of the imine proton was calculated as 6.67 (±0.08). Figure adapted from [6].

To test this hypothesis, we examined the pH dependence of the coupled PRODH-P5CDH reaction (channeling assay). Using proline as the substrate for the channeling reaction, we measured the P5CDH enzymatic rate (reflected by rate of NADH formation) and the transient time required to attain steady-state NADH formation under varying pH conditions. If the substrate channel provides a favorable condition for hydrolysis of P5C, the transient time for a channeling reaction should remain unaffected by external pH in the wild-type enzyme. BjPutA 1-986 is expected to be influenced by external pH to a greater extent due to more exposure of the substrate channel to bulk solvent than wild-

type BjPutA. Because cyclic P5C is favored at pH above 6.6, the transient time for glutamate formation may to increase substantially for BjPutA 1-986 at higher pH values. We also used a non-channeling control which is an equimolar mixture of BjPutA active site mutants that lack PRODH (R456M) and P5CDH (C792A) activity [4]. The R456M mutation inactivates PRODH but does not impair P5CDH activity, whereas the C792A mutation inactivates P5CDH but does not impair PRODH activity. In this non-channeling control, P5C formed by the C792A variant must diffuse out into bulk solvent and bind to the R456M variant before NADH is formed. Hence, for the non-channeling control, the hydrolysis of P5C to GSA should be highly dependent on the pH of the bulk solvent.

EXPERIMENTAL PROCEDURES

Materials

D,L-P5C was chemically synthesized from D,L-hydroxylysine as described previously by Williams and Frank and stored in 1 M HCl at 4^{o}C [7]. Synthesized D,L-P5C is an equimolar mixture of D-P5C and L-P5C. All chemicals were purchased from Sigma Aldrich unless noted otherwise. Tris(3-hydroxypropyl)phosphine (THP) was purchased from Santa Cruz Biotechnology Inc. CoQ_1 reduction assays and substrate channeling assays were carried out on a SF-61DX2 stopped-flow spectrophotometer (TgK Scientific, UK). CoQ_1 reduction assays for enzymatic activities of PRODH and P5CDH activity assays were carried out on a Cary-50 UV-Vis spectrophotometer (Varian) or Powerwave XS Microplate reader (BioTek). The pKA8H-BjPutA 1-986-construct was a generous gift from Dr. John tanner (University of Missouri, Columbia).

Purification of BjPutA and mutants

Wild-type BjPutA, BjPutA mutants R456M, C792A and, BjPutA 1-986 C-terminal deletion mutant were expressed and purified from *E. coli* strain BL21(DE3) pLysS with an N-terminal 6xHis tag using the pKA8H expression vector [4]. The BjPutA-pKA8H constructs were transformed into *E. coli* BL21(DE3) pLysS. Transformed cells were plated onto Luria-Bertani (LB) agar containing chloramphenicol (34 μg/ml) and ampicillin (50 μg/ml). Resulting colonies were inoculated in 5 ml of LB broth containing the necessary antibiotics and grown to an optical density at 600 nm (OD_{600}) of 1.0. 1 ml of the LB culture was then used to inoculate 1 L of LB Broth media containing chloramphenicol (34 μg/ml) and ampicillin (50 μg/ml). The 1 L cultures were incubated at 37^{o}C with shaking (250 rpm) until OD_{600} of 0.8 at which point protein expression was induced with 50 μM IPTG overnight at 20^{o}C.

The overnight cultures were centrifuged at 6000 rpm for 20 min at 4^{o}C. The resulting pellets were resuspended in a final 50 ml volume of binding buffer (20 mM Tris, 5 mM imidazole, 0.5 M NaCl, 10% glycerol, pH 7.9) supplemented with 1 mM FAD and protease inhibitors (3 mM ε-amino-N-caproic acid, 0.3 mM phenyl methyl sulfonyl chloride, 1.2 μM leupeptin, 48 μM N-*p*-tosyl-L-phenyl alanine chloromethyl ketone, 78 μM N-α-tosyl-L-lysine chloromethylketone). The cell suspension was disrupted by sonication at 4^{o}C for a total of 5 min (5 sec pulse on, 15 sec pulse off, 40% power). The cell extract was centrifuged at 16000 rpm (4^{o}C) for 60 min. The supernatant (50 ml) was passed through a 0.8 μm filter (VWR) and applied to a Ni-NTA superflow (Qiagen) resin (25 ml bed volume in a 2.8 cm x 30 cm column) equilibrated with 1X binding buffer. Wash buffer (125 ml, 20 mM Tris, 60 mM imidazole, 0.5 M NaCl, 10% glycerol, pH 7.9) was then applied to the column followed by elution buffer (20 mM Tris, 500 mM

imidazole, 0.5 M NaCl, 10% glycerol, pH 7.9) with a flow rate of 3 ml/min to elute protein fractions. Fractions from the elution step were then analyzed by SDS-PAGE and pooled. Pooled protein was then dialyzed into 50 mM Tris buffer (pH 7.9) containing 50 mM NaCl, 0.5 mM EDTA, 0.5 mM THP, 10% glycerol and concentrated using an Amicon 100-kDa cutoff filter (Millipore) and stored in -80^{o}C.

The absorbance spectra of purified protein were recorded from 600 to 250 nm. The concentration of flavin was determined using the molar extinction coefficient for enzyme-bound FAD at 450 nm (A_{450}= 13700 M^{-1} cm^{-1}) [1]. Any unbound flavin was removed by passing purified protein through a PD-10 desalting column (GE Healthcare). The concentration of total protein was determined using Pierce 660 reagent [8]. The ratio of flavin concentration to protein concentration was used to determine the amount of BjPutA containing bound FAD. The concentration of FAD bound BjPutA was used as the concentration of BjPutA in the enzyme assays.

Enzymatic assay of BjPutA and mutants

PRODH kinetics

Kinetics of the PRODH domain of BjPutA and its variants were determined by following the reduction of CoQ_1. CoQ_1 reduction was measured using 0.5 μM of BjPutA (wild-type BjPutA and mutants) in 50 mM phosphate buffer at pH 8.0. Kinetic parameters for proline were measured by varying proline (0-250 mM) with fixed CoQ_1 concentration (250 μM). Kinetic parameters for CoQ_1 were measured by varying CoQ_1 (0-300 μM) with fixed proline concentration (150 mM). Reduction of CoQ_1 was followed at 275 nm (ε=13700 cm^{-1} M^{-1}) using a 0.15 cm path length on a Hi-Tech Scientific SF-61DX2 stopped-flow instrument at 25^{o}C [9]. The kinetic parameters K_m and k_{cat} were

estimated by regression analysis of the initial reaction velocity versus proline or CoQ_1 concentration using the Michaelis-Menten equation. The specific activity of PRODH with 40 mM proline as the substrate was determined by measuring P5C complex formation with *o*-aminobenzaldehyde (*o*-AB) [10]. P5C forms a yellow dihydroquinazolinium complex with *o*-AB, which is detected by absorbance at λ = 443 nm (ε=2900 $M^{-1}cm^{-1}$ [10]). For this assay, wild type BjPutA (0.18 µM) or BjPutA 1-986 (0.18 µM) was incubated with proline (40 mM), *o*-AB (4.0 mM) and 0.1 mM CoQ_1 as an electron acceptor. The assays were performed at pH 6-10 using a mixed buffer system containing 50 mM potassium phosphate, 25 mM borate and 25 mM bicine buffer. Data were fit to the equation 4.1.

$$vel = \frac{v_{lim}}{1 + 10^{pKa1-pH} + 10^{pH-pKa2}} \quad (4.1)$$

where v_{lim} is the maximal velocity and pK_{a1} and pK_{a2} represent the acidic and alkaline ionizations that contribute to the pH dependent curve of the reaction velocity.

P5CDH kinetics

The P5CDH activity of wild-type BjPutA, BjPutA R456M and BjPutA 1-986 was measured by monitoring the formation of NADH at 340 nm (ε = 6400 cm^{-1} M^{-1} [4]) at 25 °C. The assay buffer contained 50 mM potassium phosphate (pH 7.5), 25 mM borate and 25 mM bicine. Enzyme concentration was 0.18 µM (20 µg/ml) and NAD^+ concentration was 0.2 mM. Varying concentrations of L-P5C ranging from 1 -3.9 mM were used. Initial rates were fitted to the Michaelis-Menten equation. For obtaining pH profile of kinetic parameters, P5CDH activity assays were carried out in a mixed buffer system containing

50 mM potassium phosphate, 25 mM borate and 25 mM bicine buffer pH 6-10 was used. k_{cat}/K_m for P5CDH were fit to the equation 4.1.

Substrate channeling assays at varying pH

To determine the pH activity dependence of substrate channeling, NADH formation was monitored at 340 nm in assays performed at 23 °C containing proline (40 mM), BjPutA (0.18 μM), CoQ_1 (0.1 mM), and NAD^+ (0.2 mM) in buffer containing 50 mM potassium phosphate, 25 mM borate and 25 mM bicine (pH 6-10). Identical assays were performed using 0.18 μM (20 μg/ml) BjPutA 1-986 or an equimolar mixture of the BjPutA variants C792A and R456M (0.18 μM or 20 μg/ml final concentration each). Spectral interference caused by changes in CoQ_1 absorbance at 340 nm was corrected for by subtracting progress curves from assays performed under identical conditions in the absence of NAD^+.

The progress curve for two non-interacting PRODH and P5CDH enzymes was simulated as described previously [11] for a diffusion-limited two-enzyme model using equations 4.2 and 4.3

$$[NADH] = v_1 t + \left(\frac{v_1}{v_2}\right) K_{m2} \left(e^{-\frac{v_2 t}{K_{m2}}} - 1\right) \qquad (4.2)$$

$$\tau = \frac{K_{m2}}{v_2} \qquad (4.3)$$

In the above equation, v_1 is the experimentally determined rate of PRODH activity under the specified assay conditions with 40 mM proline, t is time in sec, K_{m2} and v_2 are the steady-state Michaelis-Menten constants for P5CDH activity in BjPutA wild-type and mutants, and τ is the transient time (sec) required to attain steady-state formation of

product (i.e., NADH). The transient time was also calculated by extrapolating the linear NADH formation rate to the x-axis. The x-intercept reflects the transient time required for reaching steady-state NADH formation. pH dependent changes in transient time were fitted to equation 4.4,

$$T_{obs} = \frac{(T_{lim1} + T_{lim2} * 10^{pH-pKa})}{1 + 10^{pH-pKa}} \qquad (4.4)$$

where T_{obs} represents the observed extrapolated transient time, T_{lim1} and T_{lim2} represent the limiting values for transient time at low and high pH respectively and pK_a is the acid dissociation constant of an ionizable group in the pH range.

RESULTS

Kinetic properties of wild-type BjPutA and its mutants

Wild type BjPutA, BjPutA 1-986 and inactive mutants C792A and R456M were purified with over 90% protein bound to FAD in all cases. Each protein displays a typical UV-visible spectrum of protein bound FAD with maximum absorbance peaks at 384 and 450 nm and a shoulder near 467 nm (Figure 3) [12].

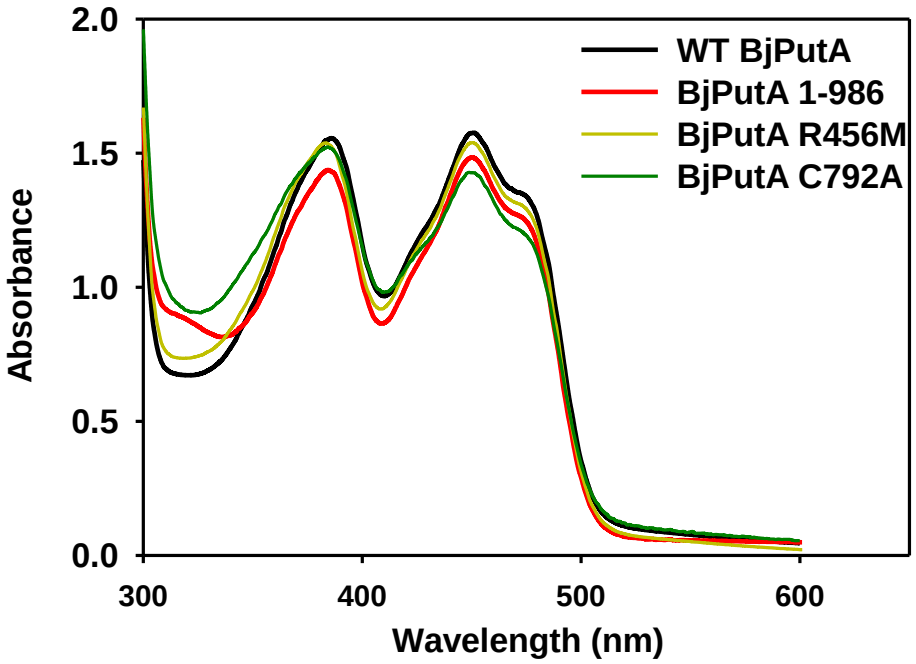

Figure 3- Absorbance spectra of purified BjPutA enzymes. Wild-type BjPutA, BjPutA 1-986, active site mutants C792A and R456M show similar flavin spectra. The shoulder at 467 nm is characteristic of flavin bound to the PRODH active site of BjPutA.

The steady-state kinetic parameters of BjPutA wild-type and the mutants are reported in Table 1. The kinetic parameters for proline using CoQ_1 as an electron acceptor are 28.6 ± 3.8 mM proline (K_m) and 1.69 ± 0.06 sec^{-1}(k_{cat}). These values are similar to the previously reported parameters (K_m = 31 ± 6 mM proline, k_{cat} = 2.0 ± 0.1 sec^{-1}) for BjPutA [4]. BjPutA 1-986 was shown to have a K_m of 40.6 ± 2.7 mM proline

and a two-fold higher k_{cat} of 3.47 ± 0.07 sec^{-1} relative to wild-type BjPutA. The BjPutA mutant C792A also shows PRODH activity similar to wild-type BjPutA whereas the R456M mutant is devoid of PRODH activity (Table 1).

CoQ_1 has been shown to act as a potential physiological electron acceptor for the PRODH activity of *E. coli* PutA (EcPutA) [13], monofunctional PRODH from *S. cerevisiae* (Put1p) [14] and *T. thermophilus* (TtPRODH) (Chapter 2). Although CoQ_1 has been previously used in assays with BjPutA [4], its steady-state kinetic parameters have not yet been determined. Here, we report that wild-type BjPutA has a K_m of 83.63 ± 13.41 µM CoQ_1. In comparison, EcPutA has a K_m of 110 ± 15 µM for CoQ_1. Monofunctional PRODHs exhibit a somewhat wider range of K_m values for CoQ_1 with Put1p and TtPRODH having K_m values of 57 ± 6 µM and 162.2 ± 7.6 µM CoQ_1, respectively. The K_m values for CoQ_1 with BjPutA 1-986 (72.41 ± 4.96 µM) and BjPutA P5CDH inactive mutant C792A (103.01 ± 20.83 µM) are similar to wild-type BjPutA.

Table 1 – Steady-state kinetic parameters of PRODH and P5CDH activities of BjPutA wild-type and mutants

Domain	**PRODH**						**P5CDH**		
Substrate	**Proline**			**CoQ_1**			**L-P5C**		
	K_m (mM)	**k_{cat} (sec^{-1})**	**k_{cat}/K_m (M^{-1} sec^{-1})**	**K_m (µM)**	**k_{cat} (sec^{-1})**	**k_{cat}/K_m (M^{-1} sec^{-1})**	**K_m (mM)**	**k_{cat} (sec^{-1})**	**k_{cat}/K_m (M^{-1} sec^{-1})**
WT BjPutA	28.6 ± 3.8	1.69 ± 0.06	5.9 x 10^1	83.63 ± 13.41	1.59 ± 0.09	1.9 x10^4	1.35 ± 0.16	3.45 ± 0.18	2.6 x 10^3
BjPutA R456M	ND	ND	ND	ND	ND	ND	1.62 ± 0.21	3.44 ± 0.21	2.1 x 10^3
BjPutA C792A	60.1 ± 10.1	1.58 ± 0.09	2.6 x 10^1	103.01 ± 20.83	1.39 ± 0.12	1.4 x 10^4	ND	ND	ND
BjPutA 1-986	40.6 ± 2.7	3.47 ± 0.07	8.5 x 10^1	72.41 ± 4.96	3.54 ± 0.08	4.9 x 10^4	1.13 ± 0.13	3.26 ± 0.16	2.88 x 10^3

ND- No Activity detected.

The P5CDH kinetic parameters of wild-type BjPutA (K_m = 1.35 ± 0.16 mM L-P5C, k_{cat} = 3.45 ± 0.18 sec^{-1}) and BjPutA 1-986 (K_m = 1.13 ± 0.13 mM L-P5C, k_{cat} = 3.26 ± 0.16 sec^{-1}) are nearly identical (Table 1). The R456M mutant exhibits P5CDH activity similar to that of wild-type BjPutA (Table 1). As anticipated, the C792A mutant has no P5CDH activity.

Substrate channeling assays

A common strategy to test for channeling is to evaluate whether there is a lag time in reaching steady-state formation of the final product in a coupled assay. Figure 4 shows the substrate proline being converted to the final product glutamate (reflected by concomitant NADH formation) via the coupled action of PRODH and P5CDH domains of BjPutA. With wild-type BjPutA, steady-state formation of NADH occurs without any apparent lag time. However, the progress curve can be fitted to equation 4.2 for a two-enzyme model to yield a lag time of 10 sec. The near absence of a lag time in the approach to steady-state is indicative of substrate channeling. Fitting the reaction progress curve for the non-channeling enzyme pair C792A and R456M to equation 4.2 estimates a lag time of 7.8 min. The lag time determined by extrapolation of the linear NADH formation rate is somewhat shorter at 5.3 min. In contrast to wild-type BjPutA, BjPutA 1-986 exhibits a noticeable lag time of about 2.5 min by extrapolating from the steady-state linear phase of the reaction. Fitting the progress curve to equation 4.2 yields a lag time of 2.4 min. The observation of a lag in NADH formation with BjPutA 1-986 indicates that deletion of C-terminal residues 987-999 diminishes substrate channeling. However, the lag time is only 50% of the non-channeling control suggesting that to some extent substrate channeling is still occurring.

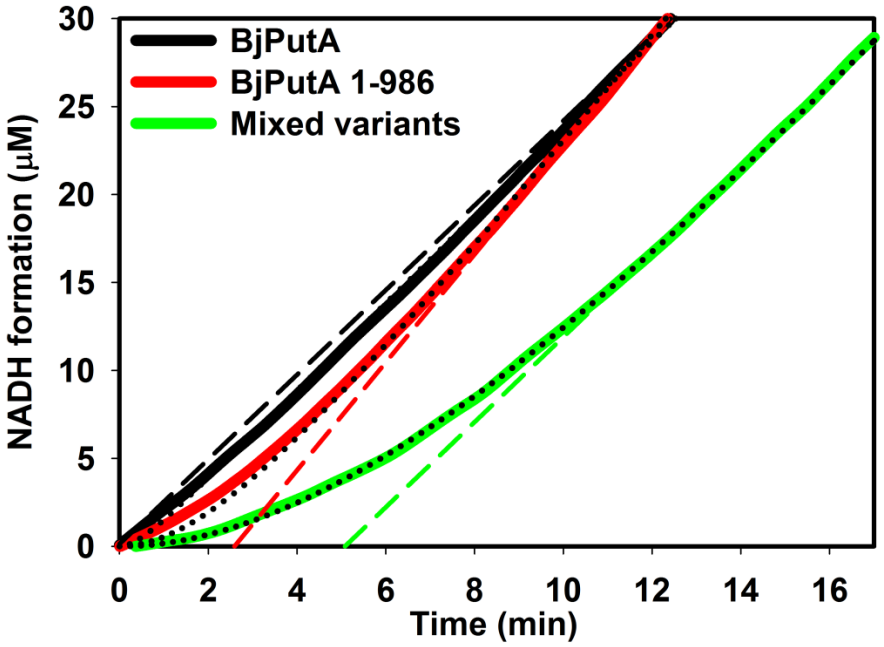

Figure 4- Transient time analysis of BjPutA and channeling variants. Colored solid lines represent the time-course of NADH formation for BjPutA, BjPutA 1-986 and non-channeling mixed variants C792A and R456M using 40 mM proline, 0.1 mM CoQ_1 and 0.2 mM NAD^+ as substrates and 0.18 μM of each enzyme. Colored dashed lines represent extrapolation of linear rate of NADH formation to the x-axis. The estimated lag time (x-intercept) from the extrapolations are 2.5 min and 5.3 min for BjPutA 1-986 and non-channeling mixed variants C792A and R456M,, respectively. The black dotted lines overlapping each trace of NADH formation are the fitting of the reaction progress curve with the two-enzyme model (equation 4.2). The estimated transient times from the fitting are 10 sec, 2.4 min, and 7.8 min for wild-type BjPutA, BjPutA 1-986 and mixed variants C792A and R456M, respectively.

pH activity dependence of substrate channeling

We next wanted to test the effect of pH on substrate channeling and explore the pH dependent hydrolysis of P5C as previously discussed. Channeling assays were performed for wild-type BjPutA, BjPutA 1-986 and the mixed variants (C792A and R456M) from pH 6-10. Figure 5A shows the time-course of NADH formation using 40 mM proline as the initial substrate for wild-type BjPutA. A plot of NADH formation

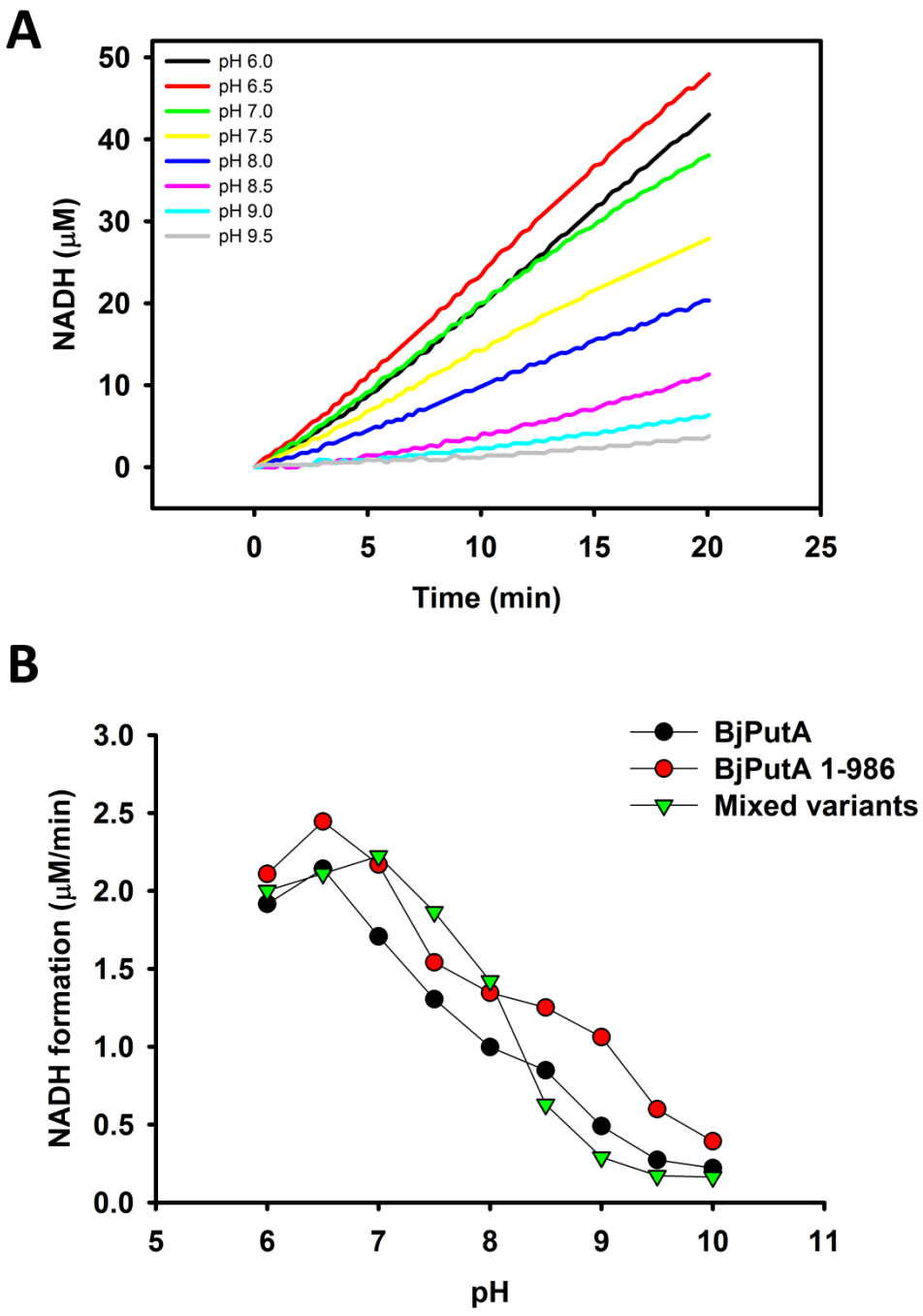

Figure 5- pH activity dependence of NADH formation. A) Time-course of NADH formation by wild-type BjPutA pH 6-9.5. B) Plot of the steady-state linear rates of NADH formation versus pH for wild-type BjPutA, mutant 1-986, and mixed variants (C792A and R456M). 50 mM potassium phosphate, 25 mM borate and 25 mM bicine mixed buffer system was used to generate a pH range of 6 to 10.

versus pH (Figure 5B) shows that the rate of NADH formation reaches a maximum at pH 6.5 and steadily declines with increased pH. BjPutA 1-986 shows an identical dependence on pH (Figure 5B). The mixed BjPutA mutants show a similar pH dependence as well except that NADH formation peaks at pH 7 (Figure 5B). The rates for NADH formation are similar for each BjPutA enzyme at pH 6.0 with 1.92 µM/min, 2.11 µM/min and 2.0 µM/min for wild-type BjPutA, BjPutA 1-986 and mixed variants respectively. These rates decrease by 8-9 fold at pH 10.0. Next, the lag time for NADH formation was plotted as a function of pH (Figure 6).

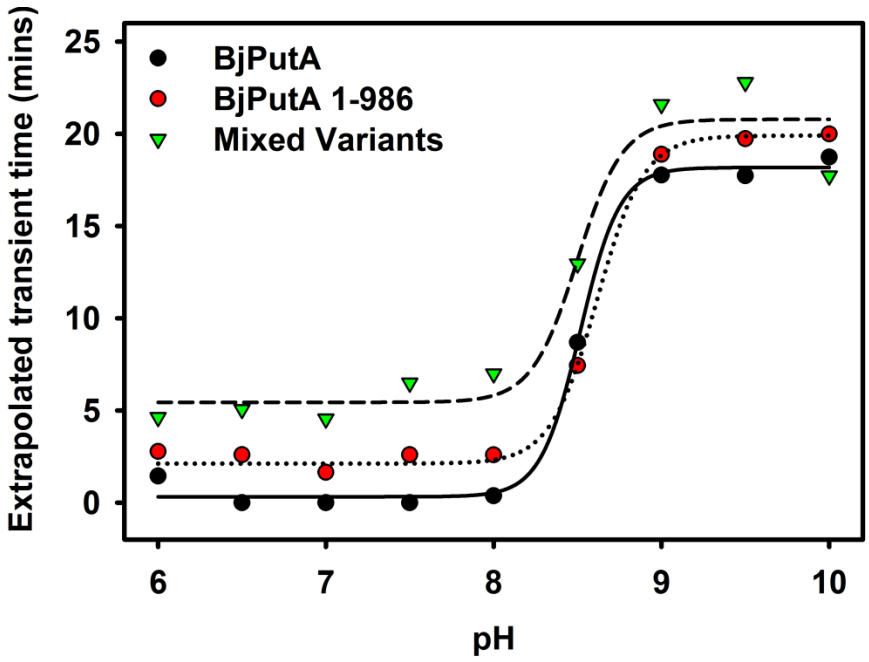

Figure 6- pH dependence of transient time in the BjPutA channeling reaction. Transient time is extrapolated from the linear rate of NADH formation and plotted against pH. The change in transient time is fitted to equation 4.4 using SigmaPlot 12 (Systat Inc.). The solid line, dotted line and dashed line correspond to the fit for BjPutA, BjPutA 1-986 and mixed variants with pK_a values of 8.64, 8.70 and 8.53 respectively.

The lag time remains unchanged within the pH range 6 to 8 for wild-type BjPutA, BjPutA 1-986 and the mixed variants. Within this pH range, wild-type BjPutA exhibits

approximately no lag in NADH formation, whereas BjPutA 1-986 and mixed variants show lag times of about 2.5 min and 6 min, respectively. Above pH 8 there is a drastic increase in the lag time to an equal extent for all three enzymes. A plateau is reached above pH 9, with apparent lag times of 17-23 min for the different BjPutA enzymes. Figures 5 and 6 show that wild-type BjPutA, BjPutA 1-986, and the mixed variants exhibit similar pH profiles of NADH formation.

Effect of pH on PRODH and P5CDH domains of BjPutA

To further probe the factors influencing the pH dependence of NADH formation in BjPutA, we examined the effect of pH on the individual PRODH and P5CDH activities. The PRODH specific activity of wild-type BjPutA , BjPutA 1-986, and the mixed variants was measured at different pH values. These assays used 40 mM proline and 0.1 mM CoQ_1 similar to the channeling assays shown in Figures 4 and 5 [4]. Figure 7 shows the dependence of PRODH activity on pH.

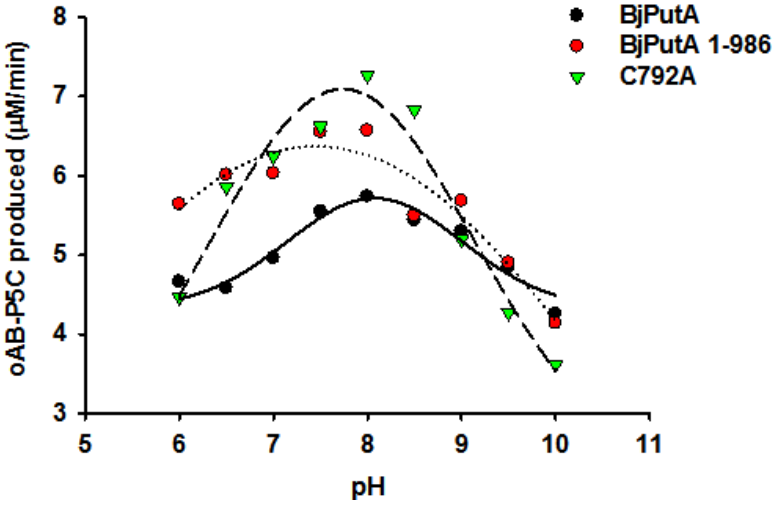

Figure 7- pH profile of PRODH specific activities. Specific activities of PRODH from BjPutA, BjPutA 1-986 and C792A measured by production of *o*-AB-P5C complex at 443 nm. The pH profiles were fit to equation 4.1 in SigmaPlot 12 (Systat Inc.). The solid line, dotted line and dashed line correspond to the fit for BjPutA, BjPutA 1-986 and C792A with peak activity estimated at pH 8.07, 7.6 and 7.75 respectively.

A bell-shaped pH profile with peak activity at pH 8 was observed for each enzyme. Wild-type BjPutA, BjPutA 1-986 and C792A reached maximal PRODH activities of 5.74, 6.56 and 7.27 μM *o*-AB-P5C/min, respectively. The pH profiles are similar to that observed for monofunctional Put1p from *S. cerevisiae* (Chapter 2).

The K_m and specificity constant (k_{cat}/K_m) of P5CDH activity of wild-type BjPutA, BjPutA 1-986, and BjPutA mutant R456M were determined at different pH. For all three BjPutA enzymes, a plot of k_{cat}/K_m versus pH yields a bell-shaped curved with k_{cat}/K_m maximum at pH 7 (Figure 8A). At pH 9.0, k_{cat}/K_m decreases by > 10-fold to about 200 M^{-1} sec^{-1} compared to 2600-3600 M^{-1} sec^{-1} at pH 7. The sharp decrease in k_{cat}/K_m at pH > 7.0 may be attributed to less favorable P5C/GSA equilibrium or a change in substrate binding. A plot of K_m versus pH (Figure 8B) shows that K_m for P5C/GSA does not significantly increase until pH > 8.5 with K_m values for P5C/GSA estimated above 10 mM at pH 9.0 for wild-type BjPutA and R456M and, above 30 mM at pH 9.5 for BjPutA 1-986.

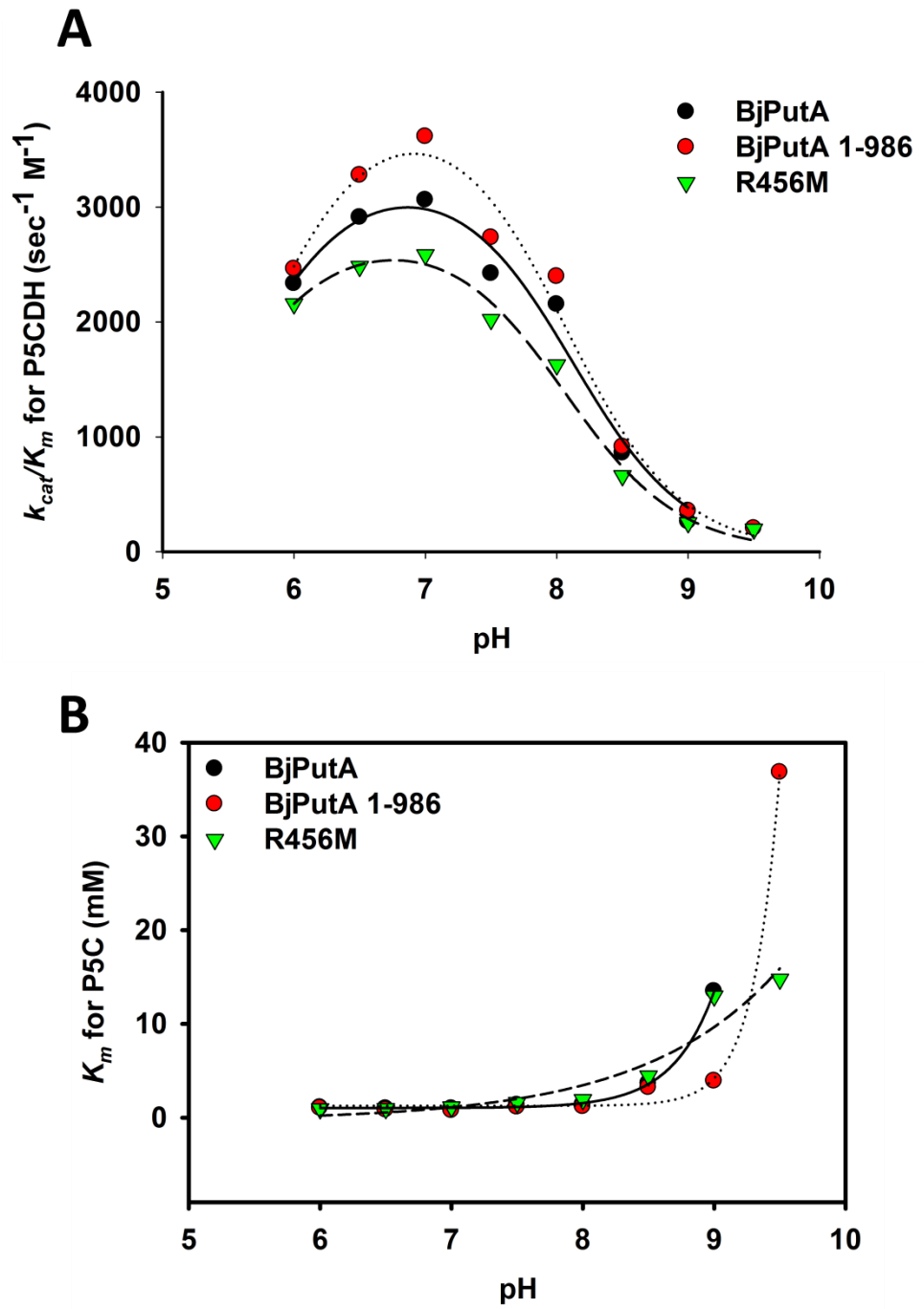

Figure 8- pH profile of P5CDH kinetic parameters. A) Specificity constant (k_{cat}/K_m) for BjPutA, BjPutA 1-986 and R456M P5CDH domains plotted versus pH. The pH profiles were fit to equation 4.1 in SigmaPlot 12 (Systat Inc.). The solid line, dotted line and dashed line correspond to the fit for BjPutA, BjPutA 1-986 and R456M with peak activity estimated at pH 6.86, 6.89 and 6.75, respectively. B) Plot of K_m (P5C/GSA mM) for P5CDH activity versus pH. Significant increase in K_m was observed at pH > 8.5.

DISCUSSION

Truncation of C-terminal residues (987-999) in PutA from *B. japonicum* was expected to increase solvent accessibility to the substrate channel by creating an additional opening into the cavity between the PRODH and P5CDH active sites. Thus, it was hypothesized that the truncated BjPutA 1-986 mutant may partially leak the intermediate P5C/GSA into the bulk solvent. In previous studies on BjPutA [4], the appearance of the intermediate P5C in the bulk medium was studied using a trapping assay using *o*-AB. In the trapping assays inverted membrane vesicles from *E. coli* (*putA*$^-$ strain) [15] were used as terminal electron acceptor in the absence and presence of 0.2 mM NAD^+. From the results of these assays, 70% of the P5C/GSA was estimated to directly channel from PRODH to P5CDH in wild-type BjPutA [4]. Unlike wild-type BjPutA, BjPutA 1-986 does not exhibit turnover with inverted membrane vesicles (data not shown). The lack of functional PRODH activity with membrane vesicles suggests that residues 987-999 are also important for BjPutA membrane binding. Thus, residues 987-99 appear not only to be important for forming the channel but also have a role in functional membrane binding. Because BjPutA 1-986 does not bind to membranes, it is not possible to directly compare the channeling efficiency of BjPutA 1-986 with wild-type PutA. Transient time analysis shows that truncation of the C-terminal residues of BjPutA increases the time required to achieve steady-state formation of NADH. Steady-state formation of NADH is reached at approximately 2.5 min for BjPutA 1-986, which is significantly longer than the ~ 10 sec lag time observed with wild-type BjPutA. These results indicate that P5C/GSA leaks into the bulk solvent in assays with BjPutA 1-986 consistent with increased solvent access to the substrate channeling cavity as predicted by the BjPutA structure.

The equilibrium of the intermediates P5C and GSA is pH dependent with the open-chain GSA favored at pH < 6.6 [6]. It is not known where the obligate hydrolysis step occurs in BjPutA. Structural analysis of the P5CDH active site indicates that P5C and GSA can both bind to the active site. The observation that proline inhibits TtP5CDH (Chapter 2) suggests that P5C may bind at the P5CDH active site and that the hydrolysis step occurs in the active site. We hypothesized that the substrate channel may facilitate the P5C/GSA equilibrium by increasing the pK_a of the pyrrolinium species above pH 6.6, making the hydrolysis of P5C to GSA more favorable at physiological pH conditions. Because BjPutA 1-986 was considered to have a more solvent exposed substrate channel, it was thought that the pH activity dependence of BjPutA and BjPutA 1-986 may be different.

The pH profile of the substrate channeling reaction and the transient time, however, showed no significant differences between wild-type BjPutA, BjPutA 1-986, and the equimolar mixture of the BjPutA monofunctional variants. The peak activity for substrate channeling reaction was observed at pH 6.5-7.0 for the three different enzyme systems. The transient time to attain steady-state NADH formation remained unchanged between pH 6-8, a range in which the equilibrium of P5C/GSA is expected to be significantly altered by the pH environment. BjPutA 1-986 and the non-channeling mixed variants did exhibit lag times (2.5 min and 5.3 min, respectively), but the lag times did not appear to change until pH > 8.0. Interestingly, the transient time for wild-type BjPutA, BjPutA 1-986, and the mixed variants all showed the same pH dependence significant increased observed at pH > 8.0. If the substrate channel was critical for facilitating the hydrolysis of P5C at a more physiological pH environment, then BjPutA

1-986 and the mixed variants would have shown significantly different pH activity dependences. The substrate channel cavity is expected to be more solvent exposed in BjPutA 1-986 and with the mixed variants P5C/GSA must equilibrate with the bulk solvent to form NADH. The similar pH profiles of wild-type BjPutA, BjPutA 1-986, and the mixed variants argue against the channel facilitating the P5C/GSA equilibrium and suggests that the hydrolysis of P5C occurs in the P5CDH active site.

To investigate the pH effect on substrate channeling further, the pH activity dependence of the individual PRODH and P5CDH domains were assessed separately. The pH profile of PRODH activity for wild-type BjPutA, BjPutA 1-986, and BjPutA mutant C792A all show a bell-shaped curve with peak activity at pH 8.0. At this point it is not clear what step in the PRODH reaction is most influencing the pH profile that is observed for PRODH activity. A straightforward experiment that could be performed would be to measure the rate of flavin reduction under single-turnover conditions at varying pH. This would help dissect out the effect of pH on the substrate binding and chemical steps of the PRODH reaction. This experiment, however, was not pursued because of difficulties with BjPutA (20-40 μM concentration) precipitating at pH > 8.0.

The activity of P5CDH for wild-type BjPutA, BjPutA 1-986, and BjPutA R456M was also significantly affected by pH (Figure 8 A) with peak activity at pH 7 for all three enzymes. pH can influence factors which are important for P5CDH catalysis such as hydrolysis of P5C to GSA, deprotonation of the active site cysteine and hydride transfer from GSA to NAD^+ [16]. Because the pH dependence of NADH formation seems to correlate more closely with the pH activity profile of P5CDH activity, it appears that catalytic steps in the P5CDH active site have a greater influence on the pH dependence of

substrate channeling than the PRODH reaction. Future experiments will need to dissect the different catalytic steps of the P5CDH reaction to provide more insights into the pH sensitive steps of P5CDH activity and the overall BjPutA substrate channeling reaction.

REFERENCES

1. Krishnan, N. and D.F. Becker, *Characterization of a bifunctional PutA homologue from Bradyrhizobium japonicum and identification of an active site residue that modulates proline reduction of the flavin adenine dinucleotide cofactor.* Biochemistry, 2005. **44**(25): p. 9130-9.
2. Tanner, J.J., *Structural biology of proline catabolism.* Amino Acids, 2008. **35**(4): p. 719-30.
3. Adams, E. and L. Frank, *Metabolism of proline and the hydroxyprolines.* Annu Rev Biochem, 1980. **49**: p. 1005-61.
4. Srivastava, D., et al., *Crystal structure of the bifunctional proline utilization A flavoenzyme from Bradyrhizobium japonicum.* Proceedings of the National Academy of Sciences, 2010. **107**(7): p. 2878-2883.
5. DeLano, W.L., *The PyMOL Molecular Graphics System.* DeLano Scientific, San Carlos, CA, USA., 2002.
6. Bearne, S.L. and R. Wolfenden, *Glutamate gamma-semialdehyde as a natural transition state analogue inhibitor of Escherichia coli glucosamine-6-phosphate synthase.* Biochemistry, 1995. **34**(36): p. 11515-20.
7. Williams, I. and L. Frank, *Improved chemical synthesis and enzymatic assay of delta-1-pyrroline-5-carboxylic acid.* Anal Biochem, 1975. **64**(1): p. 85-97.
8. Antharavally, B.S., et al., *Quantitation of proteins using a dye-metal-based colorimetric protein assay.* Anal Biochem, 2009. **385**(2): p. 342-5.
9. Grauschopf, U., A. Fritz, and R. Glockshuber, *Mechanism of the electron transfer catalyst DsbB from Escherichia coli.* Embo J, 2003. **22**(14): p. 3503-13.
10. Mezl, V.A. and W.E. Knox, *Properties and analysis of a stable derivative of pyrroline-5-carboxylic acid for use in metabolic studies.* Anal Biochem, 1976. **74**(2): p. 430-40.
11. Meek, T.D., E.P. Garvey, and D.V. Santi, *Purification and characterization of the bifunctional thymidylate synthetase-dihydrofolate reductase from methotrexate-resistant Leishmania tropica.* Biochemistry, 1985. **24**(3): p. 678-86.
12. Becker, D.F. and E.A. Thomas, *Redox properties of the PutA protein from Escherichia coli and the influence of the flavin redox state on PutA-DNA interactions.* Biochemistry, 2001. **40**(15): p. 4714-21.
13. Moxley, M.A., J.J. Tanner, and D.F. Becker, *Steady-state kinetic mechanism of the proline:ubiquinone oxidoreductase activity of proline utilization A (PutA) from Escherichia coli.* Arch Biochem Biophys, 2011. **516**(2): p. 113-20.
14. Wanduragala, S., et al., *Purification and characterization of Put1p from Saccharomyces cerevisiae.* Arch Biochem Biophys, 2010. **498**(2): p. 136-42.
15. Brown, E.D. and J.M. Wood, *Redesigned purification yields a fully functional PutA protein dimer from Escherichia coli.* J Biol Chem, 1992. **267**(18): p. 13086-92.
16. Loveridge, E.J. and R.K. Allemann, *Effect of pH on hydride transfer by Escherichia coli dihydrofolate reductase.* Chembiochem, 2011. **12**(8): p. 1258-62.